D Sanjeev Kumar
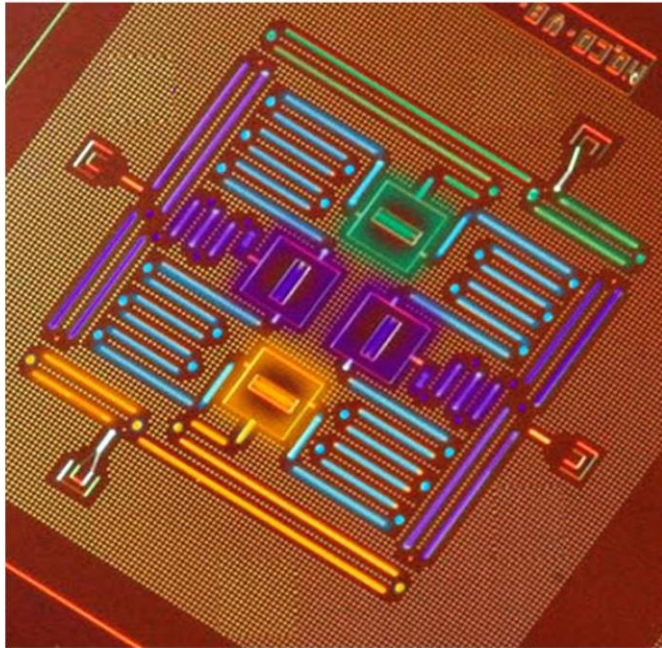
School of Physics
University of Hyderabad

Spin-Orbit interactions in parabolic quantum dots

Supervisor
Prof. Ashok Chatterjee

Spin-Orbit interactions in parabolic quantum dots

Thesis submitted for the degree

of

Doctor of Philosophy

in

Physics

By

D. Sanjeev Kumar

Supervisor:

Prof. Ashok Chatterjee

School of Physics

University of Hyderabad

Hyderabad

India-500046

June-2016

Dedicated to

All King Makers

DECLARATION

I, D. Sanjeev Kumar, hereby declare that this thesis entitled "Spin-Orbit interactions in parabolic quantum dots" submitted by me under the guidance and super-vision of Prof.. Ashok Chatterjee is a bonafide research work which is also free from plagiarism. I also declare that it has not been submitted previously in part or in full to this University or any other University or Institution for the award of any degree or diploma. I hereby agree that my thesis can be deposited in Shodganga/INFLIBNET.

A report on plagiarism statistics from the University Librarian is enclosed.

Date:

D. Sanjeev Kumar

08PHPH06

School of Physics

University of Hyderabad

CERTIFICATE

This is to certify that the research work described in this thesis entitled "**Spin-Orbit interactions in parabolic quantum dots**" has been carried out by **Mr. D. Sanjeev Kumar** under my direct supervision and this has not been submitted for any degree of diploma at this or any other University.

Place: Hyderabad

Date:

Prof. Ashok Chatterjee   Dean
 Thesis Supervisor   School of Physics

ACKNOWLEDGEMENTS

I would like to express deepest gratitude to my supervisor Prof. Ashok Chatterjee for accepting me as his student into his work group. He inspired us, motivated us, advised us, supported us and stand by us in all odds more or less like a parent besides being a research supervisor. He is highly successful in maintaining a positive work culture among the members of our work group. I am highly solemned to be a member of his work group.

I am highly thankful to Dr. Soma Mukhopadhyay for initiating the problem of this thesis, helping me during the initial stages of my research and extending it to the rest of my course.

I would like to give my sincere gratitude to Mr. Jagadeesh for motivating me in a right time. Without him, I wouldn't have continued my Ph.D.

I would like to thank my Doctoral review committee members Dr. S. Srinath, Dr. Surajith Dhara, Dr. S. V. S. Nageswararao for their critical reviews and suggestions.

It is great to mention about Mr. Abhinava for taking Physics tutions from me and Dr. M. C. Valsa Kumar for teaching a special course in materials engineering. Both of them enhanced my exposure to basics of science and rose my confidence levels.

I would like to thank former Deans and among them especially Prof. S. Chaturvedi and the current Dean, Prof. Rajenra Singh for their courageous, timely and student friendly decisions.

I would like to acknowledge Prof. A. K. Kapoor, Prof. S. Chaturvedi, Prof. K. P. N. Murthy, Prof. P. Ananthalakshmi, Dr. Soma Sanyal, Dr. Ashoka Vudayagiri, Dr. S. Srinath, Dr. G. Vaitheeswaran,

Dr. Anil K. Choudari, Dr. S Sreekanth for their friendly advises and support.

Thanks are not enough for my friends RV, Anil, Aalu, IV, Monisha, Majji, Madhu, Surya, Ephraim, Rayudu, Naveen anna, N Shankaraiah, SSN Chari, Suman Kalyan, Sudha Nirmala, Atahar, Narasimha, Raju garu, Ganga, Reddy, Prasad, Srinu, Ajay, M Vijay, V Vijay, Seshu, Bindu, Uday, Ramki, GV, Suresh, Sai, Ahmed, Soorat, Pidi, G Sriram, V Sriram, Azeem, DL Srinu, Tiru, Pavan, Ravi, Raju, Ramesh, Uma, Luhluh, Yadaiah, Naidu, Ashok, Murali, Sumantran, Chalapathi, Sukhesh, Neelotpal, Sunil, Sobhan who made my life joyful and memorable on this campus.

I would like to thank HCU for BBL and UGC for BSR JRF and SRF fellowships.

I would like to thank Mr. T. Abraham, K. Srinivas, Krishna, Sailaja, Prasad, Ravi, Sainadh, Kasyap garu, Raghunandan garu, David Raju garu, B Narsimhlu, Prof. I Ramabrahmam, Prof. E. Haribabu for their support in my non-academic jobs in this University.

Finally, I wish to pay my sincere gratitude to my parents, family and my spouse Aswathy who are giving their best for my eternal growth without any expectations.

ABSTRACT

The advanced trends in nanofabrication techniques enabled us to manufacture low dimensional structures with electron confinement in all the three dimensions. The study of spin-orbit interactions in these novel structures lead to the realization of innovative devises like spin filter, spin transistor, quantum computer etc. The aim of this work is to study the spin-orbit interaction effects in these nanostructures. Here we have considered a multi-electron quantum dot developed on a two dimensional electron gas in a perpendicular magnetic field. The confinement potential is considered to be parabolic as it is the only compliable one with the generalized Kohn's theorem. The electron-electron interaction has been taken into account by Johnson-Payne model potential as it makes the Hamiltonian of the system of interest exactly solvable. The Rashba and Dresselhaus spin-orbit interaction terms have been treated by suitable unitary transformations. Further, the effect of spin-orbit interaction on the energy spectrum, addition energy, spin splitting energy, magnetic and thermodynamic properties of a parabolic quantum dot in a perpendicular magnetic field have been studied. Besides, the problem of binding energy of a D^0 center in a Gaussian quantum dot, the problem of barrier transmission across a metal semiconductor junction with spin-orbit interaction have been studied.

List of Abbreviations

3D	Three dimensional
2D	Two dimensional
1D	One dimensional
0D	Zero dimensional
QD	Quantum Dot
PQD	Parabolic Quantum dot
GQD	Gaussian quantum dot
IR	infra-red
GS	Ground state
ES	Excited state
OAM	Orbital angular momentum
BIA	Bulk inversion asymmetry
SIA	Structure inversion asymmetry
SOI	Spin-orbit interaction
RSOI	Rashba spin-orbit interaction
DSOI	Dresselhaus spin-orbit interaction
2DEG	Two dimensional electron gas
e-e	Electron-eletron
s-t	Singlet-triplet
d-p	diamagnetic-paramagnetic

Table of Contents

1.1 Introduction

The research in semiconductor technology took a big leap with the discovery of the semiconducting nature of $InSb$ by Blum *et al.* [1] and Goryunova & Obukov [2]. Besides a systematic study by Welker [3] introduced a new class of semiconductors namely $III - V$ compounds into the arena of semiconductor research. The crystal structure of these compounds was studied a long back by Huggins [4] and Goldschmidt [5]. Further research in this area led to the discovery of quasi-binary alloys of the type $A_x B_{1-x} C$ where A and B are III_B group elements and C is a V_B group element.

On the other hand, theoretical research on dissimilar semiconductor junctions started with Gubanov [6], Shockley [7] and Kroemer [8] and took a proper shape with the schemes proposed by Anderson [9,10] in 1960 for the construction of their band diagrams. This pioneering work is an extension of the theories of Mott [11] and Schottky [12] for metal-

semiconductor junctions [13] and is considered as the foundation for the heterojunction semiconductor research. According to Anderson, when two dissimilar band-gapped semiconductors are joined together, electrons will be trapped at the junction [14–16]. The band diagram for such a heterojunction is shown in Fig. 1.1.
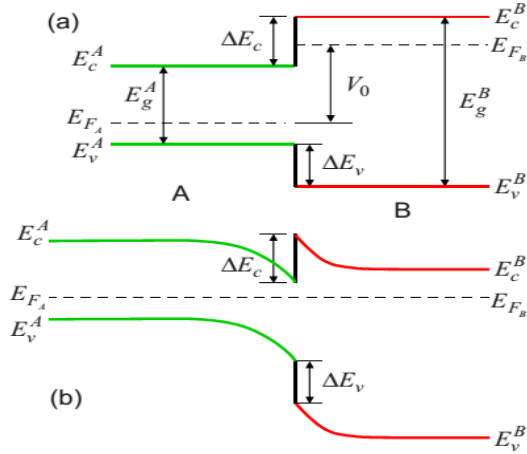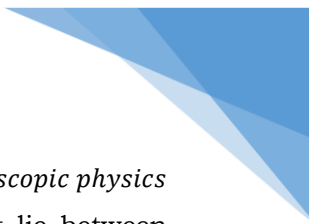

Fig. 1.1 Heterojunction band diagram.

Here the electron motion is restricted to the surface of the junction. The resultant configuration is called a two-dimensional electron gas (2DEG). This opened up a new area of "*mesoscopic physics*" in the condensed matter physics. The word *meso* in Greek

means "middle" or "intermediate" [17]. *Mesoscopic physics* studies the properties of the systems that lie between microscopic systems such as atoms and macroscopic systems such as bulk matter. The term *mesoscopic* was introduced by Kampen [18] in 1976 and also mentioned by Thouless [19] in 1977 and further utilized by Ya Azbel [20], Altshuler [21,22] in various contexts.

When a thin layer of lower bandgap material like *GaAs* is sandwiched between two layers of a wider bandgap material like *AlGaAs*, electrons are forced to move in a quasi-two dimensional (quasi-2D) planar region and the resulting structure is referred to as a Quantum well [16]. The quantum confinement effects will be clearly seen if the thickness of the lower bandgap material is of the order of the De Broglie wavelength of the charge carriers. If the confinement of the carriers further extends to one and zero dimensions (1D and 0D), one gets a quantum wire and quantum dot (QD) respectively. The effects of quantum confinement may be observed by studying the density of states. The dependence of density of states on energy for various dimensions [23,24] is given by: $DOS_{3D} \propto \varepsilon^{1/2}$, $DOS_{2D} \propto \Theta(\varepsilon - \varepsilon_i)$, $DOS_{1D} \propto \varepsilon^{-1/2}$ and $DOS_{0D} \propto \delta(\varepsilon - \varepsilon_i)$. The

variation of density of states as a function of energy in various dimensions is shown in Fig. 1.2 [25].
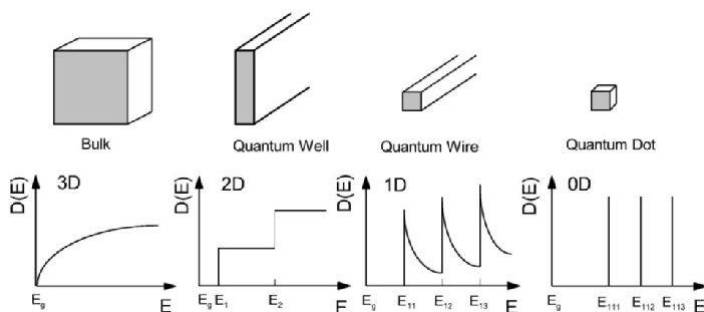
Fig. 1.2 The density of states vs. E in 3D, 2D, 1D, 0D systems.

The experimental evidence of $3D$ confinement was first demonstrated by Ekimov in 1981 in $CuCl$ microcrystal lattice [26]. They observed a blue shift in the absorption spectra with a reduction in the size of the QD. The theoretical explanation for that has been given by Efros & Efros [27] in 1982 and by Brus [28] in 1983 independently which is the starting point of the new Era of QDs in condensed matter physics. Here they have modeled the QD confinement as an infinite square well potential. The first study of electronic structure and discrete energy levels of a QD was conducted in 1987 by Bryant who clearly demonstrated the quantum size effects [29].

With the advent of micro-fabrication techniques like lithography and epitaxial growth techniques in the last two decades of 20th century, a variety of QDs have been prepared using different techniques of quantum confinement. One way to achieve the $3D$ confinement is by using metallic gates over a 2DEG developed in a heterostructure. It was first reported by Cibert *et al.* [30] in 1986. These are called lateral QDs as the electrons in the well are laterally confined by external lateral electrostatic field. An alternative method is to use chemical etching which develops QDs in vertical columns. It was first reported by Allen et al. [31] in 1983 in a single quantum well and by Reed et al. [32] in 1986 in a multiple quantum well super-lattice. However it was Reed who introduced the word "*Quantum dot*". Earlier, a $quasi-0D$ structure would be addressed as a $quantum\ box$ [31], $quantum\ bubble$ [24], $quantum\ point$ [33], $semiconductor\ crystallite$ [34] etc. Another way of obtaining $3D$ quantum confinement is by using strained layer super-lattices. Here the lattice mismatch between the layers of a super-lattice makes the $2D$ layered structure to organize into small islands and so they are called $self-assembled\ quantum\ dots$. This was first achieved by Goldstein in 1985 and further confirmed by

Leonardo in 1993. Various types of QDs developed on $III-V$ heterostructures are shown in Fig. 1.3.
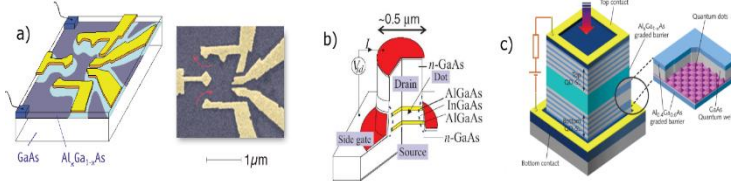
Fig. 1.3 QDs developed on $III-V$ heterostructures. a) Lateral, b) Vertical, c) Self-assembled.

1.2 Confinement potential

The fundamental magneto-optical experiments [35–40] along with generalized Kohn theorem [33,41–43] emphasized that the observed experimental facts in QDs are independent of number of electrons in the QD or in other words, independent of electron-electron (e-e) interaction in the QD. The only confinement potential which could fit into this experimentally observed fact is the parabolic potential. Likewise, any other model potential can be approximated as the enharmonic perturbative correction to the parabolic (harmonic) potential [44,45]. The parabolic potential model encompasses all the major physics of the QD and also makes the Hamiltonian of an electron in QD exactly solvable even in the presence of a perpendicular

magnetic field. Therefore throughout this thesis, the parabolic potential is considered as a model for confinement potential except for one problem where the binding energies are calculated. A QD with a parabolic confinement potential will be referred to a parabolic quantum dot (PQD).

1.3 Single electron quantum dot Hamiltonian

The Hamiltonian of a system of an electron moving in a 2D parabolic QD in the $z = 0$ plane and perpendicular magnetic field $\boldsymbol{B} = (0, 0, B)$ is given by

$$H = \frac{1}{2m^*}\left(\boldsymbol{p} + \frac{e\boldsymbol{A}}{c}\right)^2 + \frac{1}{2}m^*\omega_0^2\boldsymbol{r}^2 - \frac{1}{2}g^*\mu_B\boldsymbol{B}.\boldsymbol{\sigma} \qquad (1.1)$$

where $\boldsymbol{r}(x, y)$ is the 2D position vector of the electron and $\boldsymbol{p}(p_x, p_y)$ is the corresponding momentum operator, $-e$ is the charge of the electron (e being positive) and m^* its effective mass, $\boldsymbol{A}$ is the vector potential which is chosen in the symmetric gauge as $\boldsymbol{A} = B(y/2, -x/2, 0)$, ω_0 is the frequency of the confining parabolic potential, g^* is the
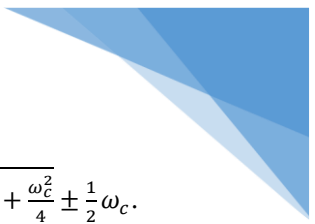
effective gyromagnetic factor of the electron, $\mu_B \left(= \frac{e\hbar}{2mc} \right)$ is the Bohr magneton and $\boldsymbol{\sigma}$'s are the Pauli spin matrices. The above Hamiltonian can be re-written as

$$H = \frac{\boldsymbol{p}^2}{2m^*} + \frac{1}{2} m^* \left(\omega_0^2 + \frac{\omega_c^2}{4} \right) r^2 + \frac{1}{2} \omega_c l_z$$
$$- \frac{1}{2} g^* \frac{m^*}{m_0} \omega_c S_z, \qquad (1.2)$$

where m_0 is the bare mass of the electron, $\omega_c \left(= \frac{eB}{m^*c} \right)$ is the cyclotron frequency, $S_z \left(= \frac{1}{2} \hbar \sigma_z \right)$ is the projection of the spin angular momentum along the field direction and $l_z (= xp_y - yp_x)$ is the projection of the orbital angular momentum along the field direction.

The solution for this Hamiltonian has been given long back in 1931 by Fock and Darwin independently as

$$E(N_A, N_B, S_z) = \left(N_A + \frac{1}{2} \right) \hbar \omega_+ + \left(N_B + \frac{1}{2} \right) \hbar \omega_-$$
$$- \frac{1}{2} g^* \frac{m^*}{m} \omega_c S_z, \qquad (1.3)$$

where N_A and N_B are integers and $\omega_\pm = \sqrt{\omega_0^2 + \frac{\omega_c^2}{4}} \pm \frac{1}{2}\omega_c$.
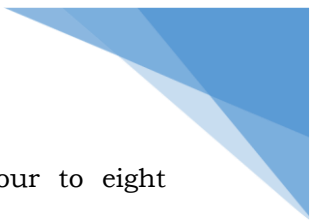
The above energy spectrum is also known as Fock-Darwin energy spectrum [46–48]. Due to the discrete and quantized nature of energy levels, QDs are also called as *Artificial atoms*. This word was coined by Kastner [49] and Chakraborty [50] independently.

1.4 Electron-electron interaction

The failure of the experimental techniques to take into account the effect of e-e interaction in QDs was explained by Chakraborty et al. [50] and Li et al. [43] independently. The reason is that when the confining potential is parabolic, the center of mass and relative motions get separated and the e-e interaction entirely goes into the relative part of the motion; whereas the long wavelength radiation couples only with the center of mass part of the motion. This revolutionary discovery grabbed the attention of contemporary researchers and directed them to quest for alternative experimental, analytical and numerical techniques that could take into account the actual e-e interaction effect in a QD.

Several analytical methods have been developed to deal with the e-e interaction in QDs. These include the constant interaction (CI) model [51,52], the Hartree [53] , Hartree-Fock [54] , unrestricted Hartree-Fock [55], and the Brueckner-Hartree-Fock [56] methods, the quantum Monte Carlo technique [57,58], the density functional theory [59–61], Green's function approaches [62,63], the WKB method [64], variational and perturbation theories [65–69], exact diagonalization [70–73] procedures and a few other numerical iterative methods [36–42]. The constant interaction method is however too simplistic and missed even some essential physics. The Hartree and other Hartree-Fock methods could not take into account the exact exchange-correlation effects. The quantum Monte Carlo method failed to explain the situations at larger magnetic fields due to computational restrictions on the configuration space that could be taken into account. Density functional methods like LSDA are suitable only for systems with low electron densities like QDs developed by etching and lithography and could not explain the properties of systems with high electron densities like self-assembled QDs. The WKB, variational and perturbation techniques are difficult to apply to higher excited states. Exact diagonalization and other numerical methods are plagued with convergence

problems for systems with more than four to eight electrons.

The coulomb potential due to a charge e in 2D is given by [81]

$$\varphi = -\frac{1}{2\pi\epsilon} \ln r. \qquad (1.4)$$

However. in QDs developed on heterostructures, field lines are not confined to 2D but pass through the surrounding material, which is often a material with a very similar dielectric constant [82]. Thus, electrons in a 2DEG or in a QD developed on a 2DEG will still feel the $1/r$ – type interaction.[83] This interesting fact was first predicted by Chaplik [84] In 1972 and revolutionized the further research in the area of low dimensional systems. The prediction of Chaplik [84] was also verified in QDs experimentally in Ref. [85,86] and theoretically in Ref. [87] and this confirmed that the Coulomb interaction in a QD is more are less 3-dimensional. It was also predicted based on experimental facts that the Coulomb interaction is screened due to a finite extension of electronic wave function perpendicular to the plane of confinement i. e., two electrons could have finite

repulsion, rather than infinite repulsion, even when the separation between them on the plane of confinement is zero as they can have finite separation along the direction perpendicular to the plane of confinement. This is due to the interaction of electrons in the 2DEG with the image charges in the adjacent layers of the semiconductor [88]. Thus the Coulomb interaction in QDs developed on 2DEG can be written as

$$V_{ee}(r, r') = \frac{1}{4\pi\epsilon} \frac{e^2}{\sqrt{|r - r'|^2 + \delta_z^2}}. \tag{1.5}$$

Since analytical and numerical models have their own drawbacks, an alternative way is to look for a model potential which could mimic the Coulomb interaction and make the QD Hamiltonian exactly soluble so that all the many- body effects are included properly. The Johnson-Payne model [89] serves exactly this purpose.

1.4.1 Johnson-Payne model

Models are of critical importance in various fields of science and especially in Physics. Models are essential to cut down and avoid the unnecessary complications in

understanding a phenomenon and are used to catch the essential facts that govern the phenomenon. Sometimes models may be over- simplified but can be further improved depending on its applicability and accuracy in predicting the experimental observations.

One of the simplest model potentials proposed to explain the observed experimental facts in the first magneto-optical experiments is the constant interaction model [51,52]. But it is an over-simplified model and failed to explain the scenario in the higher excited states as it overestimated the Coulomb interaction. There were some exactly soluble models in 2D [90–92] and 1D [93–96] with quadratic and inverse quadratic [97] potentials whose applicability to QDs has not been studied [98] extensively. But one such exactly solvable model in 2D QDs is the Johnson-Payne model [89] proposed in 1991. The validity of this model has been well established [99–102] for parabolic QDs by various authors in the recent past. Also, it is an exactly solvable model for the general case of an N-electron PQD. Hence, Johnson – Payne model has been adopted for the investigations presented in this thesis. The Johnson-Payne model potential for e-e interaction is given by

$$V(\boldsymbol{r}_i, \boldsymbol{r}_j) = 2V_o - \frac{1}{2}m^*\Omega^2 |\boldsymbol{r}_i - \boldsymbol{r}_j|^2. \qquad (1.6)$$

The Hamiltonian of an N-electron QD with e-e interaction in a perpendicular magnetic field is given by

$$H = \sum_{i=1}^{N} \left(\frac{1}{2m^*}\left(\boldsymbol{p}_i + \frac{e\boldsymbol{A}_i}{c}\right)^2 + \frac{1}{2}m^*\omega_o^2|\boldsymbol{r}_i|^2 \right.$$
$$\left. + \frac{1}{2}g^*\mu_B B\sigma_{i,z} \right)$$
$$+ \sum_{i<j} 2V_o - \frac{1}{2}m^*\Omega^2|\boldsymbol{r}_i - \boldsymbol{r}_j|^2, \qquad (1.7)$$

The advantage of this Hamiltonian (Eq. 1.7) is that it can be exactly solvable [89] for an arbitrary number of particles.

1.5 Spin-orbit interaction

The study of spin-orbit interaction (SOI) in QDs and other low-dimensional structures made a major breakthrough in the semiconductor research and opened up a new branch called *spintronics* which is an acronym for *"Spin Transport Electronics"* introduced by Wolf in

1996. The study of SOI in quantum mechanics started with the revolutionary proposal of spin of electron by Uhlembeck and Goud Smit [103,104] which made a major breakthrough in understanding basic quantum mechanics and brought in a giant leap from old quantum theory to new quantum theory. Although the empirical theory of Uhlembeck and Goud Smit has explained the Zeeman Effect and anomalous Zeeman Effect, there was a quantitative discrepancy by a factor of 2. This discrepancy was identified and resoled by Llewellyn Thomas [105,106] in 1926. The SOI Hamiltonian as given by Thomas .[107–111] and also by Dirac [112] is

$$H_{SO} = \frac{1}{2m^2c^2} \frac{1}{r} \frac{dV}{dr} (\boldsymbol{L}.\boldsymbol{S}) \qquad (1.8)$$

Thus the factor 2 in the denominator of the SOI Hamiltonian is named as $Thomas - factor$. This SOI term plays an important role in atomic physics especially in explaining the fine and the hyper-fine structures of atoms [113]. But in the case of solids, SOI utmost be treated as a perturbation.

1.6 Spin-Orbit interactions in solids

In solids, the quasi-free electrons in the conduction band may not experience strong nuclear attraction as seen in the case of atoms. However in those systems, SOI can arise due to internal fields. This SOI may not have a significant effect at any general point in the Brillouin zone. But at the symmetry points, it can lift the degeneracy and have a significant effect. In QDs developed on 2DEG of heterojunctions, SOI may arise due to two major effects. One is called the Rashba effect and the other is called the Dresselhaus effect.

1.6.1 Rashba spin-orbit interaction

This is one of the two zero-field spin splittings observed in $III - V$ heterostructures which arises due to structure inversion asymmetry (SIA) of the heterojunction. Due to the difference in the bandgap, there would be an asymmetry in the space charge accumulated on the either side of the heterojunction which creates an electric field perpendicular to the 2DEG. This leads to a SOI as described by Thomas and

is called the Rashba spin-orbit interaction (RSOI) [114–116] named after its inventor.
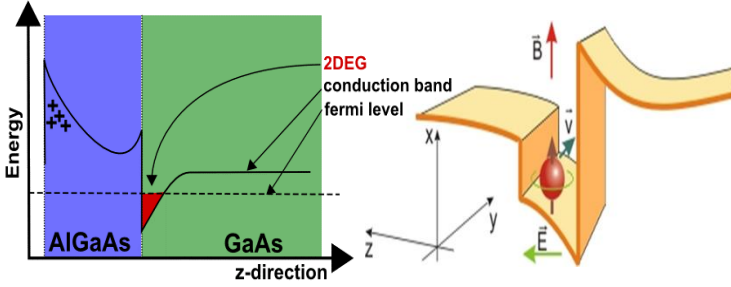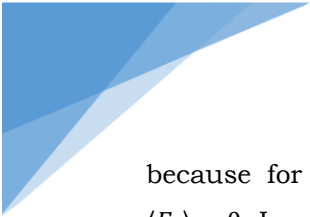
Fig. 1.5 Rashba spin-orbit interaction.

The RSOI can be enhanced by applying an external electric field across the junction and therefore it can have many experimental applications. The RSOI Hamiltonian that arises due to space charge field or due to any external electric field applied perpendicular to the 2DEG (along z direction) is given by

$$H_R = \frac{1}{2m^2c^2}(\boldsymbol{S}.\boldsymbol{L})\frac{1}{r}\frac{dV}{dr}\Big|_z = \frac{1}{2m^2c^2}S.(\boldsymbol{r}\times\boldsymbol{p})\frac{1}{r}\frac{dV}{dr}\Big|_z$$
$$= \frac{\hbar}{4m^2c^2}\nabla V.(\sigma\times p)\Big|_z$$
$$= \alpha(\sigma_x p_y - \sigma_y p_x),$$

(1.9)

where $\alpha(= \hbar\nabla V/4m^2c^2)$ is the RSOI constant. There has been a lot of discussion on the strength of RSOI constant in the literature [117]. Ando et al. [118] have argued that RSOI strength must be very small,

because for a bound state, Ehrenfest's theorem says $\langle E_z \rangle = 0$. Lassing [119] in 1985 has proved using the $k.p$ method that the major contribution to RSOI of a conduction electron comes from the electric field in the valence band. Thus the RSOI term ($\sim 0.1 - 10 meV$) has an extra contribution from the core electrons in addition to the Thomas term ($\sim 5 \times 10^{-9} - 5 \times 10^{-5} meV$) that exists in the Dirac equation.

1.6.2 Dresselhaus spin-orbit interaction

This is the other zero-field SOI observed in $III - V$ heterostructures which arises due to bulk inversion asymmetry (BIA). Diamond structure has inversion symmetry with inversion symmetry point as there will be two different atoms across every bond and inversion point chosen at the mid-point joining any two carbon atoms [120]. But $GaAs$ and $AlGaAs$ allow no such operation to bring atom on another type at every lattice point. An electrostatic potential will develop in the QD due to this inversion asymmetry in a given direction in the crystal. For the [100] crystal direction, the Dresselhaus spin-orbit interaction (DSOI) Hamiltonian is given by [121,122]
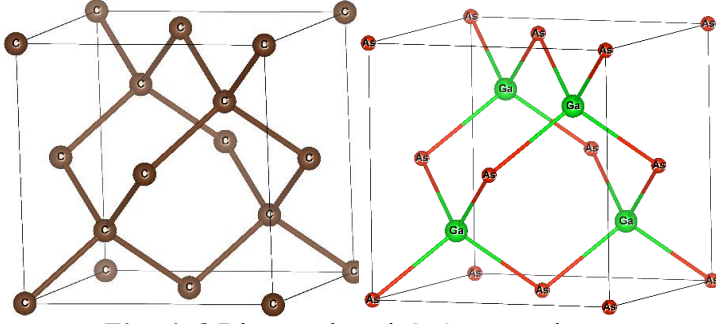
Fig. 1.6 Diamond and *GaAs* crystal structures.

$$H_D = \gamma \left(\{ \sigma_x k_x, k_y^2 - k_z^2 \} + \{ \sigma_y k_y, k_z^2 - k_x^2 \} \right.$$
$$\left. + \{ \sigma_z k_z, k_x^2 - k_y^2 \} \right) \tag{1.10}$$

Since the quantum well is confined along the z−direction, $\langle k_z \rangle = 0$ and $\langle k_z^2 \rangle \approx Const.$ So the above equation becomes [123]

$$H_D = -\gamma k_z^2 (\sigma_x k_x - \sigma_y k_y) + H_D^{Cubic}$$
$$= \beta (\sigma_x k_x - \sigma_y k_y) \tag{1.11}$$

where $\beta(= -\gamma k_z^2)$ is the DSOI constant. From the final expressions of H_R and H_D, one can see that the two terms transform into each other under the spin rotation operation given by [124]: $\sigma_x \leftrightarrow \sigma_y$, $\sigma_z \leftrightarrow -\sigma_z$. The QD
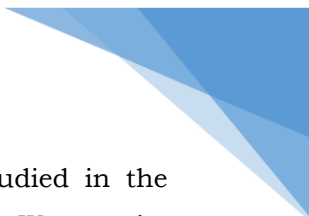
Hamiltonian with either RSOI or DSOI cannot be solved exactly analytically. Therefore one has to resort to some approximate technique [125–127] to deal with them. In the presence of external magnetic field, the momentum of the electron transforms [108] from $\boldsymbol{p}$ to $(\boldsymbol{p} + e\boldsymbol{A}/c)$ where $\boldsymbol{A}$ is the magnetic vector potential as already mentioned above.

The electronic, magnetic and thermodynamic properties of interacting electrons in PQDs with RSOI and DSOI in a perpendicular magnetic field constitute the main subject-matter of study in this thesis.

1.7 Overview of the Thesis

In the chapter immediately following, the ground state properties of a PQD with RSOI and e-e interaction in a perpendicular magnetic field is studied. The effect of RSOI and e-e interaction on chemical potential is also investigated. Then in the next chapter, we study the effect of RSOI, DSOI and e-e interaction on the energy spectrum, chemical potential, addition energy and spin-splitting energy of PQD.

In Chapter 4, the effect of RSOI, DSOI and the e-e interaction on the magnetization, susceptibility, heat

capacity and the entropy of a PQD is studied in the presence of a perpendicular magnetic field. We use the canonical ensemble approach to calculate the thermodynamic averages.
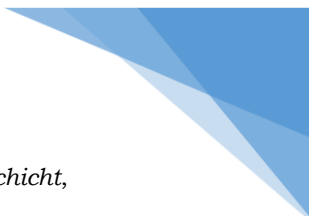
In Chapter 5, we report the results of our study on the effect of RSOI on the binding energy of a neutral hydrogenic donor [128] in a QD with Gaussian confinement [129]. We also present in this chapter our investigation on the effect of RSOI and DSOI on the tunneling conductance across a barrier separating a metal-semiconductor junction.

Finally in Chapter 6, we present our concluding remarks.

References:

1.   A. Blum, N. Mokrovski, A. Regel, *Seventh All-Union Conference on the Properties of Semiconductors (Kiev, USSR, 1950)*, Izv. Akad. Nauk SSSR Ser. Fiz. **16**, 139, (1952).

2.   N. Goryunova, A. Obukhov, *Studies on AIIIBV type (InSb, CdTe) compounds*, Seventh All-Union Conf. Prop. Semicond. (1950).

3.   H. Welker, *On new semiconducting compounds*, Zeitschrift Fur Naturforsch. **7**, 744, (1952).

4.   M.L. Huggins, *Evidence from Crystal Structures in Regard to Atomic Structures*, Phys. Rev. **27**, 286, (1926). doi:10.1103/PhysRev.27.286.

5.   V.M. Goldschmidt, *Crystal structure and chemical constitution*, Trans. Faraday Soc. **25**, 253, (1929). doi:10.1039/tf9292500253.

6.   A. Gubanov, *Theory of the contact between two semiconductors with different types of conduction*, Zh. Tekh. Fiz. **20**, 1287, (1950).

7.   W. Shockley, *Circuit element utilizing semiconductive material*, U.S. Pat. **2,569,347**, (1951). https://www.google.com/patents/US2569347.

8.   H. Kroemer, *Theory of a Wide-Gap Emitter for Transistors*, Proc. IRE. **45**, 1535, (1957). doi:10.1109/JRPROC.1957.278348.

9.   R.L. Anderson, *Germanium-Gallium Arsenide Heterojunctions [Letter to the Editor]*, IBM J. Res. Dev. **4**, 283, (1960). doi:10.1147/rd.43.0283.

10.   G. Margaritondo, ed., *Electronic Structure of Semiconductor Heterojunctions*, Springer Netherlands, Dordrecht, (1988). doi:10.1007/978-94-009-3073-5.

11.   N.F. Mott, *Note on the contact between a metal and an insulator or semi-conductor*, Math. Proc. Cambridge Philos. Soc. **34**, 568, (2008). doi:10.1017/S0305004100020570.
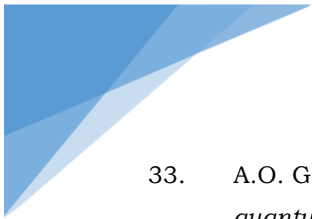
12. W. Schottky, *Halbleitertheorie der Sperrschicht*, Naturwissenschaften. **26**, 843, (1938). doi:10.1007/BF01774216.

13. B. L. Sharma, *Metal-Semiconductor Schottky Barrier Junctions and Their Applications*, Plenum Press, , (1984).

14. J.H. Davies, *The Physics of Low-dimensional Semiconductors: An Introduction*, Cambridge University Press, , (1998).

15. M. Razeghi, *Fundamentals of Solid State Engineering*, 3rd ed., Springer Science & Business Media, , (2009). doi:10.1007/978-0-387-92168-6.

16. S.M. Sze, K.K. Ng, *Physics of Semiconductor Devices*, John Wiley & Sons, Inc., , (2006).

17. Y. Murayama, *Mesoscopic Systems: Fundamentals and Applications*, John Wiley & Sons, , (2008).

18. N. Van Kampen, The expansion of the master equation, in: S.A.R. Ilya Prigogine (Ed.), Adv. Chem. Phys., : pp. 254–309.

19. D.J. Thouless, *Maximum Metallic Resistance in Thin Wires*, Phys. Rev. Lett. **39**, 1167, (1977). doi:10.1103/PhysRevLett.39.1167.

20. M. Azbel, Theory of Fluctuation Phenomena in Kinetics, in: M. Cardona P. Fulde H.-J. Queisser (Ed.),

Localization, Interact. Transp. Phenom., Springer Berlin Heidelberg, : pp. 162–168.

21.   B. Altshuler, D. Khmelnitskii, *Fluctuation properties of small conductors*, Jetp Lett. **42**, 359, (1985). http://www.jetpletters.ac.ru/ps/1435/article_21832.pdf.

22.   B.L. Al'tshuler, P.A. Lee, *Disordered Electronic Systems*, Phys. Today. **41**, 36, (1988). doi:10.1063/1.881139.

23.   Y. Arakawa, *Multidimensional quantum well laser and temperature dependence of its threshold current*, Appl. Phys. Lett. **40**, 939, (1982). doi:10.1063/1.92959.

24.   W.T. Tsang, Quantum confinement heterostructure semiconductor lasers, in: Appl. Multiquantum Wells, Sel. Doping, Superlattices, Elsevier, : pp. 397–458. doi:10.1016/S0080-8784(08)62454-0.

25.   P. Harrison, *Quantum Wells, Wires and Dots: Theoretical and Computational Physics of Semiconductor Nanostructures*, John Wiley & Sons, , (2011).

26.   A.I. Ekimov, A.A. Onushchenko, *Quantum size effect in three-dimensional microscopic semiconductor crystals*, J. Exp. Theor. Phys. Lett. **34**, 345, (1981). http://www.jetpletters.ac.ru/ps/1517/article_23187.pdf.

27. A.L. Efros, A.L. Efros, *Interband Light Absorption in Semiconductor Spheres*, Sov. Physics. Semicond. **16**, 772, (1982).

28. L.E. Brus, *A simple model for the ionization potential, electron affinity, and aqueous redox potentials of small semiconductor crystallites*, J. Chem. Phys. **79**, 5566, (1983). doi:10.1063/1.445676.

29. G.W. Bryant, *Electronic structure of ultrasmall quantum-well boxes*, Phys. Rev. Lett. **59**, 1140, (1987). doi:10.1103/PhysRevLett.59.1140.

30. J. Cibert, P.M. Petroff, G.J. Dolan, S.J. Pearton, A.C. Gossard, J.H. English, *Optically detected carrier confinement to one and zero dimension in GaAs quantum well wires and boxes*, Appl. Phys. Lett. **49**, 1275, (1986). doi:10.1063/1.97384.

31. S.J. Allen, H.L. Störmer, J.C.M. Hwang, *Dimensional resonance of the two-dimensional electron gas in selectively doped GaAs/AlGaAs heterostructures*, Phys. Rev. B. **28**, 4875, (1983). doi:10.1103/PhysRevB.28.4875.

32. M.A. Reed, R.T. Bate, K. Bradshaw, W.M. Duncan, W.R. Frensley, J.W. Lee, H.D. Shih, *Spatial quantization in GaAs–AlGaAs multiple quantum dots*, J. Vac. Sci. Technol. B. **4**, 358, (1986). doi:10.1116/1.583331.
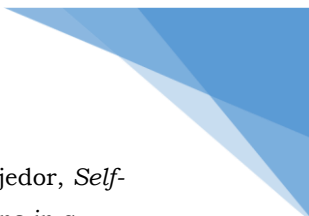
33.   A.O. Govorov, A. V. Chaplik, *Magnetoabsorption at quantum points*, J. Exp. Theor. Phys. Lett. **52**, 681, (1990). http://medvetande.dk/Quantum_point_absorbation.pdf.

34.   A.D. Yoffe, *Low-dimensional systems: quantum size effects and electronic properties of semiconductor microcrystallites (zero-dimensional systems) and some quasi-two-dimensional systems*, Adv. Phys. **42**, 173, (1993). doi:10.1080/00018739300101484.

35.   M. Reed, J. Randall, R. Aggarwal, R. Matyi, T. Moore, A. Wetsel, *Observation of discrete electronic states in a zero-dimensional semiconductor nanostructure*, Phys. Rev. Lett. **60**, 535, (1988). doi:10.1103/PhysRevLett.60.535.

36.   P. McEuen, E. Foxman, U. Meirav, M. Kastner, Y. Meir, N. Wingreen, S. Wind, *Transport spectroscopy of a Coulomb island in the quantum Hall regime.*, Phys. Rev. Lett. **66**, 1926, (1991). doi:10.1103/PhysRevLett.66.1926.

37.   K. Karrai, H.D. Drew, M.W. Lee, M. Shayegan, *Magnetoplasma effects in a quasi-three-dimensional electron gas*, Phys. Rev. B. **39**, 1426, (1989). doi:10.1103/PhysRevB.39.1426.

38.   C. Sikorski, U. Merkt, *Spectroscopy of electronic states in InSb quantum dots.*, Phys. Rev. Lett. **62**, 2164,
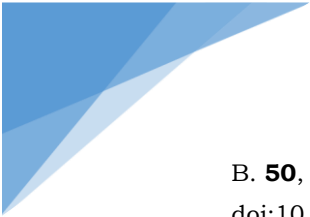
(1989). doi:10.1103/PhysRevLett.62.2164.

39.   W. Hansen, T. Smith, K. Lee, J. Brum, C. Knoedler, J. Hong, D. Kern, *Zeeman bifurcation of quantum-dot spectra.*, Phys. Rev. Lett. **62**, 2168, (1989). doi:10.1103/PhysRevLett.62.2168.

40.   R. Ashoori, H. Stormer, J. Weiner, L. Pfeiffer, K. Baldwin, K. West, *N-electron ground state energies of a quantum dot in magnetic field.*, Phys. Rev. Lett. **71**, 613, (1993). doi:10.1103/PhysRevLett.71.613.

41.   P. Bakshi, D.A. Broido, K. Kempa, *Electromagnetic response of quantum dots*, Phys. Rev. B. **42**, 7416, (1990). doi:10.1103/PhysRevB.42.7416.

42.   F.M. Peeters, *Magneto-optics in parabolic quantum dots*, Phys. Rev. B. **42**, 1486, (1990). doi:10.1103/PhysRevB.42.1486.

43.   Q.P. Li, K. Karraï, S.K. Yip, S. Das Sarma, H.D. Drew, *Electrodynamic response of a harmonic atom in an external magnetic field*, Phys. Rev. B. **43**, 5151, (1991). doi:10.1103/PhysRevB.43.5151.

44.   R.W. Haase, N.F. Johnson, *Optical absorption and addition spectra of an N -electron quantum dot: An algebraic Hamiltonian approach*, Phys. Rev. B. **49**, 14409, (1994). doi:10.1103/PhysRevB.49.14409.

45.   D. Pfannkuche, R.R. Gerhardts, *Quantum-dot helium: Effects of deviations from a parabolic confinement*

potential, Phys. Rev. B. **44**, 13132, (1991). doi:10.1103/PhysRevB.44.13132.

46. V. Fock, *Bemerkung zur Quantelung des harmonischen Oszillators im Magnetfeld*, Zeitschrift F�r Phys. **47**, 446, (1928). doi:10.1007/BF01390750.

47. C.G. Darwin, *The Diamagnetism of the Free Electron*, Math. Proc. Cambridge Philos. Soc. **27**, 86, (2008). doi:10.1017/S0305004100009373.

48. L. Jacak, P. Hawrylak, A. Wojs, *Quantum Dots*, Springer, , (1998).

49. M.A. Kastner, *Artificial Atoms*, Phys. Today. **46**, 24, (1993). doi:10.1063/1.881393.

50. P. a. Maksym, T. Chakraborty, *Quantum dots in a magnetic field: Role of electron-electron interactions*, Phys. Rev. Lett. **65**, 108, (1990). doi:10.1103/PhysRevLett.65.108.

51. C.W.J. Beenakker, *Theory of Coulomb-blockade oscillations in the conductance of a quantum dot*, Phys. Rev. B. **44**, 1646, (1991). doi:10.1103/PhysRevB.44.1646.

52. S. Tarucha, D. Austing, T. Honda, van der Hage RJ, L. Kouwenhoven, *Shell Filling and Spin Effects in a Few Electron Quantum Dot.*, Phys. Rev. Lett. **77**, 3613, (1996). doi:10.1103/PhysRevLett.77.3613.
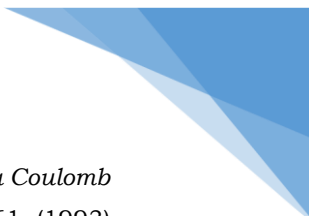
53.   J.H. Oaknin, J.J. Palacios, L. Brey, C. Tejedor, *Self-consistent Hartree description of N electrons in a quantum dot with a magnetic field*, Phys. Rev. B. **49**, 5718, (1994). doi:10.1103/PhysRevB.49.5718.

54.   N.F. Johnson, M. Reina, *The accuracy of the Hartree-Fock approximation for quantum dots*, J. Phys. Condens. Matter. **4**, L623, (1992). doi:10.1088/0953-8984/4/47/003.

55.   B. Reusch, H. Grabert, *Unrestricted Hartree-Fock for quantum dots*, Phys. Rev. B. **68**, 045309, (2003). doi:10.1103/PhysRevB.68.045309.

56.   A. Emperador, E. Lipparini, L. Serra, *Brueckner-Hartree-Fock study of circular quantum dots*, Phys. Rev. B. **73**, 235341, (2006). doi:10.1103/PhysRevB.73.235341.

57.   F. Bolton, *Fixed-phase quantum Monte Carlo method applied to interacting electrons in a quantum dot*, Phys. Rev. B. **54**, 4780, (1996). doi:10.1103/PhysRevB.54.4780.

58.   A. Harju, V.A. Sverdlov, R.M. Nieminen, V. Halonen, *Many-body wave function for a quantum dot in a weak magnetic field*, Phys. Rev. B. **59**, 5622, (1999). doi:10.1103/PhysRevB.59.5622.

59.   M. Ferconi, G. Vignale, *Current-density-functional theory of quantum dots in a magnetic field*, Phys. Rev.
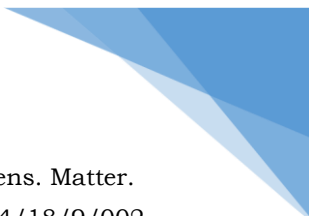
B. **50**, 14722, (1994).
doi:10.1103/PhysRevB.50.14722.

60. E. Lipparini, N. Barberán, M. Barranco, M. Pi, L. Serra,
Far-infrared edge modes in quantum dots, Phys. Rev. B.
56, 12375, (1997). doi:10.1103/PhysRevB.56.12375.

61. M. Koskinen, M. Manninen, S.M. Reimann, *Hund's
Rules and Spin Density Waves in Quantum Dots*, Phys.
Rev. Lett. **79**, 1389, (1997).
doi:10.1103/PhysRevLett.79.1389.

62. G. Cipriani, M. Rosa-Clot, S. Taddei, *Electronic-level
calculations for semiconductor quantum dots:
Deterministic numerical method using Green's functions*,
Phys. Rev. B. **61**, 7536, (2000).
doi:10.1103/PhysRevB.61.7536.

63. V. Fessatidis, N.J. M.Horing, K. Sabeeh, *Retarded
Green's function for an electron in a parabolic quantum
dot subject to a constant uniform magnetic field and an
electric field of arbitrary time dependence and
orientation*, Philos. Mag. B. **79**, 77, (1999).
doi:10.1080/13642819908206783.

64. R.M.G. García-Castelán, W.S. Choe, Y.C. Lee,
*Correlation energies for two interacting electrons in a
harmonic quantum dot*, Phys. Rev. B. **57**, 9792, (1998).
doi:10.1103/PhysRevB.57.9792.

65. M. Taut, *Two electrons in an external oscillator*

potential: Particular analytic solutions of a Coulomb correlation problem, Phys. Rev. A. **48**, 3561, (1993). doi:10.1103/PhysRevA.48.3561.

66. S. Mukhopadhyay, A. Chatterjee, *Rayleigh-Schrödinger perturbation theory for electron-phonon interaction effects in polar semiconductor quantum dots with parabolic confinement*, Phys. Lett. A. **204**, 411, (1995). doi:10.1016/0375-9601(95)00530-G.

67. A. Harju, V.A. Sverdlov, B. Barbiellini, R.M. Nieminen, *Variational wave function for a two-electron quantum dot*, Phys. B Condens. Matter. **255**, 145, (1998). doi:10.1016/S0921-4526(98)00461-X.

68. Y.Z. Hu, S.W. Koch, M. Lindberg, N. Peyghambarian, *Theoretical and Experimental Results on Coulomb Effects in Semiconductor Quantum Dots*, Phys. Status Solidi. **159**, 249, (1990). doi:10.1002/pssb.2221590129.

69. R.J. Warburton, B.T. Miller, C.S. Dürr, C. Bödefeld, K. Karrai, J.P. Kotthaus, G. Medeiros-Ribeiro, P.M. Petroff, S. Huant, *Coulomb interactions in small charge-tunable quantum dots: A simple model*, Phys. Rev. B. **58**, 16221, (1998). doi:10.1103/PhysRevB.58.16221.

70. S. Yang, A. MacDonald, M. Johnson, *Addition spectra of quantum dots in strong magnetic fields.*, Phys. Rev. Lett. **71**, 3194, (1993). doi:10.1103/PhysRevLett.71.3194.

71. S. V. Nair, L.M. Ramaniah, K.C. Rustagi, *Electron states in a quantum dot in an effective-bond-orbital model*, Phys. Rev. B. **45**, 5969, (1992). doi:10.1103/PhysRevB.45.5969.

72. M.B. Tavernier, E. Anisimovas, F.M. Peeters, B. Szafran, J. Adamowski, S. Bednarek, *Four-electron quantum dot in a magnetic field*, Phys. Rev. B. **68**, 205305, (2003). doi:10.1103/PhysRevB.68.205305.

73. P.A. Maksym, T. Chakraborty, *Effect of electron-electron interactions on the magnetization of quantum dots*, Phys. Rev. B. **45**, 1947, (1992). doi:10.1103/PhysRevB.45.1947.

74. U. Merkt, J. Huser, M. Wagner, *Energy spectra of two electrons in a harmonic quantum dot*, Phys. Rev. B. **43**, 7320, (1991). doi:10.1103/PhysRevB.43.7320.

75. F. V Prudente, L.S. Costa, J.D.M. Vianna, *A study of two-electron quantum dot spectrum using discrete variable representation method.*, J. Chem. Phys. **123**, 224701, (2005). doi:10.1063/1.2131068.

76. O.M. Al-Dossary, *Ordering of Ground State Energy Levels of Two-Electron Quantum Dot in a Magnetic Field*, Int. J. Theor. Phys. **49**, 1187, (2010). doi:10.1007/s10773-010-0298-1.

77. O. Ciftja, M.G. Faruk, *Two interacting electrons in a one-dimensional parabolic quantum dot: exact*

numerical diagonalization, J. Phys. Condens. Matter. **18**, 2623, (2006). doi:10.1088/0953-8984/18/9/002.

78.   O. Ciftja, A.A. Kumar, *Ground state of two-dimensional quantum-dot helium in zero magnetic field: Perturbation, diagonalization, and variational theory*, Phys. Rev. B. **70**, 205326, (2004). doi:10.1103/PhysRevB.70.205326.

79.   R. Pino, V.M. Villalba, *Calculation of the energy spectrum of a two-electron spherical quantum dot*, J. Phys. Condens. Matter. **13**, 11651, (2001). doi:10.1088/0953-8984/13/50/324.

80.   R.G. Nazmitdinov, N.S. Simonović, J.M. Rost, *Semiclassical analysis of a two-electron quantum dot in a magnetic field: Dimensional phenomena*, Phys. Rev. B. **65**, 155307, (2002). doi:10.1103/PhysRevB.65.155307.

81.   E. Moreno, J. Rivas, *On electromagnetism in R 2+1*, Eur. J. Phys. **5**, 15, (1984). doi:10.1088/0143-0807/5/1/005.

82.   H. Haug, S.W. Koch, *Quantum Theory of the Optical and Electronic Properties of Semiconductors*, World Scientific, , (2004).

83.   R. Dick, *Advanced Quantum Mechanics: Materials and Photons*, Springer Science & Business Media, , (2012).

84.   A.V. Chaplik, *Possible Crystallization of Charge*

Carriers in Low-density Inversion Layers, Sov. Phys. JETP. **35**, 395, (1972). http://www.jetp.ac.ru/cgi-bin/dn/e_035_02_0395.pdf.

85. A. Kumar, S. Laux, F. Stern, *Electron states in a GaAs quantum dot in a magnetic field*, Phys. Rev. B. **42**, 5166, (1990). doi:10.1103/PhysRevB.42.5166.

86. P.L. McEuen, E.B. Foxman, J. Kinaret, U. Meirav, M.A. Kastner, N.S. Wingreen, S.J. Wind, *Self-consistent addition spectrum of a Coulomb island in the quantum Hall regime*, Phys. Rev. B. **45**, 11419, (1992). doi:10.1103/PhysRevB.45.11419.

87. M. Rontani, F. Rossi, F. Manghi, E. Molinari, *Coulomb correlation effects in semiconductor quantum dots: The role of dimensionality*, Phys. Rev. B. **59**, 10165, (1999). doi:10.1103/PhysRevB.59.10165.

88. L.C. Andreani, A. Pasquarello, *Accurate theory of excitons in GaAs- Ga 1 − x Al x As quantum wells*, Phys. Rev. B. **42**, 8928, (1990). doi:10.1103/PhysRevB.42.8928.

89. N.F. Johnson, M.C. Payne, *Exactly solvable model of interacting particles in a quantum dot*, Phys. Rev. Lett. **67**, 1157, (1991). doi:10.1103/PhysRevLett.67.1157.

90. R.B. Laughlin, *Quantized motion of three two-dimensional electrons in a strong magnetic field*, Phys. Rev. B. **27**, 3383, (1983).
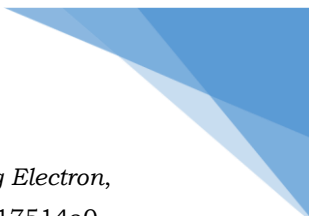
doi:10.1103/PhysRevB.27.3383.

91. S.M. Girvin, T. Jach, *Interacting electrons in two-dimensional Landau levels: Results for small clusters*, Phys. Rev. B. **28**, 4506, (1983). doi:10.1103/PhysRevB.28.4506.

92. J.M. Kinaret, Y. Meir, N.S. Wingreen, P.A. Lee, X.-G. Wen, *Many-body coherence effects in conduction through a quantum dot in the fractional quantum Hall regime*, Phys. Rev. B. **46**, 4681, (1992). doi:10.1103/PhysRevB.46.4681.

93. F. Calogero, *Solution of the One-Dimensional N-Body Problems with Quadratic and/or Inversely Quadratic Pair Potentials*, J. Math. Phys. **12**, 419, (1971). doi:10.1063/1.1665604.

94. F. Calogero, *Solution of a Three-Body Problem in One Dimension*, J. Math. Phys. **10**, 2191, (1969). doi:10.1063/1.1664820.

95. F. Calogero, *Ground State of a One-Dimensional N-Body System*, J. Math. Phys. **10**, 2197, (1969). doi:10.1063/1.1664821.

96. F. Calogero, *Exact solution of a one-dimensional three-body scattering problem with two-body and/or three-body inverse-square potentials*, J. Math. Phys. **15**, 1425, (1974). doi:10.1063/1.1666827.

97. N. Johnson, L. Quiroga, *Analytic results for N particles*

with 1/r2 interaction in two dimensions and an external magnetic field., Phys. Rev. Lett. **74**, 4277, (1995). doi:10.1103/PhysRevLett.74.4277.

98.   N.F. Johnson, *Quantum dots : few-body , low-dimensional systems*, J. Phys. Condens. Matter. **7**, 965, (1995).

99.   B.L. Johnson, G. Kirczenow, *Electrons in quantum dots: A comparison of interaction energies*, Phys. Rev. B. **47**, 10563, (1993). doi:10.1103/PhysRevB.47.10563.

100.   N.F. Johnson, *Quantum-dot excitation spectrum: Laughlin-like states*, Phys. Rev. B. **46**, 2636, (1992). doi:10.1103/PhysRevB.46.2636.

101.   B.A. Al-Riyami, *Carrier states in a quantum dot*, J. Phys. Condens. Matter. **7**, 4697, (1995). doi:10.1088/0953-8984/7/24/009.

102.   K.-H. Ahn, J.H. Oh, K.J. Chang, *Correlation effects in a quantum dot at high magnetic fields*, Phys. Rev. B. **52**, 13757, (1995). doi:10.1103/PhysRevB.52.13757.

103.   S. Goudsmit, G. Uhlenbeck, *Over Het Roteerende Electron En de Structuur der Spectra,* Physica. **6**, 273, (1926).

104.   S. Goudsmit, R. de L. Kronig, *Die Intensität der Zeemankomponenten*, Naturwissenschaften. **13**, 90, (1925). doi:10.1007/BF01558737.

105. L.H. THOMAS, *The Motion of the Spinning Electron*, Nature. **117**, 514, (1926). doi:10.1038/117514a0.

106. H. Kroemer, *The Thomas precession factor in spin–orbit interaction*, Am. J. Phys. **72**, 51, (2004). doi:10.1119/1.1615526.

107. J.D. Jackson, *Classical Electrodynamics*, John Wiley & Sons, Inc., , (1962).

108. H. Goldstein, *Classical Mechanics*, Addison-Wesley, , (1965).

109. R.D. Sard, *Relativistic mechanics: special relativity and classical particle dynamics*, W. A. Benjamin, , (1970).

110. G.P. Fisher, *The Thomas Precession*, Am. J. Phys. **40**, 1772, (1972). doi:10.1119/1.1987061.

111. J.A. Rhodes, M.D. Semon, *Relativistic velocity space, Wigner rotation, and Thomas precession*, Am. J. Phys. **72**, 943, (2004). doi:10.1119/1.1652040.

112. Schiff, *Quantum mechanics*, McGraw-Hill Education (India) Pvt Limited, , (1968).

113. A.M. Boring, J.L. Smith, The Quasi-Periodic Table and Anomalous Metallic Properties, in: J.P. Connerade, J.M. Esteva, R.C. Karnatak (Eds.), Giant Reson. Atoms, Mol. Solids, Springer US, : pp. 311–320. doi:10.1007/978-1-4899-2004-1_20.

114. E.I. Rashba, V.I. Sheka, *Symmetry of Energy Bands in*
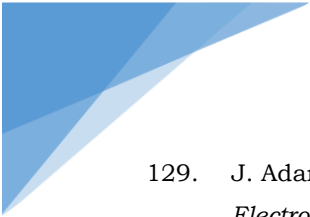
Crystals of Wurtzite Type II. Symmetry of Bands with Spin-Orbit Interaction Included, New. J. Phys. Phys.-Solid State. **17**, 50202, (2015).

115.   Y.A. Bychkov, E.I. Rashba, *Oscillatory effects and the magnetic susceptibility of carriers in inversion layers*, J. Phys. C Solid State Phys. **17**, 6039, (1984). doi:10.1088/0022-3719/17/33/015.

116.   G. Bihlmayer, O. Rader, R. Winkler, *Focus on the Rashba effect*, New J. Phys. **17**, 050202, (2015). doi:10.1088/1367-2630/17/5/050202.

117.   R. Winkler, *Spin-orbit Coupling Effects in Two-Dimensional Electron and Hole Systems*, Springer Science & Business Media, , (2003).

118.   A. Därr, J.P. Kotthaus, T. Ando, Electron-spin resonance in an inversion layer on InSb, in: Proc. 13 Th Int. Conf. Phys. Semicond. Semicond., : p. 774.

119.   R. Lassnig, $k\rightarrow \cdot p\rightarrow$ *theory, effective-mass approach, and spin splitting for two-dimensional electrons in GaAs-GaAlAs heterostructures*, Phys. Rev. B. **31**, 8076, (1985). doi:10.1103/PhysRevB.31.8076.

120.   B.B. Pate, *The diamond surface: atomic and electronic structure*, Surf. Sci. **165**, 83, (1986). doi:10.1016/0039-6028(86)90665-5.

121.   G. Dresselhaus, *Spin-Orbit Coupling Effects in Zinc Blende Structures*, Phys. Rev. **100**, 580, (1955).

doi:10.1103/PhysRev.100.580.

122. S. Bandyopadhyay, M. Cahay, *Introduction to Spintronics*, CRC Press, , (2008).

123. R.H. Eric, S.J. Yong, *Spintronics in Nanoscale Devices*, CRC Press, , (2013).

124. E. Tsitsishvili, G.S. Lozano, A.O. Gogolin, *Rashba coupling in quantum dots: An exact solution*, Phys. Rev. B. **70**, 115316, (2004). doi:10.1103/PhysRevB.70.115316.

125. I.L. Aleiner, V.I. Fal'ko, *Spin-orbit coupling effects on quantum transport in lateral semiconductor dots.*, Phys. Rev. Lett. **87**, 256801, (2001). doi:10.1103/PhysRevLett.87.256801.

126. P. Tonello, E. Lipparini, *Spin-orbit splitting of the cyclotron resonance in GaAs*, Phys. Rev. B. **70**, 1, (2004). doi:10.1103/PhysRevB.70.081201.

127. M. Valín-Rodríguez, A. Puente, L. Serra, *Spin splitting and precession in quantum dots with spin-orbit coupling: The role of spatial deformation*, Phys. Rev. B. **69**, 085306, (2004). doi:10.1103/PhysRevB.69.085306.

128. J.-L. Zhu, *Exact solutions for hydrogenic donor states in a spherically rectangular quantum well*, Phys. Rev. B. **39**, 8780, (1989). doi:10.1103/PhysRevB.39.8780.

129.   J. Adamowski, M. Sobkowicz, B. Szafran, S. Bednarek, *Electron pair in a Gaussian confining potential*, Phys. Rev. B. **62**, 4234, (2000). doi:10.1103/PhysRevB.62.4234.

Chapter 2. Ground state properties of parabolic quantum dot with Rashba spin-orbit interaction in a magnetic field

2

2.1 Introduction

The study of spin-orbit interaction (SOI) in zero-dimensional (0D) structures started long back in 1986 by Brus et al. [1,2] and the effect of Rashba spin-orbit interaction (RSOI) has been studied in parabolic quantum dot (PQD) with interacting electrons in a magnetic field was first studied by Darnhofer et al. [3] in 1993 using the $k \cdot p$ method. Later several numerical, analytical, exact and semi-exact methods have been proposed [4–9] to solve the Hamiltonian of PQD with RSOI and electron-electron (e-e) interaction. The study of RSOI has more practical applications [10,11] as its strength can be controlled very easily by using an external electrostatic field [12]. The dipole transition energy or the resonance tunneling energy [13–17] also has much practical importance and has therefore received a lot of theoretical attention and led to the proposal of generalized Kohn's theorem [18–21]. In the

present chapter we study the effect of RSOI on the ground state energy of one-electron and few-electron quantum dots (QDs) and also on the resonance tunneling energy of the QD. For our numerical investigations, we consider a *GaAs* QD which has a small value of g^*, i.e., $g^* = -0.44$. Because of small value of g^*, the spin Zeeman effects are negligible in a GaAs QD, and hence SOI effects can be observed more clearly.

2.2 The Hamiltonian

We consider a system of N electrons in a QD developed on a heterojunction, grown along the *z*-direction and confined by a lateral isotropic parabolic potential in the x-y plane, with an applied perpendicular magnetic field along the growth direction. The Hamiltonian for such a system with e-e interaction and RSOI can be written as

$$H = \sum_{i=1}^{N} \left(\frac{1}{2m^*} \left(\boldsymbol{p}_i + \frac{e\boldsymbol{A}_i}{c} \right)^2 + \frac{1}{2} m^* \omega_o^2 |\boldsymbol{r}_i|^2 \right.$$

$$\left. + \frac{1}{2} g^* \mu_B B \sigma_{i,z} \right) \qquad (2.1)$$

$$+ \frac{\alpha}{\hbar} \sum_i \left[\left(p_{i,y} + \frac{e}{c} A_{i,y} \right) \sigma_{i,x} \right.$$

$$\left. - \left(p_{i,x} + \frac{e}{c} A_{i,x} \right) \sigma_{i,y} \right]$$

$$+ \sum_{i<j} 2V_o - \frac{1}{2} m^* \Omega^2 |\boldsymbol{r}_i - \boldsymbol{r}_j|^2$$

where i refers to the $i-$th electron with the spatial coordinate $\boldsymbol{r}_i$, momentum $\boldsymbol{p}_i$, effective mass m^* and effective g factor g^*. $\boldsymbol{A}_i$ is the vector potential for the $i-$th electron, α is the RSOI coupling constant and $\boldsymbol{\sigma}$'s are the Pauli spin matrices.

2.3 Analytical solution

To proceed further we choose for the vector potential $\boldsymbol{A}$ the symmetric gauge, i.e., we take $\boldsymbol{A}_i = \widehat{\boldsymbol{A}} B(-y_i/2 , x_i/2 , 0)$, so that the total Hamiltonian becomes

$$H = \sum_i \left[\frac{\boldsymbol{p}_i^2}{2m^*} + \frac{1}{2} m^* \omega_o^2(B) |\boldsymbol{r}_i|^2 + \frac{\omega_c}{2} L_{i,z} \right.$$

$$+ \frac{1}{2} g^* \mu_B B \sigma_{i,z} + i\alpha (\sigma_{i,x} p_{i,y} - \sigma_{i,y} p_{i,x})$$

$$\left. + \frac{\alpha m^* \omega_c}{2\hbar} (x_i \sigma_{i,x} + y_i \sigma_{i,y}) \right]$$

$$+ \sum_{i<j} \left(2V_o - \frac{1}{2} m^* \Omega^2 |\boldsymbol{r}_i - \boldsymbol{r}_j|^2 \right), \qquad (2.2)$$

where $\omega_o^2(B) = [\omega_o^2 + \omega_c^2/4]$, $\omega_c = [eB/m^* c]$ and $L_{i,z}(= [x_i p_{i,y} - y_i p_{i,x}])$ is the z component of the angular momentum of the ith particle. We now perform a unitary transformation [8] on H by the operator: $U = \exp[i(\alpha m^*/\hbar^2) \sum_i (y_i \sigma_{i,x} - x_i \sigma_{i,y})]$ and expand the transformed Hamiltonian in powers of α (assuming $H_o \gg H_R \gg H_z$) to obtain $\tilde{H} (= e^U H e^{-U})$ as

$$\tilde{H} = \sum_i \left[\frac{\boldsymbol{p}_i^2}{2m^*} + \frac{1}{2} m^* \tilde{\omega}_o^2(B) |\boldsymbol{r}_i|^2 + \frac{\tilde{\omega}_c}{2} L_{i,z} \right.$$

$$\left. + \frac{1}{2} g^* \mu_B B \sigma_{i,z} - \frac{\alpha^2 m^*}{\hbar^2} + \mathcal{O}(\alpha^3) \right]$$

$$+ \sum_{i<j} \left(2V_o - \frac{1}{2} m^* \Omega^2 |\boldsymbol{r}_i - \boldsymbol{r}_j|^2 \right),$$

$$(2.3)$$

where $\widetilde{\omega}_o^2(B) = [\omega_o^2(B) - (\alpha^2 m^*/\hbar^3)\omega_c\sigma_z]$, $\widetilde{\omega}_c = [\omega_c - (\alpha^2 m^*/\hbar^3)\sigma_z]$. Since $\widetilde{H}$ is independent of SOI, it can be separated into space part and spin part as [22]: $\widetilde{H} = H_{space} + H_{spin}$, with

$$H_{space} = \sum_i \left[\frac{p_i^2}{2m^*} + \frac{m^*}{2}\widetilde{\omega}_o^2(B)|r_i|^2 + \frac{\widetilde{\omega}_c}{2}L_{i,z} - \frac{m^*}{\hbar^2}\alpha^2 \right]$$

$$+ \sum_{i<j}\left(2V_o - \frac{1}{2}m^*\Omega^2|r_i - r_j|^2 \right); \qquad (2.4)$$

$$H_{spin} = \sum_i \frac{1}{2}g^*\mu_B B\sigma_{i,z} . \qquad (2.5)$$

H_{space} can be further separated into center of mass coordinates and relative coordinates (H_{cm} and H_{rel} respectively) using the transformations [22]

$$\mathbf{R} = (X, Y) = \sum_i \frac{r_i}{N}, \qquad \mathbf{P} = (P_X, P_Y) = \sum_i \mathbf{p}_i;$$

$$\mathbf{r}_{ij} = (x_{ij}, y_{ij}) = (r_i - r_j),$$

$$\mathbf{p}_{ij} = (p_{ij,x}, p_{ij,y}) = (\mathbf{p}_i - \mathbf{p}_j). \qquad (2.6)$$

One can introduce the corresponding raising and lowering operators for center-of-mass mode and the relative mode as follows:

$$A^{\pm} = F(B)[Nm^*\widetilde{\omega}_0(B)(X \mp iY) \mp i(P_X \mp P_Y)],$$

$$B^{\pm} = F(B)[Nm^*\widetilde{\omega}_0(B)(X \pm iY) \mp i(P_X \pm P_Y)],$$

$$F = 1/\sqrt{4Nm^*\hbar\widetilde{\omega}_0(B)}; \tag{2.7}$$

$$a_{ij}^{\pm} = G[m^*\Omega_o(x_{ij} \mp iy_{ij}) \mp i(p_{ij,x} \mp p_{ij,y})];$$

$$b_{ij}^{\pm} = G[m^*\Omega_o(x_{ij} \pm iy_{ij}) \mp i(p_{ij,x} \pm p_{ij,y})],$$

$$G = 1/\sqrt{4m^*\hbar\Omega_o}, \tag{2.8}$$

with $\Omega_o{}^2 = [\widetilde{\omega}_o^2(B) - N\Omega^2]$, $[A^-, A^+] = 1$, $[A^{\pm}, a_{ij}^{\pm}] = [A^{\pm}, B^{\pm}] = 0$, $[a_{ij}^-, a_{kl}^+] = [b_{ij}^-, b_{kl}^+] = c_{ijkl}$, where $c_{ijkl} = 2$ if $i = k$ and $j = l$; $c_{ijkl} = -2$ if $i = l$ and $j = k$; $c_{ijkl} = 1$ if $i = k$ and $j \neq l$; $c_{ijkl} = -1$ if $i = l$ and $j \neq k$ and $c_{ijkl} = 0$ if $i \neq k, l$ and $j \neq l, k$.

Then H_{cm} and H_{rel} are given by

$$H_{cm} = (\hbar\widetilde{\omega}_0(B) - \frac{1}{2}\hbar\widetilde{\omega}_c)A^+A^- + (\hbar\widetilde{\omega}_0(B)$$

$$+ \frac{1}{2}\hbar\widetilde{\omega}_c)B^+B^- + \hbar\widetilde{\omega}_0(B), \tag{2.9}$$

$$H_{rel} = \frac{1}{2N}[(2\hbar\Omega_o - \hbar\widetilde{\omega}_c)\sum_{i<j}a_{ij}^+ a_{ij}^- + (2\hbar\Omega_o +$$
$$\hbar\widetilde{\omega}_c)\sum_{i<j}b_{ij}^+ b_{ij}^-] + (N-1)[\hbar\Omega_o + NV_o] - \qquad (2.10)$$
$$\frac{Nm^*}{\hbar^2}\alpha^2.$$

The ground state energy of the system can be obtained in the limit of large magnetic field as

$$E = \hbar[\widetilde{\omega}_0(B) + \frac{N-1}{4}\{2(N+2)\Omega_o - N\widetilde{\omega}_c + 4NV_o\}$$
$$- \frac{m^*}{4m_o}g^*\omega_c] - \frac{Nm^*}{\hbar^2}\alpha^2 \qquad (2.11)$$

with $\Omega_o{}^2 = [\widetilde{\omega}_o^2(B) - N\Omega^2]$. In the absence of e-e interaction [16,22], we have

$$E = \frac{\hbar}{4}[2N(N+1))\widetilde{\omega}_0(B) - N(N-1)\widetilde{\omega}_c - \frac{m^*}{m_o}g^*\omega_c]$$
$$- \frac{Nm^*}{\hbar^2}\alpha^2 \qquad (2.12)$$

2.4 Numerical results and discussion

In our numerical investigations, we have considered a GaAs QD with parameters $m^*/m_0 = 0.063$, $\varepsilon = 12.9$,

$g^* = -0.44$, parabolic confinement strength $\omega_0 = 7.5\ meV$ and RSOI constant equal to $20\ meV.nm$. In Fig. 2.1, we plot the total ground state (GS) energy of a one-electron system as a function of the applied magnetic field B with and without the RSOI. One can see that the RSOI reduces the energy of the system. We have shown the exact numerical results of Pietilainen et. al.[23] for the sake of comparison. In the absence of SOI, the problem can of course be solved exactly and hence our results are in complete agreement with the numerical results of Pietilainen et. al. [23].
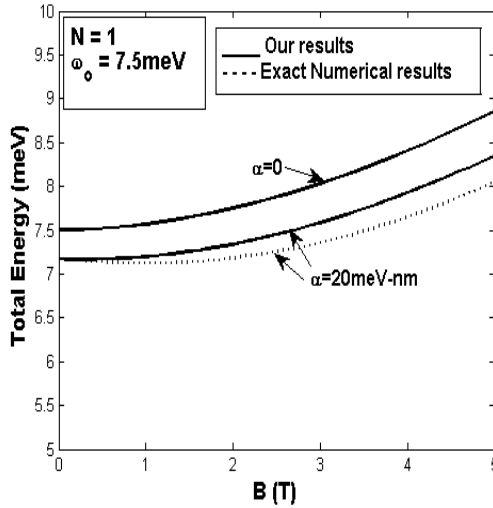
Fig: 2.1 Total GS energy vs B for $N = 1$ with and without RSOI

In the presence of SOI, the total GS energy estimated by our method turns out to be a little larger than the exact numerical result. Also the disagreement becomes more with higher magnetic fields. This is probably because of our neglecting the higher order terms in α in our calculation.

The variation of the GS energy of a two-electron system as a function of the applied magnetic field is shown in Fig. 2.2 (a). As the number of electrons in the system becomes more than one, the e-e interaction comes into play. Following Johnson and Payne [22], we have used the parabolic interaction as the model for the e-e interaction which contains two parameters V_0 and Ω, whose values have been fixed by fitting our GS energy vs. magnetic field curve with the exact numerical result of Pietilainen et al. [23] in the absence of RSOI (i. e., for $\alpha = 0$). For $N = 2$, and $\omega_0 = 7.5\ meV$, fairly exact agreement is obtained between our results and the exact numerical results of Pietilainen et al. [23] with $V_0 = 6.4\ meV$ and $\Omega = 5.1 meV$ in the magnetic field range of $2\ T$ to $5\ T$. We have therefore performed our calculation for the two-electron system in the presence of RSOI in the range $2T$ to $5T$ with the above values of V_0 and Ω so that we can compare our results with those of Pietilainen et al. [23] for non-zero α.

Fig. 2.2 (a) Total GS energy vs B (b) Energy difference $\Delta E = [E_{V_{ee} \neq 0} - E_{V_{ee}=0}]$ vs. B for $N = 2$ with and without RSOI.

One can notice from the figure that in the presence of SOI, though at a low magnetic field, our energy results are slightly lower than the exact numerical results of Pietilainen et al. [23], there is an excellent agreement at higher magnetic fields. Inclusion of higher-order terms in α is expected to improve the results even at low B. The difference between the energy with e-e interaction and that without e-e interaction, i. e., $\Delta E = [E_{V_{ee} \neq 0} - E_{V_{ee}=0}]$, which may be referred to the effective Coulomb correlation energy, is plotted as a function of the magnetic field B in Fig. 2.2 (b). It may be observed that the effective Coulomb interaction energy ΔE (= $[E_{V_{ee} \neq 0} - E_{V_{ee}=0}]$) increases more or less linearly with B. The increase in the e-e interaction energy with the magnetic field is an expected behaviour, because the magnetic field reduces the effective e-e separation which in turn increases the e-e interaction energy.

The variation of the total GS energy with B for a three-electron system is shown in Fig. 2.3(a) for $\alpha = 0$ and $\alpha = 20\ meV$- nm. The corresponding e-e interaction energy ($\Delta E = [E_{V_{ee} \neq 0} - E_{V_{ee}=0}]$) is shown in Fig. 2.3(b). The values of V_0 and Ω have been chosen in this case to be 5.13 meV and 4.01meV as obtained by fitting the $N = 3$ Johnson-Payne results with the corresponding

Fig. 2.3 (a) Total GS energy vs B (b) Energy difference $\Delta E = [E_{V_{ee} \neq 0} - E_{V_{ee}=0}]$ vs. B for $N = 3$ with and without RSOI.

results of Pietilainen et al. [23] for $\alpha = 0$ in the range, $B = 1\,T$ - $4\,T$. It is clearly evident that our results are in very good agreement with the exact numerical results of Pietilainen et al. [23]. Similar results are presented for a four-electron system in Fig. 2.4 (a) and 2.4 (b). Again the agreement is found to be fairly good. Comparison of Figs. 2.2(b), 2.3(b) and 2.4(b) shows that the variation of the effective Coulomb interaction energy ΔE as a function of B in the presence of RSOI is qualitatively similar to that in the absence of it. Also, in both cases, the curves ($\alpha = 0$ and $\alpha \neq 0$) are essentially linear and parallel to each other throughout the range of the applied magnetic field. Thus the effects of the e-e interaction and the RSOI seem to be independent of each other.

The variation of the GS energy of the system with RSOI constant α is presented in Fig. 2.5 for $N = 1,2,3$ and 4. The curves show that as a function of α, the GS energy decreases in a nonlinear way and the dependence is slightly more complex than just being quadratic. In fact, one can observe that the energy decreases with increasing α much faster if the electron number is larger and also at larger values of α.
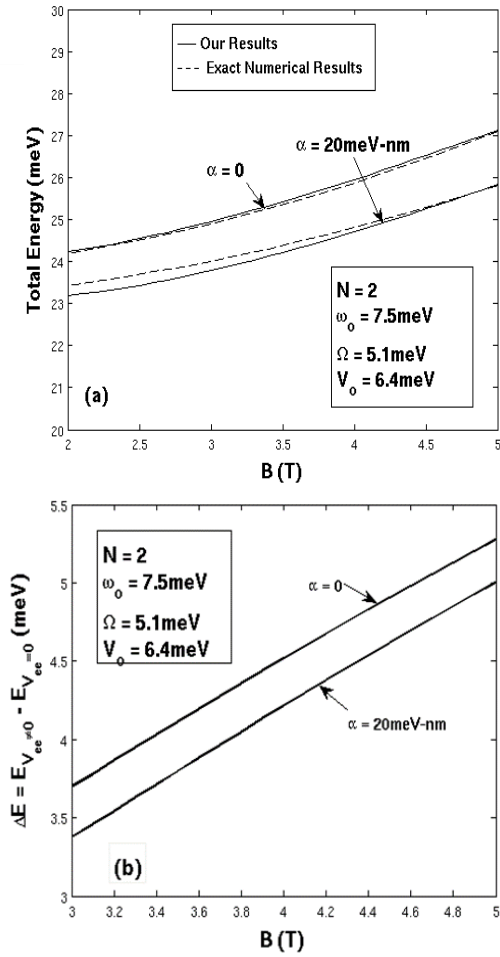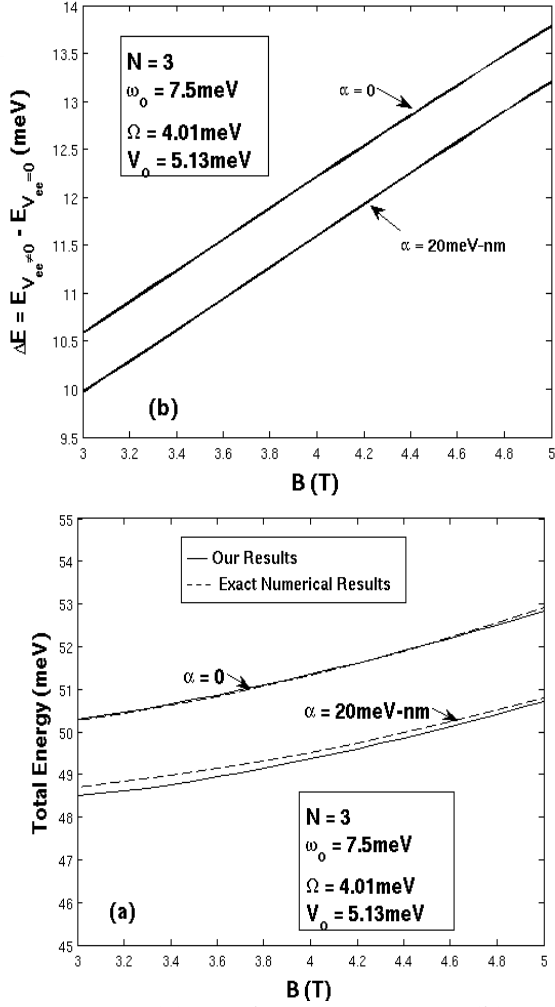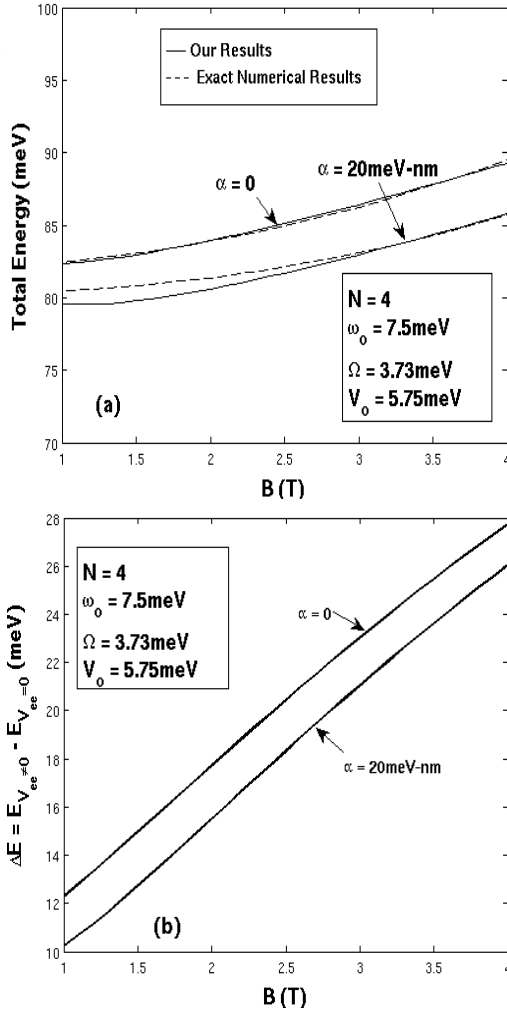
Fig. 2.4 (a) Total GS energy vs B (b) Energy difference $\Delta E = [E_{V_{ee} \neq 0} - E_{V_{ee}=0}]$ vs. B for $N = 4$ with and without RSOI.
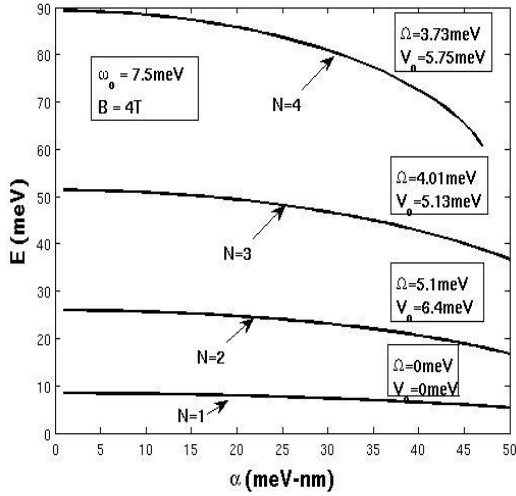
Fig. 2.5 GS energy as a function of SOI constant.
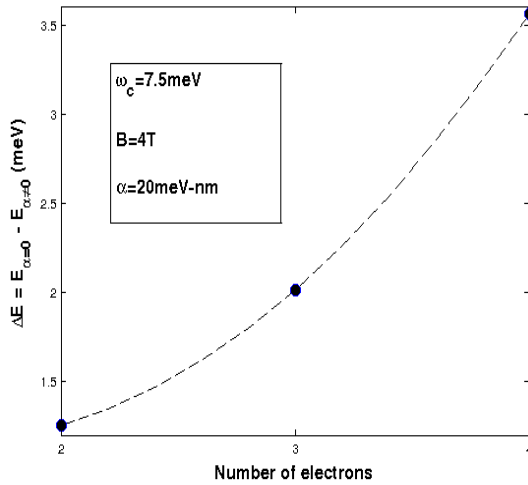
Fig. 2.6 SOI-dependent energy vs N for $\alpha = 20 meV \cdot nm$

The figure also shows, as expected, that the energy increases with the increase in the number of electrons but interestingly the dependence of the energy on N is also nonlinear. The explicit dependence of RSOI contribution to the energy on the number of electrons is plotted in Fig. 2.6.

The resonance tunneling energy or the addition energy, $\Delta E = [E(N+1) - E(N)]$ as a function of the applied magnetic field is presented in Fig. 2.7. Fig. 2.7 (a) gives the results for $N = 2$ and Fig. 2.7 (b) for $N = 3$. We have shown results for both $\alpha = 0$ and $\alpha = 20\ meV \cdot nm$ for the sake of comparison. As expected, for both $N = 2$ and $N = 3$, RSOI reduces the addition energy. For $N = 2$, the addition energy $\Delta E = [E(3) - E(2)]$ as a function of the magnetic field B exhibits a minimum which is found to shift towards right as the RSOI is switched on. For $N = 3$, however, there exists no such minimum structure and the addition energy, $\Delta E = [E(4) - E(3)]$ shows a monotonic increase in B. This stark difference between the behavior of the addition energy for $N = 2$ and that for $N = 3$ is not clearly understood.
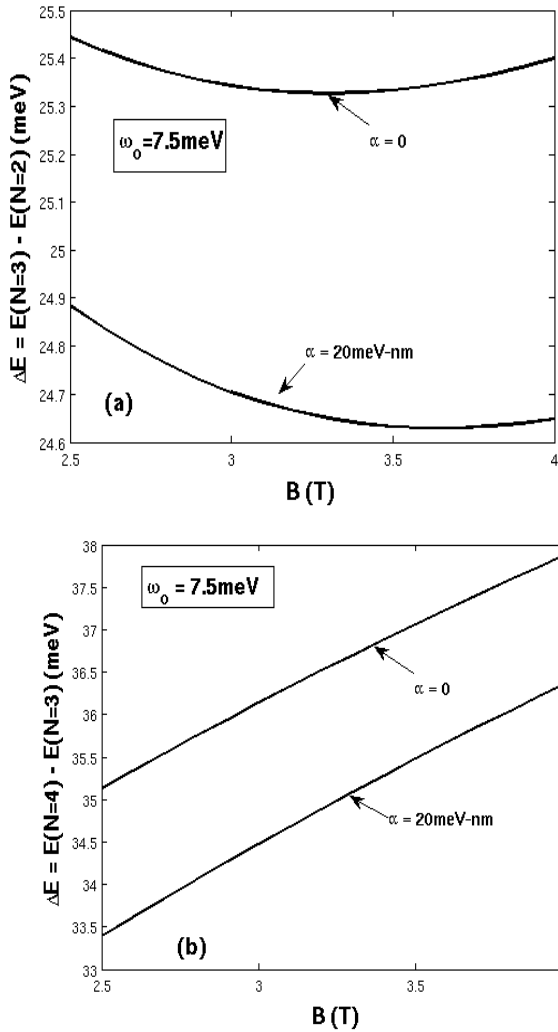
Fig. 2.7 $\Delta E = [E(N+1) - E(N)]$ vs B for (a) $N = 2$ and (b) $N = 3$ (b) with and without RSOI.

2.5 Conclusions

We have studied the ground state energy of a parabolically confined QD in the presence of an external magnetic field incorporating both the e-e interaction and the RSOI. We have considered systems with the electron number equal to 1, 2, 3 and 4. For the e-e interaction, a simple, exactly soluble and physically reasonable model potential as suggested by Johnson and Payne is used. A unitary transformation is performed to eliminate the effect of the RSOI beyond quadratic in RSOI constant α. The transformed haniltonian is then solved exactly for the GS energy following Johnson and Payne. We have observed that the GS energy increases with increasing magnetic field and in general the RSOI reduces the total energy of the system. The dependence of the GS energy on the RSOI constant α is slightly more complex than just quadratic. RSOI energy is found to decrease with the increase in the number of electrons in the system. This decrease looks more or less quadratic. The total energy however increases with the number of electrons as expected. The e-e interaction energy is found to increase almost linearly with the magnetic field. It also increases with the electron number but decreases with the RSOI.

Our results are found to be in very good agreement with the numerical results[23] available in the literature.

References

1.   N. Chestnoy, R. Hull, L.E. Brus, *Higher excited electronic states in clusters of ZnSe, CdSe, and ZnS: Spin-orbit, vibronic, and relaxation phenomena*, J. Chem. Phys. **85**, 2237, (1986). doi:10.1063/1.451119.

2.   M.G. Bawendi, M.L. Steigerwald, L.E. Brus, *The Quantum Mechanics of Larger Semiconductor Clusters ("Quantum Dots")*, Annu. Rev. Phys. Chem. **41**, 477, (1990). doi:10.1146/annurev.pc.41.100190.002401.

3.   T. Darnhofer, U. Rössler, *Effects of band structure and spin in quantum dots*, Phys. Rev. B. **47**, 16020, (1993). doi:10.1103/PhysRevB.47.16020.

4.   E. Tsitsishvili, G.S. Lozano, A.O. Gogolin, *Rashba coupling in quantum dots: An exact solution*, Phys. Rev. B. **70**, 115316, (2004). doi:10.1103/PhysRevB.70.115316.

5.   H. Tütüncüler, R. Koç, E. Ol ar, *Solution of a Hamiltonian of quantum dots with Rashba spin–orbit coupling: quasi-exact solution*, J. Phys. A. Math. Gen. **37**, 11431, (2004). doi:10.1088/0305-4470/37/47/011.

6.   F.M. Hashimzade, A.M. Babayev, S. Çakmak, Ş.

Çakmaktepe, *Rashba splitting in Kane type quantum disk*, Phys. E Low-Dimensional Syst. Nanostructures. **25**, 78, (2004). doi:10.1016/j.physe.2004.06.045.

7. H. Hassanabadi, H. Rahimov, S. Zarrinkamar, *Analytical Treatment of a Three-Electron-Quantum Dot Under Rashba Spin–Orbit Interaction*, Few-Body Syst. **52**, 87, (2011). doi:10.1007/s00601-011-0234-9.

8. I.L. Aleiner, V.I. Fal'ko, *Spin-orbit coupling effects on quantum transport in lateral semiconductor dots.*, Phys. Rev. Lett. **87**, 256801, (2001). doi:10.1103/PhysRevLett.87.256801.

9. S. Bandyopadhyay, M. Cahay, *Rashba effect in an asymmetric quantum dot in a magnetic field*, Superlattices Microstruct. **32**, 171, (2002). doi:10.1016/S0749-6036(03)00017-X.

10. G. Bihlmayer, O. Rader, R. Winkler, *Focus on the Rashba effect*, New J. Phys. **17**, 050202, (2015). doi:10.1088/1367-2630/17/5/050202.

11. S. Datta, B. Das, *Electronic analog of the electro-optic modulator*, Appl. Phys. Lett. **56**, 665, (1990). doi:10.1063/1.102730.

12. R. Winkler, *Spin-orbit Coupling Effects in Two-Dimensional Electron and Hole Systems*, Springer Science & Business Media, , (2003).

13. P. McEuen, E. Foxman, U. Meirav, M. Kastner, Y. Meir,

N. Wingreen, S. Wind, *Transport spectroscopy of a Coulomb island in the quantum Hall regime.*, Phys. Rev. Lett. **66**, 1926, (1991). doi:10.1103/PhysRevLett.66.1926.

14.   M. Reed, J. Randall, R. Aggarwal, R. Matyi, T. Moore, A. Wetsel, *Observation of discrete electronic states in a zero-dimensional semiconductor nanostructure*, Phys. Rev. Lett. **60**, 535, (1988). doi:10.1103/PhysRevLett.60.535.

15.   van der Vaart NC, S. Godijn, Y. Nazarov, C. Harmans, J. Mooij, L. Molenkamp, C. Foxon, *Resonant tunneling through two discrete energy states.*, Phys. Rev. Lett. **74**, 4702, (1995). doi:10.1103/PhysRevLett.74.4702.

16.   N.F. Johnson, M.C. Payne, *Many-body effects in resonant tunneling through quantum dots*, Phys. Rev. B. **45**, 3819, (1992). doi:10.1103/PhysRevB.45.3819.

17.   P.L. McEuen, E.B. Foxman, J. Kinaret, U. Meirav, M.A. Kastner, N.S. Wingreen, S.J. Wind, *Self-consistent addition spectrum of a Coulomb island in the quantum Hall regime*, Phys. Rev. B. **45**, 11419, (1992). doi:10.1103/PhysRevB.45.11419.

18.   L. Brey, N.F. Johnson, B. Halperin, *Optical and magneto-optical absorption in parabolic quantum wells*, Phys. Rev. B. **40**, 10647, (1989). doi:10.1103/PhysRevB.40.10647.

19.   Q.P. Li, K. Karraï, S.K. Yip, S. Das Sarma, H.D. Drew, *Electrodynamic response of a harmonic atom in an external magnetic field*, Phys. Rev. B. **43**, 5151, (1991). doi:10.1103/PhysRevB.43.5151.

20.   F.M. Peeters, *Magneto-optics in parabolic quantum dots*, Phys. Rev. B. **42**, 1486, (1990). doi:10.1103/PhysRevB.42.1486.

21.   P. a. Maksym, T. Chakraborty, *Quantum dots in a magnetic field: Role of electron-electron interactions*, Phys. Rev. Lett. **65**, 108, (1990). doi:10.1103/PhysRevLett.65.108.

22.   N.F. Johnson, M.C. Payne, *Exactly solvable model of interacting particles in a quantum dot*, Phys. Rev. Lett. **67**, 1157, (1991). doi:10.1103/PhysRevLett.67.1157.

23.   P. Pietilainen, T. Chakraborty, *Energy levels and magneto-optical transitions in parabolic quantum dots with spin-orbit coupling*, Phys. Rev. B. **73**, 155315, (2005). doi:10.1103/PhysRevB.73.155315.

Chapter 3.   Effect of Rashba and Dresselhaus spin-orbit interactions on the energy spectrum, chemical potential, addition energy and spin-splitting energy in a parabolic GaAs quantum dot in the presence of an external magnetic field.

3

3.1 Introduction

The study of Dresselhaus spin-orbit interaction (DSOI) has been kept aside for a long time after the discovery of quantum dots (QDs) as it could not be tuned as easily as Rashba spin orbit interaction (RSOI). It was Voskaboynikov et al. [1] who studied, a decade after the invention of QD, the effect of DSOI and RSOI together on the zero-field spin splitting in a parabolic quantum dot (PQD). Before Voskaboynikov et al., it was Pikus et al. [2, 3] who studied the effect of DSOI on the spin-splitting in $III - V$ heterojunctions. Later in 2004, Lipparini et al. [4] have studied the effect of DSOI alone on the spin-splitting of cyclotron resonances in $GaAs$ QD.   Later several studies [5–8] were made on a PQD incorporating

the effect of DSOI and RSOI. In this chapter we study the effect of both RSOI and DSOI on the energy spectrum, chemical potential, addition energy and spin-splitting energy in a *GaAs* PQD.

3.1.1 Chemical potential

Chemical potential was first introduced by Gibbs [9] through his pioneering publications "A Method of Geometrical Representation of the Thermodynamic Properties of Substances by Means of Surfaces" in 1873 and "On the Equilibrium of Heterogeneous Substances" In 1876. In solid state physics chemical potential or electrochemical potential is used to define the Fermi energy at $T = 0\,K$. The study of chemical potential in QDs has attracted attention in the recent past both from the point of view of theory [10–12] and experiments [13–16]. Chemical potential $\mu(N)$ is defined as the energy required to add an Nth electron to an $(N-1)$ electron system: $\mu(N) = E(N) - E(N-1)$.

3.1.2 Addition energy

Addition energy studies have made an important breakthrough in the theoretical understanding and experimental applications of QDs [17]. The addition energy for N^{th} electron is defined as the difference between Ionization potential (I_N) and the electron affinity (A_N) of the Nth electron i. e, $E_{Add} = I_N - A_N$, where the ionization energy which is the energy required to remove an electron from an N-electron system is given by: $I(N) = E(N-1) - E(N)$ and the electron affinity which is the energy released when an electron is added to an N-electron system is given by: $A(N) = E(N) - E(N+1)$. Thus, $E_{Add} = E(N+1) - 2E(N) + E(N-1)$ and so the addition energy is just the energy required to overcome the Coulomb barrier and can also be defined as [18, 19]: $E_{Add}(N) = \mu(N+1) - \mu(N)$. Here $\mu(N+1)$ represents the energy corresponding to an average $(N+1/2)$ electron system and $\mu(N)$ corresponds to the energy of an average $(N-1/2)$ electron system. Hence, the addition energy $E_{Add}(N)$ represents the energy of the Nth electron.

3.1.3 Spin splitting energy

The effect of SOI reflects directly in the spin-splitting energy. The interest in the study of spin-splitting energy has continued unabated from the inception of QD

research [20–25]. In recent years the study of spin-spilling energy has also found applications in the fields of quantum information and quantum computing [26]. The spin splitting energy [27–30] is defined as the difference between the energies of two oppositely spinning electrons in a given spatial and orbital angular momentum (OAM) state. For a single-electron QD in an external field, the spin-splitting energy without spin polarization is given by: $E_{ss} = E(N_a, N_b, +S_z) - E(N_a, N_b, -S_z)$. Our results are valid for any parabolic QD with a small value of g^*. But for the sake of concreteness, we have applied our theory to a $GaAs$ QD.

3.2 The Hamiltonian

Our model consists of a system of N electrons, each with effective mass m^*, charge "-e" and spin s, moving in a radially symmetric two-dimensional (2D) PQD grown on a heterojunction, in the presence of an external magnetic field applied perpendicular to the QD (i.e., along z-axis). We also take into account the RSOI and the DSOI and for the electron-electron (e-e) interaction we use the prescription of Johnson and Payne [31]. The relevant Hamiltonian is given by

$$H = \sum_{i=1}^{N} \left(\frac{1}{2m^*} \left(\boldsymbol{p}_i + \frac{e\boldsymbol{A}_i}{c} \right)^2 + \frac{1}{2} m^* \omega_o^2 |\boldsymbol{r}_i|^2 \right.$$

$$\left. + \frac{1}{2} g^* \mu_B B \sigma_{i,z} \right)$$

$$+ \sum_{i<j} 2V_o - \frac{1}{2} m^* \Omega^2 |\boldsymbol{r}_i - \boldsymbol{r}_j|^2$$

$$+ \frac{\alpha}{\hbar} \sum_i \left[\left(p_{i,y} + \frac{e}{c} A_{i,y} \right) \sigma_{i,x} \right.$$

$$\left. - \left(p_{i,x} + \frac{e}{c} A_{i,x} \right) \sigma_{i,y} \right]$$

$$+ \frac{\beta}{\hbar} \sum_i \left[\sigma_{i,x} \left(p_{i,x} + \frac{e}{c} A_{i,x} \right) \right. \qquad (3.1)$$

$$\left. - \sigma_{i,y} \left(p_{i,y} + \frac{e}{c} A_{i,y} \right) \right],$$

where all the symbols have been introduced earlier.

3.3 Analytical solution

To make progress, we choose the gauge of $\boldsymbol{A}$ as: $\boldsymbol{A}_i = B(-y_i/2, x_i/2, 0)$. In the limit, $H_o \gg H_R \approx H_D \gg H_z$, one can now diagonalize the Hamiltonian by a unitary transformation [32] with a generator: S= $im^*[\alpha \sum_i (y_i \sigma_{i,x} -$

$x_i\sigma_{i,y}) + \beta \sum_i(x_i\sigma_{i,x} - y_i\sigma_{i,y})]/\hbar^2$. Neglecting terms of order higher than quadratic in α and β, the transformed Hamiltonian can now be separated [31, 33] into a space part H_p and a spin part H_s where

$$H_p = \sum_i \left[\frac{p_i^2}{2m^*} + \frac{m^*}{2}\widetilde{\omega}_o^2|r_i|^2 + \frac{\widetilde{\omega}_c}{2}L_{i,z} - \frac{m^*}{\hbar^2}(\alpha^2 + \beta^2)\right]$$

$$+ \sum_{i<j}\left(2V_o - \frac{1}{2}m^*\Omega^2|r_i - r_j|^2\right) \qquad (3.2)$$

$$H_s = \sum_i \frac{1}{2}g^*\mu_B B\sigma_{i,z} \qquad (3.3)$$

where $\widetilde{\omega}_o^2 = [\omega^2 - \frac{m^*}{\hbar^3}(\alpha^2 - \beta^2)\omega_c\sigma_z]$, $\omega_c = [eB/m^*c]$, $\omega^2 = [\omega_o^2 + \omega_c^2/4]$, $\widetilde{\omega}_c = \omega_c - \frac{m^*}{\hbar^3}(\alpha^2 - \beta^2)\sigma_z$ and $L_{i,z} = [x_ip_{i,y} - y_ip_{i,x}]$ is the z-component of the OAM of the ith particle. H_p can be further separated into center of mass and relative coordinates using the transformations given in [31, 33] to obtain the energy spectrum of the system at large magnetic field as

$$E = E_0(S_Z) + N_A \hbar \left[\widetilde{\omega}_0 - \frac{\widetilde{\omega}_c}{2} \right] + N_B \hbar \left[\widetilde{\omega}_0 + \frac{\widetilde{\omega}_c}{2} \right]$$

$$+ \sum_{i<j} \left[\alpha_{ij} \hbar \left(\Omega_0 - \frac{\widetilde{\omega}_c}{2} \right) \right.$$

$$\left. + \beta_{ij} \hbar \left(\Omega_0 + \frac{\widetilde{\omega}_c}{2} \right) \right] - \frac{Nm^*}{\hbar^2} (\alpha^2 + \beta^2)$$

$$(3.4)$$

where $N_A, N_B, \alpha_{ij}, \beta_{ij}$ can take any positive integer values, $\Omega_o{}^2 = [\widetilde{\omega}_o^2 - N\Omega^2]$ and $E_0(S_Z)$ is the ground state (GS) energy given by

$$E_0 = \hbar\widetilde{\omega}_0 + (N-1)[\hbar\Omega_0 + NV_o] - \frac{m^* g^*}{2m_0} \omega_c S_Z .$$

$$(3.5)$$

The second term in the total energy expression represents the excitation energy corresponding to the electron with orbital OAM along the field direction. The third term gives the excitation energy corresponding to the electron with OAM opposite to the magnetic field. The fourth term denotes the excitation energy corresponding to the electrons with parallel OAM whereas the last term is that with antiparallel OAM. The space part of the total wave function is symmetric if the sum of all the quantum numbers $N_A, N_B, \alpha_{ij}, \beta_{ij}$ is even and is anti-symmetric if the

sum is odd. The spin part of wave function and the corresponding total spin has been considered in such a way as to preserve the anti-symmetry of the total wave function. In the case of a spin-polarized system, since the spin part of the wave function is symmetric, the space part of the wave function must be anti-symmetric to preserve the anti-symmetric nature of the fermionic system. Furthermore, since the center of mass part of wave function is always symmetric, N_A and N_B can take any positive integer values. Hence the relative part of the wave function must be anti-symmetric for a spin-polarized system. For this to happen, the sum of α_{ij} and β_{ij} should take odd positive integer values.

3.4 Numerical results and discussion

In our numerical investigation we have considered a *GaAs* QD with parameters [34] $m^*/m_0 =0.063$, $\varepsilon =12.9$, $g^* = -0.44$, $V_0 = 7.5 \, \text{meV}$, $\alpha = 20 \, \text{meV} \cdot \text{nm}$ and $\beta = 20 \, \text{meV} \cdot \text{nm}$.

3.4.1 One electron system

We have the exact analytical expression for the energy spectrum of a one-electron system as a function of the magnetic field in the absence of SOI. This energy spectrum is presented in Fig. 3. 1 and and obviously the results are identical with those available in the literature [34].
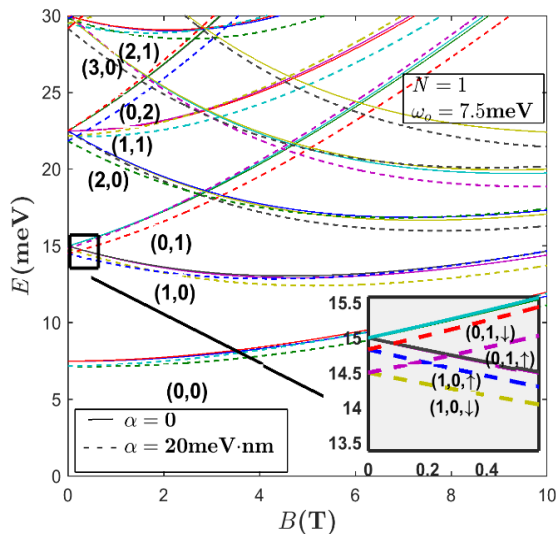
Fig. 3.1 Energy spectrum of a one-electron system with and without RSOI.

In the presence of the magnetic field, first, the orbital Zeeman splitting occurs leading to two branches, one increasing with the magnetic field and the other decreasing with it. The spin-degeneracy of these energies is further split by the spin-Zeeman interaction leading to two energy curves from each one. The effect of RSOI is to shift the spin-split energies downward. At zero magnetic field, the states with the same value of $(N_A + N_B)$ are degenerate. As the strength of the magnetic field increases, at $B = 1.65$T, the states (3,0) and (0,2) which have the same value of $(N_A + 1.5N_B)$ become degenerate. As the field strength increases further, at $B = 2.85T$, the states (2,0) and (0,1) which have the same value of $(N_A + 2N_B)$ become degenerate. As the magnetic field is further increased to $B = 4.75$T, the states (3,0) and (0,1) which have the same value of $(N_A + 3N_B)$ become degenerate. Finally at very large magnetic fields, the states with same value of N_B group together i.e, the states (0,0), (1,0), (2,0), (3,0) etc. group together and states (0,1), (1,1), etc. group together. This happens because in the presence of the magnetic field, the energy of the electrons with OAM antiparallel to the field increases while that parallel to the field decreases. Finally when the field strength is made very large, complete polarization takes place and all the electron states with the same OAM opposite to the

applied field are grouped together. The figure also depicts the energy spectrum with RSOI. For a spin-up electron, the plot shows that the RSOI reduces the total energy of the system and the reduction is larger for a stronger magnetic field. Also, RSOI has a negligible effect on the electrons with OAM parallel to the applied field. This is due to the fact that the energy of an electron with OAM parallel to the magnetic field is reduced by the Zeeman Effect which in turn is reduced by RSOI. So, indirectly through Zeeman effect RSOI increases the energy of the electron with OAM parallel to the magnetic field. At the same time RSOI directly reduces the energy of the system.

These two effects combine to nullify the overall effect of RSOI on the electron with OAM parallel to the applied field. Exactly the opposite effect is observed in the case of a spin-down electron. The energy spectrum of a one-electron system with and without DSOI is presented in Fig. 3.2. In the case of a spin-up electron, DSOI has a very little effect on an electron with OAM antiparallel to the applied field. This is due to the fact that the energy of such an electron is increased by the Zeeman interaction which in turn is enhanced by DSOI. Thus

through the Zeeman Effect, DSOI increases the energy of an electron with OAM antiparallel to the magnetic field.
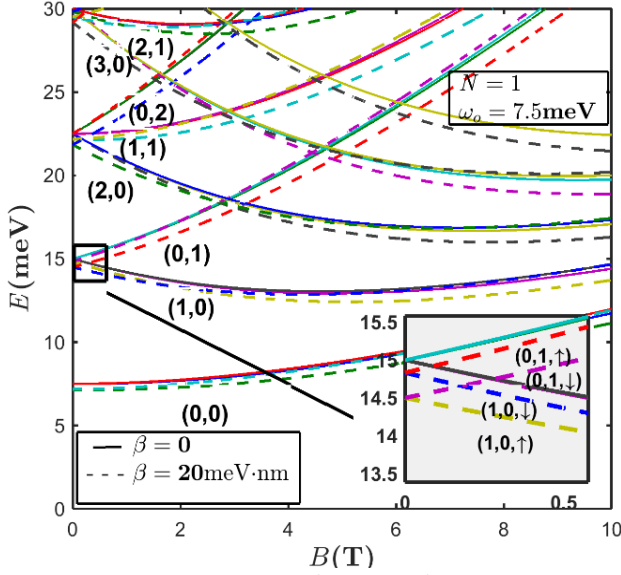
Fig. 3.2 Energy spectrum of a one-electron system with and without DSOI.

On the other hand, DSOI, in general, reduces the energy of the electron. Thus the resultant effect of DSOI on an electron with OAM antiparallel to the external field is negligible. So the effects of RSOI and DSOI with equal strengths on an electron's energy with a given spin are equal and opposite. Hence without any loss of generality, one can consider either a spin-up or a spin-down electron system for simplicity. The plots of a spin

polarized single-electron system with and without RSOI and DSOI are shown in Fig. 3.3. In this work we consider only spin-polarized systems (unless mentioned otherwise) to distinguish the effects of RSOI and DSOI. Here the reduction effect of RSOI and the enhancement effect of DSOI on Zeeman interaction get cancelled for equal strengths of Rashba and Dresselhaus terms and only the over-all reduction effect of SOI on the total electron energy persists.
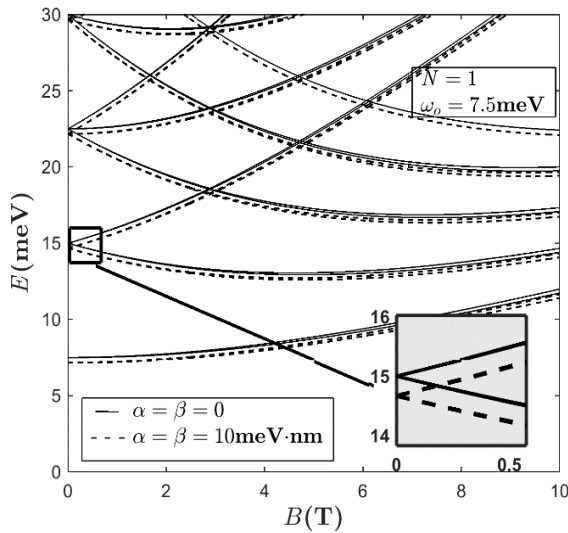
Fig. 3.3 Energy spectrum of a one-electron system with and without both SOI's.

Thus one can see that the spectrum obtained taking into account both SOI's shifts down by a constant value from that obtained without SOI's.

To examine the effect of SOI explicitly, we calculate the electron energy with SOI's and also without them and subtract the latter from the former. The results are presented in Fig. 3.4 as a function of the applied magnetic field. Here the levels are labeled by two quantum numbers (N_A, N_B), since the spin-Zeeman term (having negligible effect on SOI terms) can be neglected.
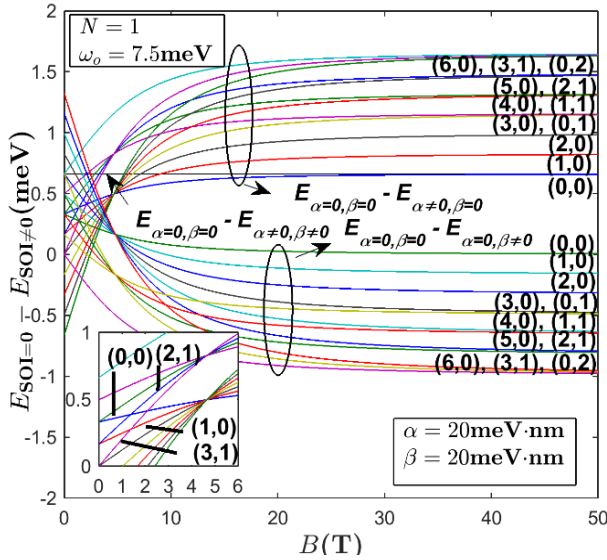
Fig. 3.4 Effect of RSOI, DSOI and the both on the energy of a one- electron system as a function of B.

Thus effectively, SOI's have the same effect on spin-up and spin-down electrons. The difference between the energy of an electron without RSOI and that with RSOI monotonically increases with the applied field and eventually saturates to a constant positive value. Obviously, RSOI always reduces the energy of the electron. The effect of the external field on DSOI is opposite to that on RSOI. In the absence of an external field, the states with the same value of $(\Delta N)_{AB}^a = (N_A^a - N_B^a)$, where a denotes a particular state, have the same energy. For example the pairs $(0,0)$ & $(1,1)$ and $(1,0)$ & $(2,1)$ have same energies. Also the states with larger magnitude of OAM have lesser RSOI energy. For example, the $(6,0)$ state $(l = -6)$ has a lower energy than the $(0,0)$ state $(l = 0)$. The scenario changes if an external field is applied and if it becomes large enough to dominate over the confinement potential. In the presence of the magnetic field, the direction of OAM also matters and the state with a larger OAM vector corresponds to a lesser energy, i.e., the RSOI energy of the $(0,0)$ state becomes less than that of the state $(6,0)$. We observe an interesting behavior for states a, b, c etc. for which $(\Delta N)_{AB}^b - (\Delta N)_{AB}^a = (\Delta N)_{AB}^c - (\Delta N)_{AB}^b$. We call this difference as $(\Delta^2 N)_{AB}$. The figure shows that states with even N_A's and with $(\Delta^2 N)_{AB} = 1$ attain the same energy at

$B = 1.4$T. Thus, for example, the energy levels for the states $(0,0)$, $(2,1)$ & $(4,2)$ which satisfy the condition $(\Delta^2 N)_{AB} = 1$ show a crossing behavior at $B = 1.4T$. Interestingly, the energy levels for the states with odd N_A's and $(\Delta N)_{AB}^{CD} = 1$ also show the crossing phenomenon at the same magnetic field, but at a different energy value. Thus, the energy levels for the states $(1,0)$, $(3,1)$ & $(5,2)$ also undergo crossing at $B = 1.4$T. The energy levels with $(\Delta^2 N)_{AB} = 2$ exhibit the crossing behavior at a higher magnetic field and this crossing behavior continues to occur for states with even higher values of $(\Delta^2 N)_{AB}$. For example, at $B = 2.1$T, the states $(0,0)$, $(3,1)$, $(6,2)$ have the same energy and the states $(0,0)$, $(4,1)$, $(8,2)$ have the same energy at $B = 4.65T$. At $B = 4.75T$, the states $(N_A, 0)$, $(N_A, 1)$ with $N_A = 0, 1, 2, 3,$ etc undergo crossing (though at different energies) for both RSOI and DSOI. Crossing of states also occurs for states with negative values of $(\Delta^2 N)_{AB}$. Furthermore, pairs of states with the same value of $(\Delta^2 N)_{AB}$ also cross at certain magnetic field. For example, at $B = 9$T, the pairs of states $(6,0)$ & $(1,1)$ and $(5,0)$ & $(0,1)$ have the same energy and at $B = 12$T, the pairs of states $(5,0)$ & $(1,1)$ and $(4,0)$ & $(0,1)$ have same energy. We find that at very large magnetic fields, the states with same $N_A + 3N_B$ obtain the same energy.
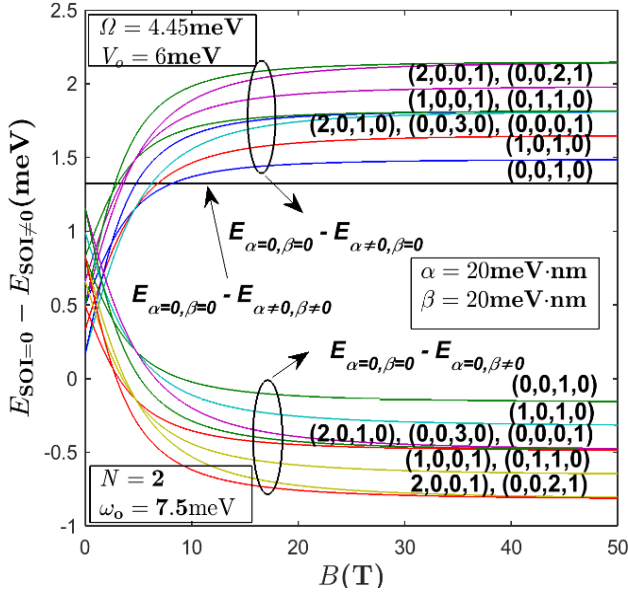
Fig. 3.5 Effect of RSOI, DSOI and the both on the 2-electron QD energy as a function of B with e-e interaction.

Once the complete polarization occurs, RSOI has no effect on the energy of the states. Similar observations are also made for the DSOI energies but in this case energies become negative if the magnetic field is sufficiently large. When both the interactions are considered, terms containing the orbital Zeeman interaction get cancelled leaving a constant term that leads to a straight horizontal line independent of the magnetic field. The RSOI energy for (0,0) state coincide

with the straight line corresponding to both the interactions at large magnetic fields. This is due to the fact that at large magnetic fields, the RSOI and DSOI contributions approach $-N(m^*/\hbar^2)\alpha^2$ and $-N(m^*/\hbar^2)\beta^2$ respectively and become equal for $\alpha = \beta$. The separations between two consecutive RSOI and DSOI energy levels in the asymptotic limit are found to be $(m^*/2\hbar^2)\alpha^2$ and $(m^*/2\hbar^2)\beta^2$ respectively.

3.4.2 Two-electron system

(a) The SOI energy

The variation of the SOI energy as a function of the magnetic field for a two-electron system is presented in Fig. 3.5. In this case, the e-e interaction comes into picture. Here we consider for the e-e interaction the exactly soluble Johnson- Payne model potential (Eq. 1.1) and fix the values of V_0 and Ω appearing in it by fitting the GS energy of the system without SOI with that of the numerical result [34]. As evident from the analytic expression, the states with the same value of $(\Delta N)_{AB}^{ij} =$

$[(N_A + \alpha_{ij}) - (N_B + \beta_{ij})]$ are degenerate at zero field. For example, at $B = 0$, the states $(0,0,1,0)$, $(2,0,0,1)$ and $(0,0,2,1)$ have the same SOI energy. Also, at a certain strength of the magnetic field, the SOI energy curves for states with the same $(N_B + \beta_{ij})$ and $(\Delta N)_{AB} = 1, 2, 3$, *etc* cross one another. Thus the SOI energy curves for the states $(0,0,01)$, $(1,0,0,1)$ and $(2,0,0,1)$ cross one another at $B = 5T$ and at the same magnetic field, the states $(0,0,1,0)$, $(1,0,1,0)$ and $(2,0,1,0)$ also cross one another but at a different SOI energy. Beyond a certain magnetic field, the states with $N_A = 0 = N_B$ have a smaller SOI energy than those having finite values for both N_A, N_B or a finite value for one of them. For example, the state $(0,0,0,1)$ has a lower energy than the state $(1,0,0,1)$ and $(0,0.1,0)$ has a smaller energy than $(0,1,10)$. At very large magnetic fields, the states with the same value of $[(N_A + \alpha_{ij}) + 3(N_B + \beta_{ij})]$ merge together. We also observe that the magnitude of both RSOI and DSOI energies are only slightly enhanced in the presence of the e-e interaction (not shown here).

(b) Electron-electron interaction

The difference between the energy with e-e interaction and that without it for two and three-electron QD's is presented in Figs. 3.6 and 3.7 as a function of magnetic field. Fig. 3.6 gives the results for a 2-electron system, while Fig. 3.7 for a 3- electron system. In this case, only the quantum numbers corresponding to e-e interaction, namely α_{ij}, β_{ij}, matter. One can observe that the e-e interaction energy is same for states with the same value of $(\alpha_{ij} + \beta_{ij})$. This is because we have considered a spin-polarized system.
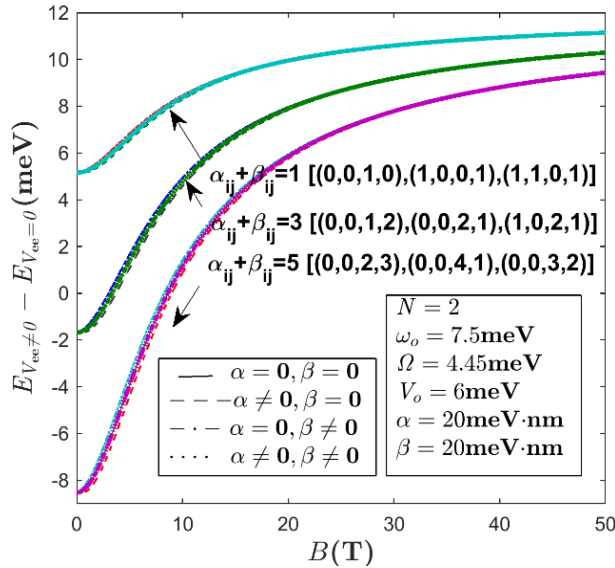
Fig. 3.6 Electron-electron interaction energy as a function of B for a 2-electron system.

Also one can see that the e-e interaction energy is lower for higher excited states. Also, RSOI marginally enhances the effect of e-e interaction and DSOI reduces it. When both interactions are present, SOI has no effect on the e-e interaction. Also the e-e interaction varies linearly for low-lying excited states and almost quadratically for the higher excited states. At larger magnetic fields, the e-e interaction energy saturates. This is because the magnetic field leads to localization which becomes maximum at a certain magnetic field.
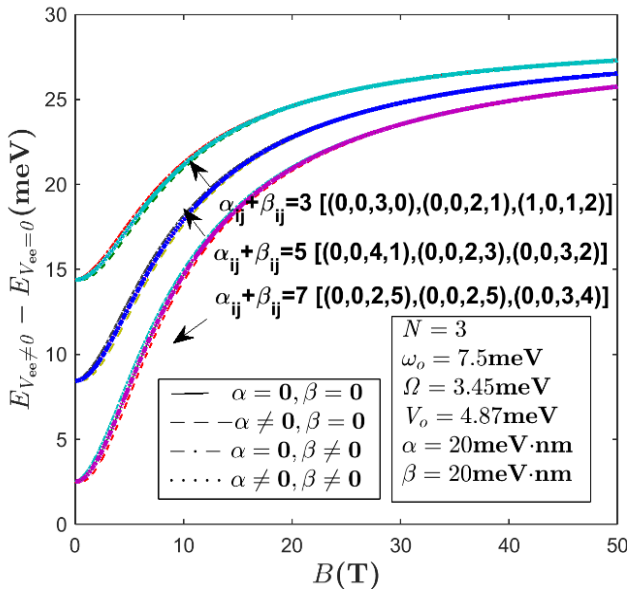
Fig. 3.7 Electron-electron interaction energy as a function of B for a 3-electron system.

Comparison of Fig. 3.6 with Fig. 3.7 clearly shows that e-e interaction contribution is larger for a three-electron system than a two-electron system. This reason is of course understandable.

(c) Effect of SOI

The total variational energy is presented as a function of RSOI in Fig. 3.8 and as a function of DSOI in Fig. 3.9. Fig. 3.8 shows that RSOI reduces the total energy and the reduction increases for the higher excited states. However, Fig. 3.9 shows that while DSOI also reduces the total energy, the reduction decreases for the higher excited states. As one can see, the additional reduction in energy due to the inclusion of DSOI increases for states with OAM parallel to the external field, namely (0,0), (1,0), (2,0) whereas it decreases and also changes sign if we consider the states with OAM antiparallel to the applied field i.e., as we go from (0,0) to (0,1) and (0,2) states. The opposite effect is observed while considering RSOI in addition to DSOI (Fig. 3.9).
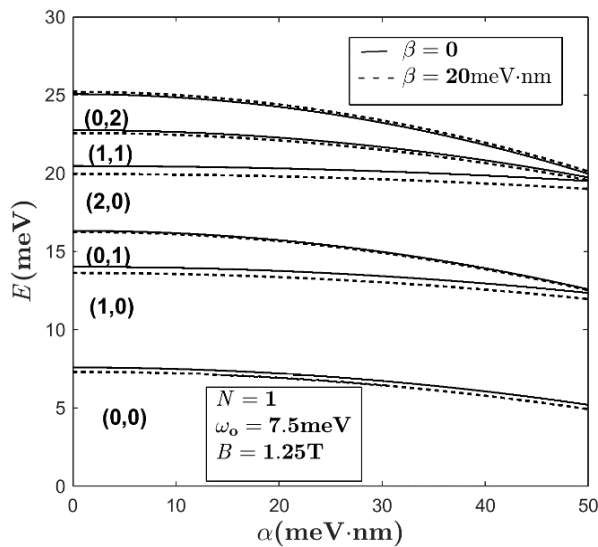
Fig. 3.8. Energy spectrum as a function of α.
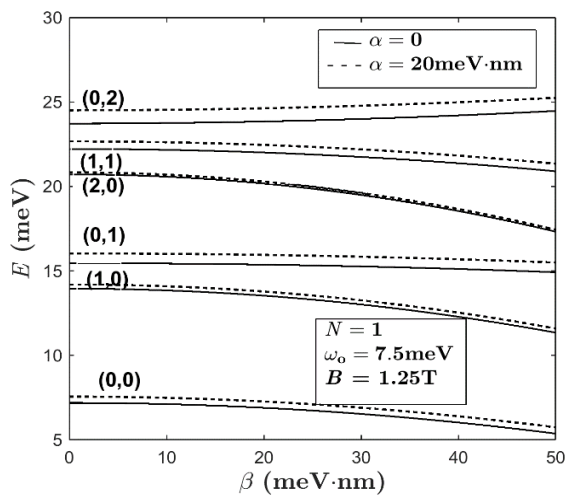
Fig. 3.9. Energy spectrum as a function of β.

Thus, in the presence of DSOI, additional inclusion of RSOI increases the energy of the system. This increase in energy becomes larger for electrons with OAM antiparallel to the applied field and becomes smaller for the states with OAM parallel to the field. Thus the increase in energy for (0, 1) is larger than (0, 0) and that in (0, 2) is larger than (0, 1), while the increase in (1,0) is smaller than (1,0) and that in (2, 0) is smaller than (1, 0).

(d) Chemical potential

The variation of the chemical potential as a function of the applied magnetic field B for $N = 2$ is presented in Fig. 3.10. When we add a second electron to a single-electron system, the separation between the incoming electron and the existing electron increases if the existing electron lies in a higher excited state since the incoming electron enters the lower-most state (0,0). Thus the chemical potential $\mu(2)$ will be smaller if the system is initially in a higher excited state. We say $\mu(2)$ is larger for higher excited states to describe this situation. Also there is a uniform spacing between the chemical potential levels for the higher excited states. This is because the model potential introduces equal spacing in energy levels as it is parabolic in nature.
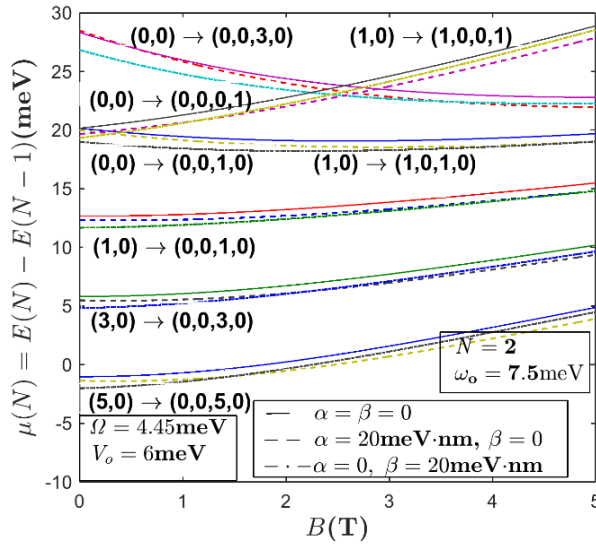
Fig. 3.10 Chemical potential as a function of magnetic field for $N = 2$.

If the incoming electron enters some excited state keeping the existing electron in the GS (0,0) itself, the chemical potential behaves in the same way as that of the total energy spectrum as a function of magnetic field since a constant energy for a given magnetic field will be subtracted from the entire spectrum i. e., the energy of the single electron in the GS. The effect of SOI on chemical potential is same as that on the total energy i.e., RSOI reduces the chemical potential and the reduction increases with applied field. Dresselhaus interaction also

reduces the chemical potential at lower magnetic fields but tends to increase it at higher applied fields.
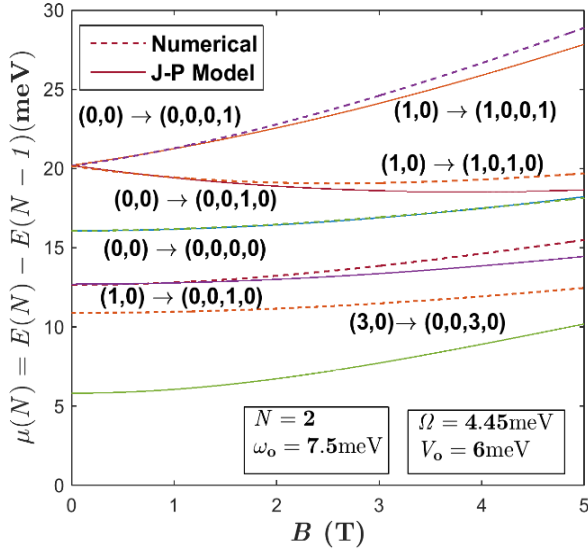
Fig. 3.11 Comparison of our chemical potential results for $N = 2$ with the exact diagonalization results.

When both the interactions are present, there is a uniform reduction in energy independent of applied magnetic field. To examine the accuracy of our results, we have compared our chemical potential plot for $N = 2$ with that obtained by exact numerical diagonalization in the Fock-Darwin basis. The results are presented in Fig. 3.11. The $(0,0)$ to $(0,0,0,0)$ transition results match

exactly as we have fixed our model parameters by fitting with the corresponding numerical results. For the excited states, at lower magnetic fields, our results are in very good agreement with the numerical results but at larger magnetic fields, our results are little lower as we have neglected the higher order terms. For very high excited states, our results are not so close to the numerical results and so the present theory is valid for low-energy excitations. This has already been emphasized in the literature [35].

In the case of $N = 3$ and $N = 4$, the chemical potential becomes larger for higher excited states. We plot the chemical potential as a function of the magnetic field in Fig. 3.12. Consider the case in which the two-electron system is in the spin-polarized (0,0,1,0) state i.e., there is one electron in (0,0) state and another electron in (1,0) state. Hence the incoming electron must go to the (2,0) state as it is the lowest accessible spin-polarized state. Thus the new configuration for the 3-electron system becomes (0,0,3,0). It is easy to visualize that the chemical potential in the case $(0,0,2,0) \rightarrow (0,0,3,0)$ is smaller than that in $(0,0,1,0) \rightarrow (0,0,3,0)$. We now consider a two-electron system in the state (0,0,3,0) i. e., one electron in the state (0,0) and the other in (3,0). On adding a third electron to the state (2,0), the state of the three-electron

system becomes (0,0,5,0). The chemical potential in this case is higher than that in the case (0,0,1,0) to (0,0,3,0). In fact, one can easily show that $\mu(3)_{(0,0,n,0)\to(0,0,n+1,0)}$ depends on n i. e., on the state of the second electron.
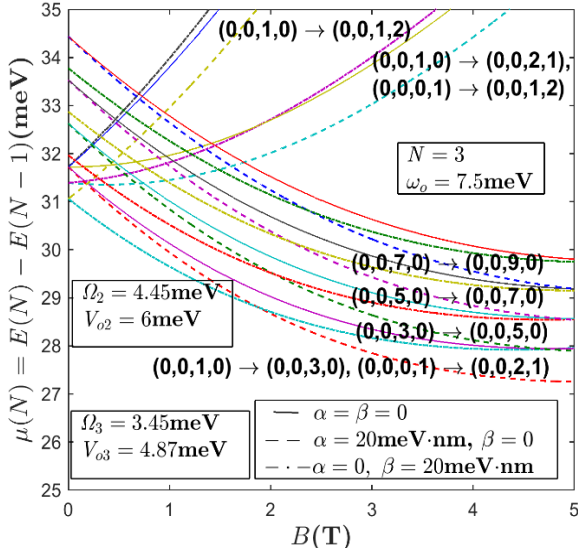
Fig. 3.12 Chemical potential as a function of magnetic field for $N = 3$.

If the second electron lies in a higher state, then the third electron experiences a stronger repulsion from the (0,0) electron because of the weaker screening. Thus the chemical potential results clearly show the effect of the electron-electron interaction. A similar behavior is also observed in the chemical potential spectrum for $N = 4$ (Fig. 3.13). In this case, if the GS of a spin-polarized

three-electron system is (0,0,3,0) i.e, if initially the electrons are in (0,0), (1,0) and (2,0) states, the incoming fourth electron goes into the (3,0) state and the GS of the four-electron system is given by (0,0,6,0).
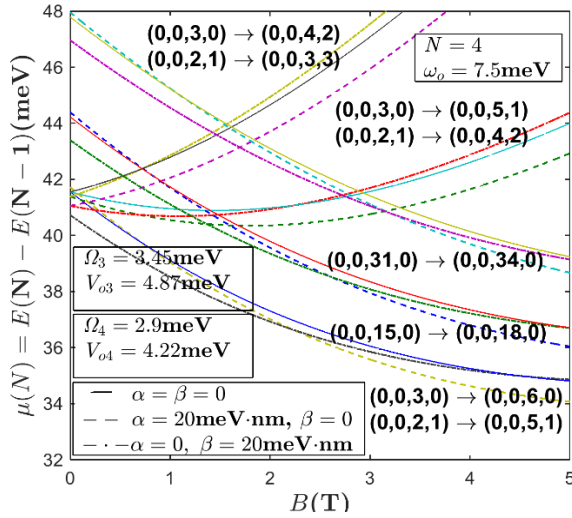
Fig. 3.13 Chemical potential as a function of magnetic field for $N = 4$.

The separation between the chemical potential levels in the $N = 4$ case reduces considerably as compared to the $N = 3$ case due to the shielding effect of the second electron in the (1,0) state.

To see the effect of SOI explicitly on the chemical potential we calculate the difference in μ with and

without SOI i. e., $\mu(SOI = 0) - \mu(SOI \neq 0)$. The results for $N = 2$ and $N = 3$ are presented in Figs. 3.14 and 3.15 respectively.
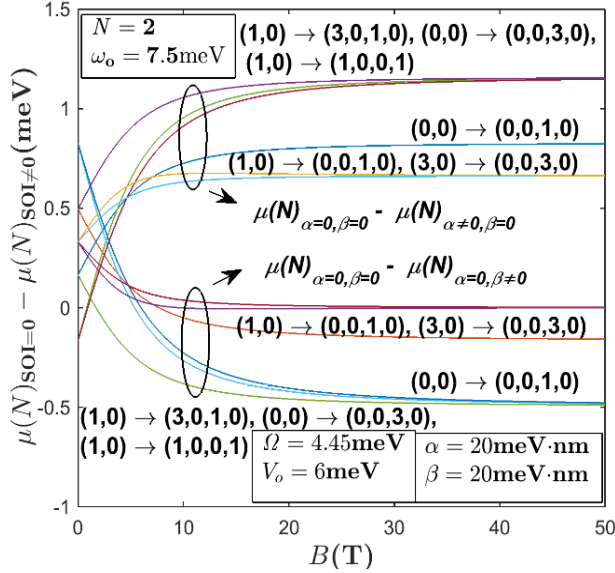
Fig. 3.14 Effect of RSOI, DSOI and both SOI's on chemical potential as a function of B for $N = 2$.

The curves show a behavior similar to the energy spectrum. Also, as the strength of the magnetic field increases, the SOI effect depends only on the state into which the incoming electron enters and is independent of the initial configuration of the system. Thus the chemical potential for the transitions $(0,0,1,0) \rightarrow (0,0,3,0)$

and (0,0,7,0) → (0,0,9,0) have the same strength of SOI contribution at larger magnetic fields in the case of $N = 3$. When the additional electron goes into some excited state keeping the original system in the GS, contribution of RSOI to chemical potential increases in both the cases for $N = 2$ and $N = 3$.
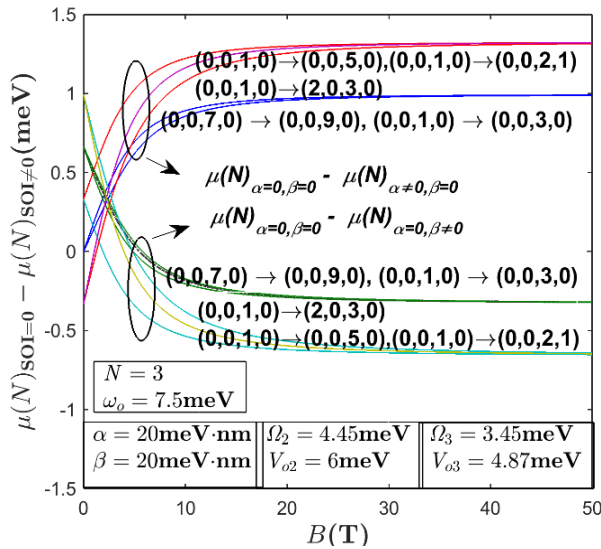
Fig. 3.15 Effect of RSOI, DSOI and both SOI's on chemical potential as a function of B for $N = 3$.

This is quite obvious as in this case the chemical potential includes excitation energy also and the behavior will be similar to the effect of RSOI on the total energy. DSOI also has a similar contribution to chemical

potential as that of RSOI except for a sign change, as happens in case of its effect on the total energy spectrum.

(e) Addition energy

The variation of addition energy as a function of the applied magnetic field is shown in Fig. 3.16 for three values of N. At low magnetic fields, RSOI enhances the addition energy whereas DSOI reduces it. As the magnetic field exceeds a certain critical value, DSOI enhances the addition energy and RSOI reduces it. This is shown in the inset of Fig. 3.16. For $N = 1$ and $N = 3$, the addition energy goes through a minimum as a function of B, whereas for $N = 2$, it shows a monotonically decreasing behavior. In fact, above a certain value of B, the addition energy for $N = 3$ becomes even larger than that for $N = 2$. In all cases, however, the variation is much stronger at low magnetic field. As the magnetic field increases and attains a large value, RSOI reduces the addition energy and DSOI increases it, thus leading to an overall reduction in the effect of SOI on the addition energy. For all the N values considered, the addition energy as a function of B seems to saturate asymptotically.
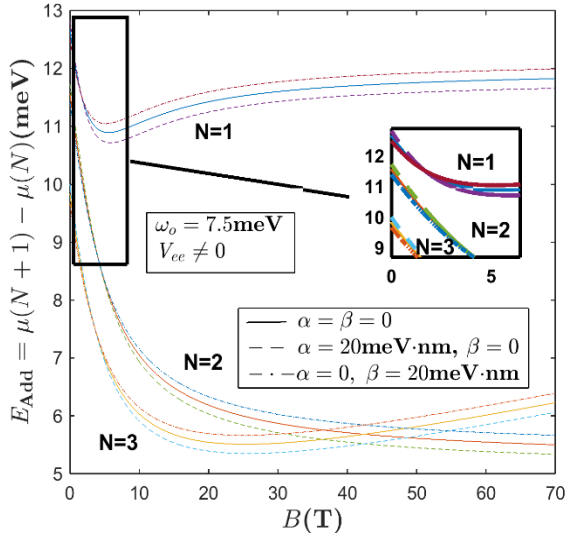
Fig. 3.16 variation of addition energy as a function of magnetic field for three values of N ($N = 1,2,3$).

The variation of addition energy as a function of number of electrons in the presence of V_{ee} is shown in Fig. 3.17 and that for $V_{ee} = 0$ is shown in Fig. 3.18. Fig. 3.17 shows that as N increases, the addition energy in general decreases, if the magnetic field is not too strong.
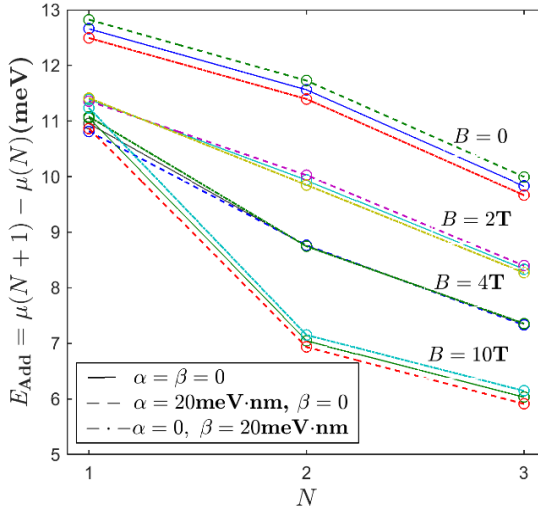
Fig. 3.17 E_{Add} vs. N with and without RSOI, DSOI for various B values for $V_{ee} \neq 0$.

In the zero applied field case, RSOI enhances the addition energy whereas DSOI reduces it. As the magnetic field is increased beyond a certain value, the effects of RSOI and DSOI switch their sign i. e., DSOI enhances the addition energy while RSOI reduces it. Fig. 3.18 shows that in the absence of the electron-electron interaction, the addition energy remains essentially unaffected by the number of electrons at low magnetic field. However at large magnetic fields, the electron number may have a small effect on the addition energy.
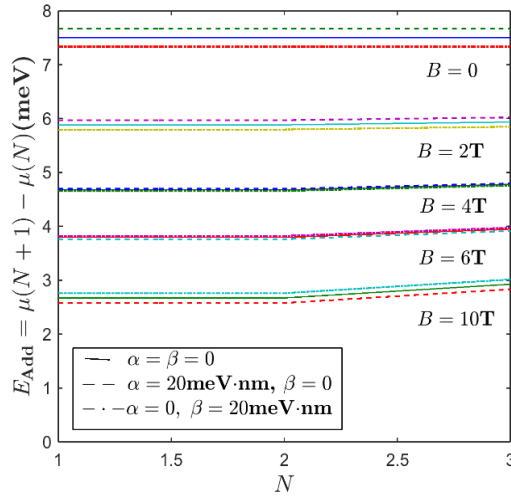
Fig. 3.18 E_{Add} vs. N with and without RSOI, DSOI for various B values for $V_{ee} = 0$.

(f) Spin-splitting energy

The variation of E_{ss} as a function of the magnetic field is presented in Fig. 3.19. The figure shows that in the absence of SOI, the spin-splitting energy decreases with increasing magnetic field in a linear way. However, in the presence of RSOI, the spin-splitting energy initially increases quadratically with the magnetic field and once complete polarization occurs, it saturates and then starts decreasing linearly. A similar behavior is observed in the

case of DSOI except for a sign change. At low magnetic fields, the spin-splitting energies of an up-OAM electron and a down-OAM electron are of opposite sign and the sign becomes same above a certain value of the magnetic field. The effect of SOI on the spin-splitting energy turns out to be greater in the case of electrons with parallel OAM i. e for larger N_A.
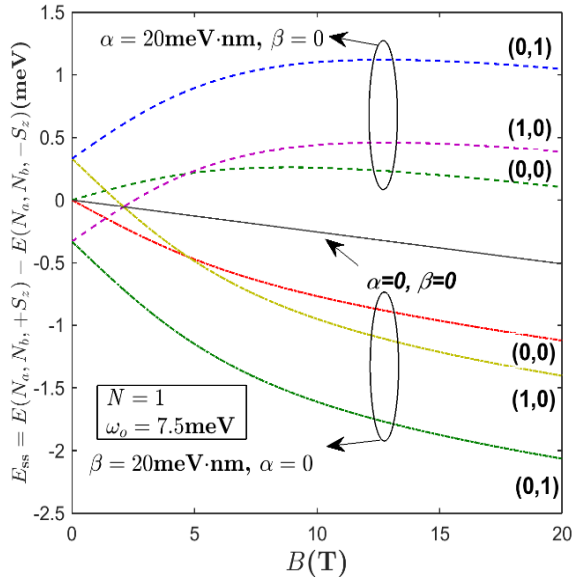
Fig. 3.19. Spin splitting energy as a function of B.

The variation of the spin-splitting energy as a function of RSOI strength is explicitly shown in Fig. 3.20. The figure

shows that the spin-splitting energy of a state with $+ve$ OAM quantum number decreases with increasing α and that with $-ve$ OAM increases. The effect of DSOI on the spin-splitting energy, in this case, is to reduce it for $-ve$ OAM and to increase it for $+ve$ OAM.
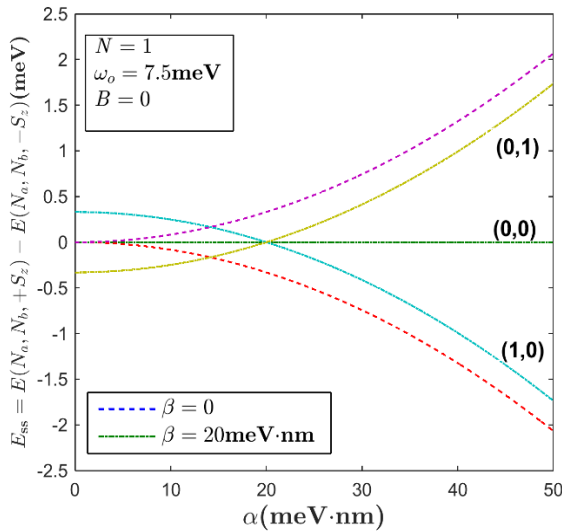
Fig. 3.20 Variation of spin-splitting energy as a function of RSOI strength.

In Fig. 3.21, we show the behavior of the spin-splitting energy as a function of DSOI strength β. Again the spin-splitting energy of a state with $+ve$ OAM quantum number is found to decrease with increasing β

and that with $-ve$ OAM is found to increase. The effect of RSOI on this spin-splitting energy is to enhance it for $+ve$ OAM and to reduce it for $-ve$ OAM. For zero-OAM state, the spin-splitting energy remains unaltered by any change in α or β or both.
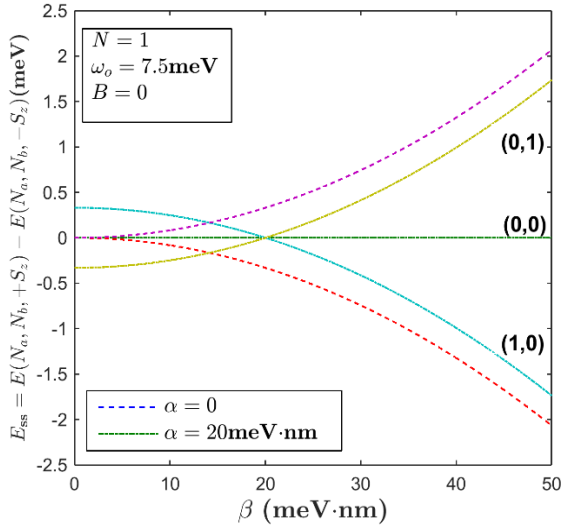
Fig. 3.21 Variation of spin-splitting energy as a function of DSOI strength.

3.5 Conclusions

We have studied the GS energy of a parabolically confined N-electron QD in the presence of an external magnetic field incorporating electron-electron

interaction, RSOI and DSOI. We have considered one, two and three-electron systems. For the e-e interaction, a simple, exactly soluble and physically reasonable model potential as suggested by Johnson and Payne is used. A unitary transformation is performed to eliminate the effect of the SOI beyond quadratic term. The transformed Hamiltonian is then solved exactly for the GS energy following Johnson and Payne. Our results show that both RSOI and DSOI reduce the total energy of the system. In the case of RSOI, the reduction is more for higher excited states, whereas in the case of DSOI, it is less and changes sign at a certain level and then it increases the total energy of the system. We also observe that RSOI reduces the effect of Zeeman interaction, while DSOI enhances it. It turns out that the states with the same value of $(\Delta N)_{AB}^{ij} = [(N_A + \alpha_{ij}) - (N_B + \beta_{ij})]$ are degenerate at zero field. In the presence of a magnetic field, the SOI energy curves cross one another at a certain magnetic field for states with the same $(N_B + \beta_{ij})$ and $(\Delta N)_{AB} = 1, 2, 3, etc$. At very large magnetic fields, the states with the same value of $[(N_A + \alpha_{ij}) + 3(N_B + \beta_{ij})]$ merge together. We furthermore observe that the magnitude of both RSOI and DSOI energies are only slightly enhanced in the presence of the e-e interaction.

For a spin-polarized system, the e-e interaction energy is found to be the same for states with the same value of $(\alpha_{ij} + \beta_{ij})$. Also we have shown that the e-e interaction energy is lower for higher excited states. RSOI marginally enhances the effect of e-e interaction and DSOI reduces it. When both interactions are present, SOI has no effect on the e-e interaction. Also the e-e interaction varies linearly for lower excited states and almost quadratically for the higher excited states. At larger magnetic fields, the e-e interaction energy saturates. This is because the magnetic field leads to localization and localization becomes maximum at a certain magnetic field.

The chemical potential is found to be smaller if the system is initially in a higher excited state. Also there is a uniform spacing between the chemical potential levels for the excited states. The effect of SOI on chemical potential is same as that on the total energy. The addition energy follows the Pauli principle i. e., addition of an electron to an odd-electron system reduces the energy of the system whereas in the case of an even-electron system it increases the total energy. If the magnetic field is not very large, the addition energy decreases with increasing N. In the absence of a magnetic field, RSOI enhances the addition energy whereas DSOI reduces it.

As the magnetic field is increased beyond a certain value, the effects of RSOI and DSOI become opposite i. e., DSOI enhances the addition energy while RSOI reduces it. In the absence of the e-e interaction, the addition energy is not much affected by the number of electrons at low magnetic field, though at large fields, the addition energy may develop a weak dependence on the electron number.

In the presence of RSOI, the spin-splitting energy initially increases quadratically with the magnetic field and once complete polarization occurs, it saturates and then starts decreasing linearly. A similar behavior is observed in the case of DSOI except for a sign change. The spin-splitting energy of a state with a $+ve$ OAM decreases with increasing α and that with $-ve$ OAM increases. The effect of DSOI on the spin-splitting energy is to reduce it for $-ve$ OAM and to increase it for $+ve$ OAM. Again the spin-splitting energy of a state with $+ve$ OAM quantum number is found to decrease with RSOI and that of a state with $-ve$ OAM quantum number is found to increase with RSOI. For zero-angular momentum state, the spin-splitting energy remains unaltered by any change in α or β or both.

References

1. O. Voskoboynikov, C. P. Lee, and O. Tretyak, "*Spin-orbit splitting in semiconductor quantum dots with a parabolic confinement potential*", Phys. Rev. B **63**, 165306 (2001).

2. G. Pikus and V. Marushchak, "*Spin splitting of energy bands and spin relaxation of carriers in cubic III-V crystals*", Sov. Physics--Semiconductors(English Transl. **22**, 115 (1988).

3. F. G. Pikus and G. E. Pikus, "*Conduction-band spin splitting and negative magnetoresistance in A 3 B 5 heterostructures*", Phys. Rev. B **51**, 16928 (1995).

4. P. Tonello and E. Lipparini, "*Spin-orbit splitting of the cyclotron resonance in GaAs*", Phys. Rev. B **70**, 1 (2004).

5. C. F. Destefani, S. E. Ulloa, and G. E. Marques, "*Spin-orbit coupling and intrinsic spin mixing in quantum dots*", Phys. Rev. B **69**, 125302 (2004).

6. M. Valín-Rodríguez, A. Puente, and L. Serra, "*Spin splitting and precession in quantum dots with spin-orbit coupling: The role of spatial deformation*", Phys. Rev. B **69**, 085306 (2004).

7. S. Weiss and R. Egger, "*Path-integral Monte Carlo simulations for interacting few-electron quantum dots with spin-orbit coupling*", Phys. Rev. B **72**, 245301

(2005).

8.   G. A. Intronati, P. I. Tamborenea, D. Weinmann, and R. A. Jalabert, "*Spin-orbit effects in nanowire-based wurtzite semiconductor quantum dots*", Phys. Rev. B **88**, 045303 (2013).

9.   J. W. Gibbs, *The Scientific Papers of J. Willard Gibbs, Volume 1*, Longmans, Green and Company (1906).at <https://books.google.com/books?id=uaU5AQAAMAAJ&pgis=1>

10.   A. Emperador, E. Lipparini, and F. Pederiva, "*Role of spin-orbit interaction in the chemical potential of quantum dots in a magnetic field*", Phys. Rev. B **70**, 125302 (2004).

11.   S. M. Reimann and M. Manninen, "*Electronic structure of quantum dots*", Rev. Mod. Phys. **74**, 1283 (2002).

12.   C. W. J. Beenakker, "*Theory of Coulomb-blockade oscillations in the conductance of a quantum dot*", Phys. Rev. B **44**, 1646 (1991).

13.   T. H. Oosterkamp, J. W. Janssen, L. P. Kouwenhoven, D. G. Austing, T. Honda, and S. Tarucha, "*Maximum-Density Droplet and Charge Redistributions in Quantum Dots at High Magnetic Fields*", Phys. Rev. Lett. **82**, 2931 (1999).

14.   D. . Austing, Y. Tokura, S. Tarucha, T. . Oosterkamp, J. . Janssen, M. W. . Danoesastro, and L. .

Kouwenhoven, "*Vertical quantum dots at high magnetic fields beyond the few-electron limit*", Phys. E Low-dimensional Syst. Nanostructures **6**, 358 (2000).

15. M. Ciorga, A. Wensauer, M. Pioro-Ladriere, M. Korkusinski, J. Kyriakidis, A. S. Sachrajda, and P. Hawrylak, "*Collapse of the spin-singlet phase in quantum dots.*", Phys. Rev. Lett. **88**, 256804 (2002).

16. R. Ashoori, H. Stormer, J. Weiner, L. Pfeiffer, S. Pearton, K. Baldwin, and K. West, "*Single-electron capacitance spectroscopy of discrete quantum levels.*", Phys. Rev. Lett. **68**, 3088 (1992).

17. G. J. Iafrate, K. Hess, J. B. Krieger, and M. Macucci, "*Capacitive nature of atomic-sized structures*", Phys. Rev. B **52**, 10737 (1995).

18. M. A. Kastner, "*Artificial Atoms*", Phys. Today **46**, 24 (1993).

19. S. Bandyopadhyay and H. S. Nalwa, *Quantum dots and nanowires*, American Scientific Publishers (2003).at <https://books.google.com/books?id=5yVTAAAAMAAJ&pgis=1>

20. M. Wagner, U. Merkt, and A. V. Chaplik, "*Spin-singlet–spin-triplet oscillations in quantum dots*", Phys. Rev. B **45**, 1951 (1992).

21. D. Pfannkuche, V. Gudmundsson, and P. A. Maksym, "*Comparison of a Hartree, a Hartree-Fock, and an exact*

treatment of quantum-dot helium", Phys. Rev. B **47**, 2244 (1993).

22. M. Bayer, V. B. Timofeev, T. Gutbrod, A. Forchel, R. Steffen, and J. Oshinowo, "*Enhancement of spin splitting due to spatial confinement in In x Ga 1 − x As quantum dots*", Phys. Rev. B **52**, R11623 (1995).

23. L. Besombes, Y. Léger, L. Maingault, D. Ferrand, H. Mariette, and J. Cibert, "*Probing the spin state of a single magnetic ion in an individual quantum dot.*", Phys. Rev. Lett. **93**, 207403 (2004).

24. S. Prabhakar and R. Melnik, "*Electric field control of spin splitting in III–V semiconductor quantum dots without magnetic field*", Eur. Phys. J. B **88**, 273 (2015).

25. M. R. Molas, A. A. L. Nicolet, B. Pietka, A. Babinski, and M. Potemski, "*The excited spin-triplet state of a charged exciton in quantum dots*", 6 (2016).at <http://arxiv.org/abs/1602.03789>

26. J. Berezovsky, M. H. Mikkelsen, N. G. Stoltz, L. A. Coldren, and D. D. Awschalom, "*Picosecond coherent optical manipulation of a single electron spin in a quantum dot.*", Science **320**, 349 (2008).

27. E. Tsitsishvili, G. S. Lozano, and A. O. Gogolin, "*Rashba coupling in quantum dots: An exact solution*", Phys. Rev. B **70**, 115316 (2004).

28. J. Lee, H. N. Spector, W. C. Chou, and C. S. Chu,

"*Rashba spin splitting in parabolic quantum dots*", J. Appl. Phys. **99**, 113708 (2006).

29. V. M. Ramaglia, D. Bercioux, V. Cataudella, G. De Filippis, C. A. Perroni, and F. Ventriglia, "*Conductance of a large point contact with Rashba effect*", Eur. Phys. J. B - Condens. Matter **36**, 365 (2003).

30. Y. Li, C. P. Lee, S. M. Sze, and O. Tretyak, "*Electron energy state spin-splitting in 3D cylindrical semiconductor quantum dots*", Eur. Phys. J. B **28**, 475 (2002).

31. N. F. Johnson and M. Payne, "*Exactly solvable model of interacting particles in a quantum dot*", Phys. Rev. Lett. **67**, 1157 (1991).

32. M. Valín-Rodríguez, A. Puente, and L. Serra, "*Spin splitting and precession in quantum dots with spin-orbit coupling: The role of spatial deformation*", Phys. Rev. B **69**, 085306 (2004).

33. D. Sanjeev Kumar, S. Mukhopadhyay, and A. Chatterjee, "*Effect of Rashba interaction and Coulomb correlation on the ground state energy of a GaAs quantum dot with parabolic confinement*", Phys. E Low-dimensional Syst. Nanostructures **47**, 270 (2013).

34. P. Pietilainen and T. Chakraborty, "*Energy levels and magneto-optical transitions in parabolic quantum dots with spin-orbit coupling*", Phys. Rev. B **73**, 155315

(2005).

35.   B. L. Johnson and G. Kirczenow, "*Electrons in quantum dots: A comparison of interaction energies*", Phys. Rev. B **47**, 10563 (1993).

Chapter 4   Thermodynamic and magnetic properties of a parabolic quantum dot with spin-orbit interaction in the presence of an external magnetic field

4

4.1 Introduction

The pioneering work of Chakraborthy at al. [1] and Li et al. [2] highlighted that the results of the magneto-optical experiments do not depend on the electron-electron (e-e) interaction. The reason is that the IR radiation used in those experiments couples only with the center of mass motion while the e-e interaction goes entirely into the relative motion part and therefore could not be probed by IR magneto-optical experiments. In the same paper Chakraborthy et al. [1] suggested that the effect of e-e interaction in parabolic quantum dots would show up in thermodynamic quantities. In the present chapter we shall investigate some of the thermodynamic

and temperature-dependent magnetic properties of a quantum dot. To be specific, we shall study magnetization, susceptibility, heat capacity and entropy of a parabolic quantum dot. We investigate all these quantities incorporating the effect of e-e interaction, RSOI and DSOI in the presence of a perpendicular magnetic field. As usual, for the e-e interaction we choose the model prescribed by Johnson and Payne. Though there have been several theoretical investigations on magnetization and susceptibility of a parabolic quantum dot, only a very few studies have reported on the heat capacity and entropy. Especially, to our knowledge, no work on the effect of SOI on heat capacity and entropy of a quantum dot has been reported so far.

The theoretical study on the magnetization of a quantum dot started with the work of Yigal Meir at al. [3] who have studied the magnetization, persistent current and the spin-orbit interaction effects using some solvable models in a quantum dot developed on a two dimensional electron gas (2DEG) with non-interacting electrons. Maksym and chakraborthy [4] studied the magnetization of a parabolic quantum dot with interacting electrons numerically. Chaplik et al. [5,6] have studied the thermodynamic properties of quantum dots in a magnetic field with Coulomb interaction numerically.

Voskaboynikov et al. [7] have studied the magnetization and susceptibility of a few-electron quantum dot in the presence of spin-orbit interaction neglecting the electron-electron interaction. Sheng and Xu [8] studied the magnetization of a quantum dot with interacting electrons using a numerical diagonalization method. Dias Da Silva et al. [9,10] have studied the effect of electron-electron interaction on the orbital magnetic properties of quantum dots. Chatterjee and collaborators [11–13] have studied the magnetic properties of Gaussian quantum dots. So far, to our knowledge, no studies have been conducted on the magnetic properties of quantum dots with both RSOI and DSOI in the presence of e-e interaction. The purpose of the present chapter is to make an attempt in this direction.

In the case of heat capacity calculations, Maksym and Chakraborthy [1] studied the effect of magnetic field on the heat capacity of a parabolic quantum dot without the Zeeman interaction. Boyacioglu and Chatterjee have [14] studied the heat capacity and entropy of a Gaussian quantum dot. Oh et al. [15] have studied the magnetization and heat capacity of a 3D quantum dot with e-e interaction. De Groote et al. [6] have studied the magnetization, susceptibility and specific heat of a helium-like confined quantum dot with spin-Zeeman

interaction. Muller et al. [16] have studied the heat capacity of a electron quantum dot using the Hartree-Fock approximation for the e-e interaction. Zhai et al. [17] have studied the heat capacity of 2D Boltzmann gas in an elliptical parabolic quantum dot. Gao et al. [18] have studied the effect of spin-orbit interaction on the thermodynamic properties of a 2D quantum well. Lee et al. [19,20] have studied the heat capacity of a quantum dot super lattice with Zeeman interaction. So far no investigation has been made on the effects of spin-orbit interaction (SOI) on the heat capacity and entropy of quantum dots. In the present chapter we shall present our results on the heat capacity and specific heat of a quantum incorporating the SOI.

4.2 Thermodynamic properties

We use the canonical ensemble approach to calculate the thermodynamic averages of various physical quantities. As already mentioned, we are interested in a parabolic quantum dot with RSOI, DSOI and e-e interaction in the presence of a perpendicular magnetic field. The partition function, average energy, magnetization, susceptibility, heat capacity and entropy

of the system are calculated using the following formulae.

$$Z = \sum_{N_A, N_B, \alpha_{ij}, \beta_{ij}} e^{-E(N_A, N_B, \alpha_{ij}, \beta_{ij})/k_b T} \quad ; \quad E_a$$

$$= \frac{1}{Z} \sum E e^{-E/k_b T}$$

$$M = \frac{1}{Z} \sum \left(-\frac{\partial E}{\partial B} \right) e^{-E/K_B T} \quad ; \quad \chi = \frac{\partial M}{\partial B}$$

$$C_V = \frac{\partial E_a}{\partial T} \quad ; \quad S$$

$$= \frac{\partial}{\partial T} (k_b T \ln Z)$$

where K_B is the Boltzmann constant and $E(N_A, N_B, \alpha_{ij}, \beta_{ij})$ is given by Eq. (3.1).

4.3 Numerical results and discussion

4.3.1 Energy spectrum and Average Thermodynamic Energy

For the sake of concreteness, we apply our theory to an *InAs* QD with $m^*/m_0 = 0.042$, $\varepsilon = 14.6$, $g^* = -14$, $\alpha = 20\ meV - nm$, $\beta = 20\ meV - nm$ and $\omega_0 = 7.5\ meV$. The energy spectra of a two-electron InAs QD with and without e-e interaction are presented in Fig. 4.1. The values of V_o and Ω are obtained by matching our ground state energy with the numerical results of Pietilainen and Chakraborty [21]. Here the energy levels are labeled by two quantum numbers (L, S), where L is the total orbital angular momentum and S is the total spin angular momentum of the two electron system. In the absence of applied magnetic field (B), the first excited state is six-fold degenerate. This is due to three possible spin angular momenta and two possible orbital angular momenta which can be lifted by external magnetic field due to Zeeman interaction. One can see that the magnetic field B at which the energy-level crossing occurs giving rise to singlet-triplet (s-t) transition is lower in the presence of e-e interaction than in the absence of it.
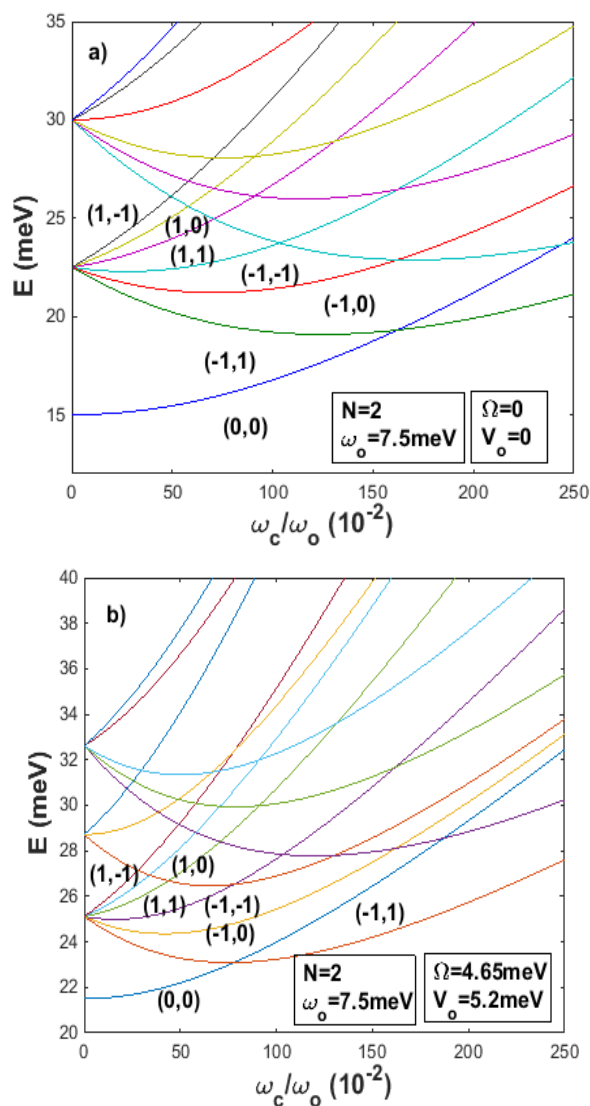
Fig. 4.1 Energy spectrum of InAs QD vs. magnetic field
(a) without e-e interaction , (b) with e-e interaction.

This transition occurs due to the interplay between confinement potential and the applied magnetic field for a finite value of g^*. The first transition occurs between states with the same value of total angular momentum $J = J_1 + J_2 = 0$ [21]. This s-t transition occurs at lower magnetic fields in the presence of e-e interaction as it is a repulsive interaction and acts against the confinement potential. If the finite width of the quantum dot along z direction is considered, the transition point shifts towards larger magnetic fields as in that case, the Coulomb interaction gets screened at smaller electron separations. Thus the effect of the third dimension can be incorporated by considering a screened Coulomb interaction. This has been observed and studied by several authors [22–24]. The effect of the third dimension for s-t transitions in two-electron quantum dots at zero temperature has been discussed first by Dineykhan and Nazmitdinov [25] where the Coulomb interaction has been treated quite accurately. Later, the effects of the third dimension and the exact electron-electron interaction on the position of the s-t transitions have been thoroughly analyzed in [26,27]. Many issues related to two-electron quantum dots have been recently reviewed by Birman et al. [28] In the present work, we take into account the effect of extension of the quantum

dot along the z-direction by choosing to work with the Johnson-Payne model [29].

The average thermodynamic energy (E_a) vs. magnetic field is plotted at different temperatures (T) in Fig. 4.2 both in the absence and presence of the e-e interaction (V_{ee}). In the case of $V_{ee} = 0$, the s-t transition shows a peak structure. It is also evident that the s-t transition occurs at a lower value of B for $V_{ee} \neq 0$ and is also sharper. As T increases, the sharpness of the peak decreases.
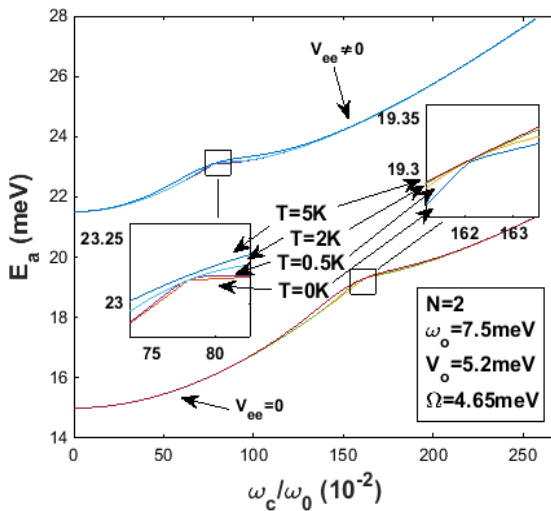
Fig. 4.2 Average thermodynamic energy as a function of the magnetic field with and without e-e interaction.

4.3.2 Magnetization and Susceptibility

The variation of the magnetization (M) as a function of B at various values of T is shown in Fig. 4.3(a) with and without e-e interaction. In the case of $B = 0$, since the electrons pair up in the ground state, $M = 0$. As B increases, M decreases (or $|M|$ increases) till B reaches a critical value at which the s-t transition takes places. At this critical field, M undergoes a rapid increase in its value and after that it decreases monotonically as B is further increased. At $T = 0\,K$, the change in M at the critical B is discontinuous, while at $T \neq 0$, though the change is still rapid but it is continuous. The jump in M at the s-t transition is smaller for $V_{ee} \neq 0$. At very large B, M is larger for the case $V_{ee} = 0$ than for $V_{ee} \neq 0$. In Fig. 4.3(b), we plot the corresponding susceptibility (χ) as a function of B at different T values for $V_{ee} = 0$ and $V_{ee} \neq 0$. At low B, χ is negative i. e., the system is diamagnetic. As B increases, at a certain B, the system turns paramagnetic. At $T = 0$, this transition is accompanied with the s-t transition and it occurs at a particular value of B. At higher T, first the diamagnetism-paramagnetism (d-p) transition
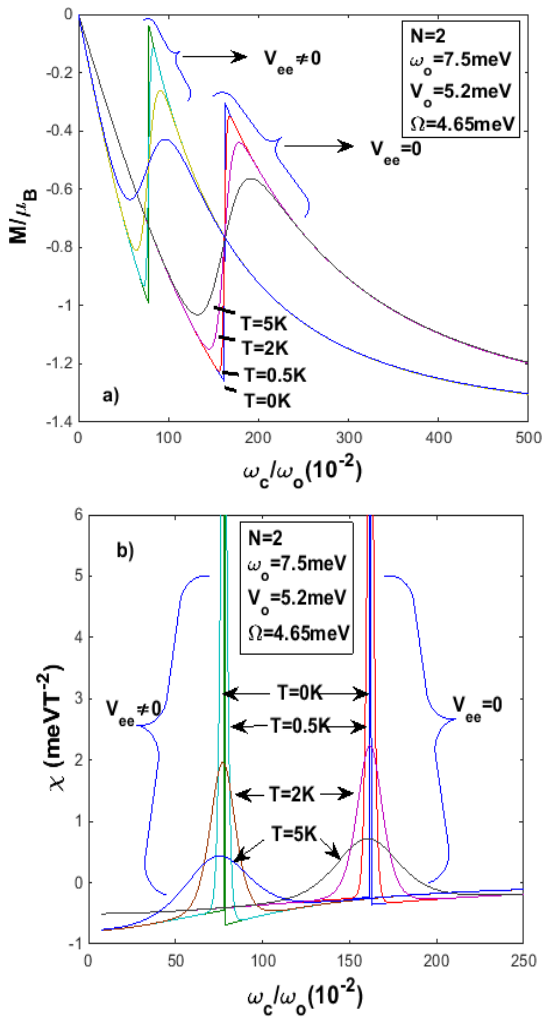
Fig. 4.3 (a) Magnetization (M) vs. ω_c at different temperatures (T) with and without V_{ee}. (b) Susceptibility (χ) vs. ω_c at different T with and without V_{ee}.

takes place at a lower B at which the s-t transition also starts and as B is increased further, the s-t transition becomes complete. Once the system enters into the fully triplet state, a further increase in B increases only the diamagnetic susceptibility and consequently, above this field the total susceptibility decreases with increasing B and subsequently at another critical field a re-entrant paramagnetic-diamagnetic (p-d) transition occurs. The width and height of the paramagnetic peaks decrease with both T and V_{ee}.

The variation of χ with T at different B is presented in Fig. 4.4(a) for $V_{ee} = 0$ and in Fig. 4.4(b) for $V_{ee} \neq 0$. Let us first discuss the case for $V_{ee} = 0$. At small values of B, the paramagnetic contribution is negligible while the diamagnetic effect dominates and therefore the system will be in a diamagnetic state. As B increases, the paramagnetic effect sets in and χ increases as the same T unless T is very large. In general, as T increases, thermodynamic fluctuations increase and the

diamagnetism starts dominating and so at higher T, χ decreases with increasing T.

Fig. 4.4 (a) χ vs. T for $V_{ee} = 0$; (b) χ vs. T for $V_{ee} \neq 0$ at different values of B.

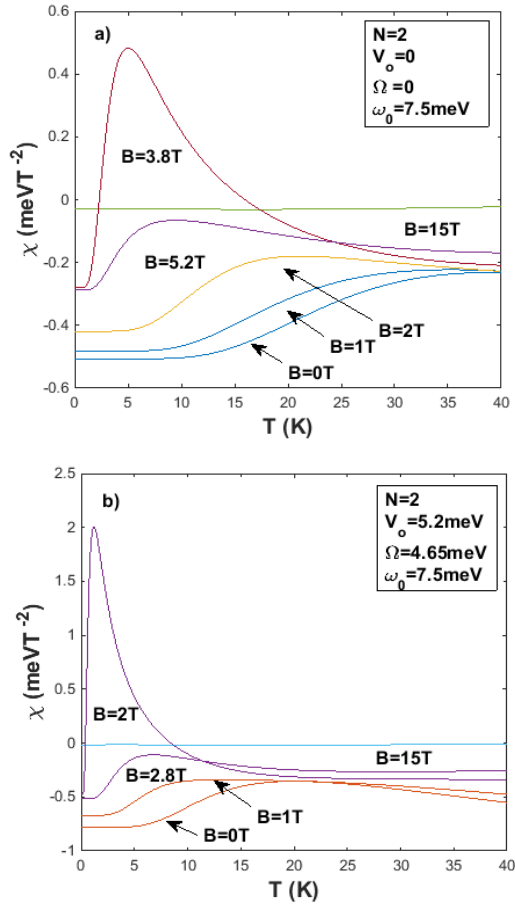Thus one can see that there exists a range of values of B for which the system will be in a paramagnetic state within certain temperature windows. As T becomes very large, χ seems to saturate to a negative constant irrespective of the value of B implying that the system becomes diamagnetic at large T as would ordinarily be expected. The situation is qualitatively similar for $V_{ee} \neq 0$. Again for a certain range of B, as T increases, χ increases and turns positive i. e., the system turns paramagnetic. However, the d-p transition is faster in the case of $V_{ee} \neq 0$.

To understand the effects of RSOI and DSOI on M and χ, it is more convenient to consider a spin-polarized system because RSOI and DSOI have similar effect on electrons with opposite spins or opposite effect on electrons with same spin. Here we consider a two-electron QD with spin-polarized states. The variation of M of the spin-polarized system as a function of B at various T is shown in Fig. 4.5(a) with and without e-e interaction. Since the system is polarized, there is a non-zero value of M at $T = 0$ and $B = 0$. In this case, the system is completely in a paramagnetic state with maximum possible M. As T increases, there will be a drop in the paramagnetic part of M due to the fluctuations in the polarized state by thermal agitations.
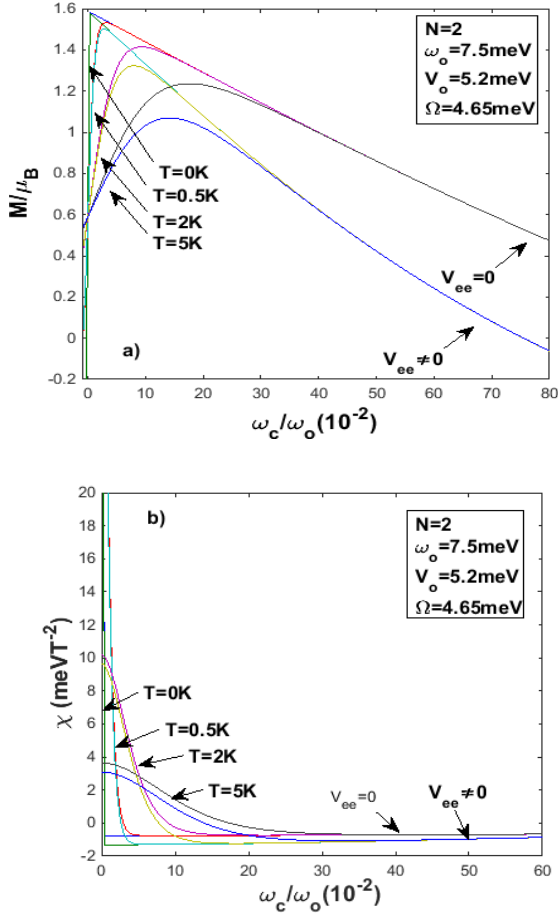
Fig. 4.5 (a) M vs. ω_c , (b) χ vs. ω_c , at different T with and without V_{ee} for a spin-polarized system.

The system still paramagnetic below a certain magnetic depending on T. In the paramagnetic phase, **M** increases with B up to a certain critical value at which the d-p

transition takes place. After this M decreases with B. As T increases, the height of the paramagnetic peak reduces and its position shifts towards larger B. One can also observe that the paramagnetic peaks are lowered by the e-e interaction. As B becomes very large, M becomes independent of the T and at very low B, M becomes independent of the e-e interaction. In Fig. 4.5(b), we plot the corresponding χ as a function of B at different T values for $V_{ee} = 0$ and $V_{ee} \neq 0$. Since the system is completely polarized, an increase in B increases only the diamagnetic susceptibility and consequently, total χ decreases with increasing B. At T increases, the paramagnetic part of χ decreases due to thermal agitations and so the overall χ decreases. At a finite T and B, there would be competition between diamagnetic and paramagnetic effects. Thus, for a certain range finite of B, χ increases with T as the system still remains in the paramagnetic phase. Finally at very large B, χ saturates to a negative value and the system becomes diamagnetic.

In Fig. 4.6(a), we show the variation of M as a function of B for nonzero α, β and with and without V_{ee}. The plot shows that in the diamagnetic region, while V_{ee} reduces M, both RSOI and DSOI enhance it, DSOI having a stronger effect. In the paramagnetic region, RSOI shifts the curve towards higher B and DSOI shifts it to lower B.
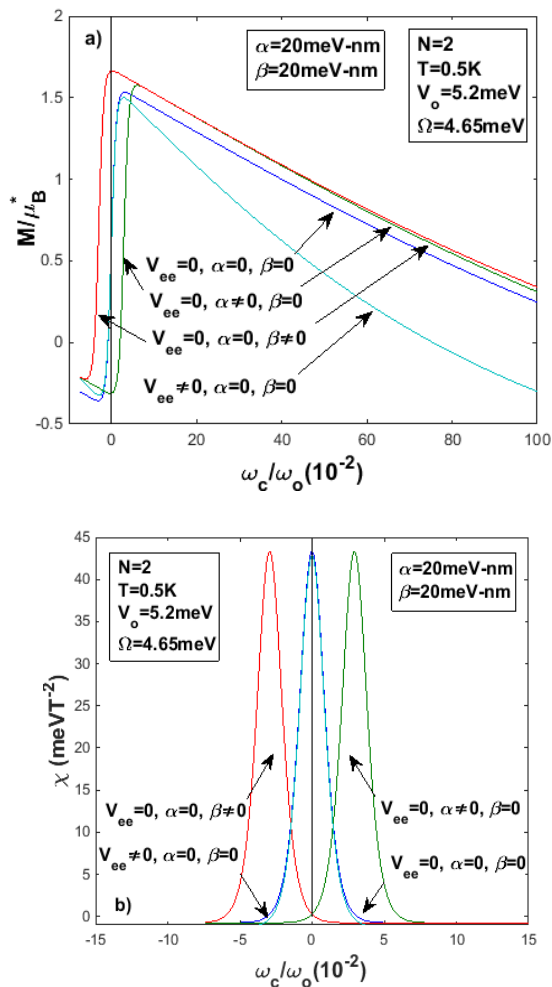
Fig. 4.6 (a) Magnetization (b) Susceptibility with pure RSOI, pure DSOI, pure e-e interaction and with no interaction vs. ω_c

This implies that DSOI lowers the critical B for the p-d transition and RSOI increases it. The e-e interaction does not have much effect in the paramagnetic region. Both RSOI and DSOI increase the height of the paramagnetic peak. In the diamagnetic region, the e-e interaction reduces M. The variation of χ of a two-electron spin-polarized system with RSOI, DSOI and V_{ee} is presented in Fig. 4.6 (b). The figure shows that DSOI shifts the p-d transition towards lower B, while RSOI shifts it towards higher B. Apart from that both the curves are qualitatively identical.

The variation of M as a function of T at $B = 0$ with RSOI, DSOI and V_{ee} is presented in Fig. 4.7 (a). The figure shows that at $T = 0$ and $B = 0$, RSOI lowers the magnetization and DSOI increases it. In the absence of SOI, there is a finite M at $T = 0$ and $B = 0$ as the system is spin-polarized. As the T increases more and more, M reaches a saturation value in all the cases. M with $V_{ee} \neq 0$ is found to be little higher compared to the case with $V_{ee} = 0$ at very large T. The variation of χ as a function of T for a system with RSOI, DSOI and V_{ee} is presented in Fig. 4.7 (b). The figure shows that the T-dependence of the paramagnetic peaks is same for RSOI and DSOI. At $B = 0$, the paramagnetic peak in the presence of SOI is lower than that in the absence of it.
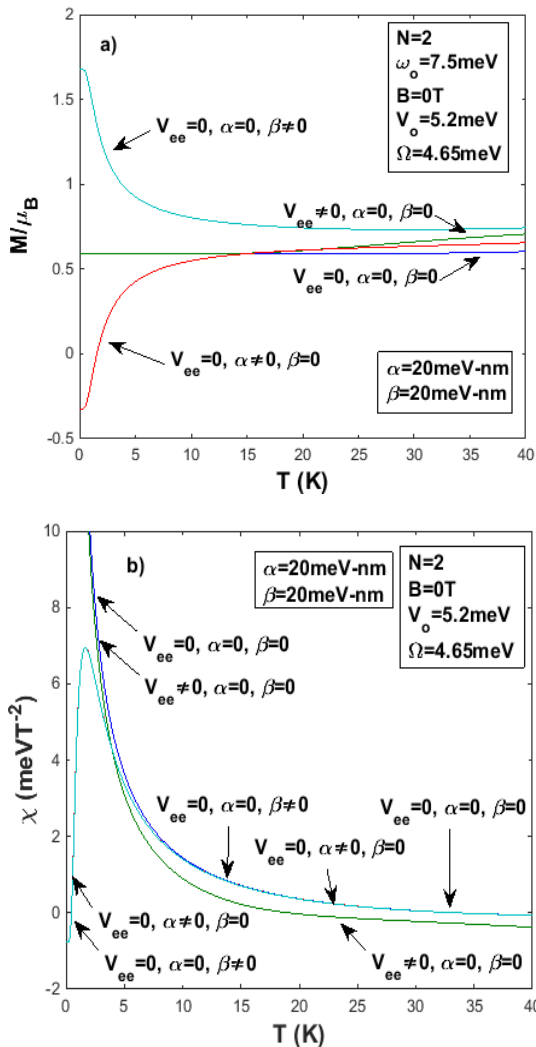
Fig. 4.7 (a) Magnetization; (b) Susceptibility vs. T with only RSOI, only DSOI, only e-e interaction and with no interaction.

As T increases, χ turns $-ve$. In the diamagnetic regime, the magnetization with RSOI and DSOI approaches to that without V_{ee}. In the diamagnetic regime, the system with $V_{ee} \neq 0$ has even lower χ compared to the other cases. As $T \to 0$, the χ of the system without SOI approaches infinity and falls to zero at $T = 0$.

4.3.3 Heat capacity and Entropy

To study the nature of heat capacity and entropy we first plot of energy spectrum with and without e-e interaction as shown in Figs. 4.8 (a, b). Here the ground state of electron at zero applied field is a singlet and the first excited state is a triplet. As the applied magnetic field strength increases from zero, the singlet state energy increases and the triplet state energy decreases and at a critical field, the ground state shifts from singlet to triplet. Ie; there will be a transition from singlet state to triplet state. This occurs due to the interplay between the confinement potential and the applied magnetic field for a finite value of g. The plots clearly show that the e-e interaction makes the singlet triplet transition to occur at lower magnetic field strength.
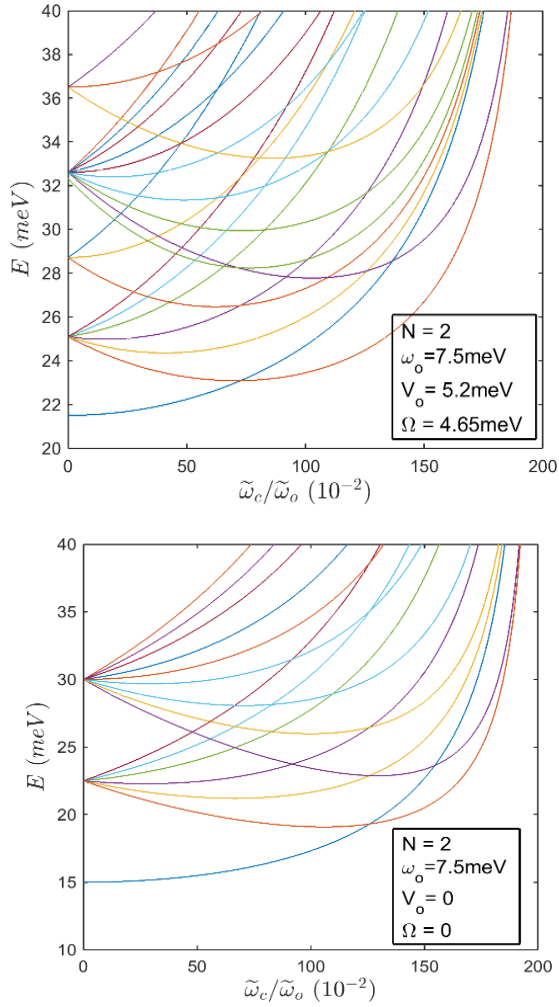
Fig. 4.8 Energy spectrum a) with and b) without e-e interaction.

The thermodynamic average energy E_a as a function of magnetic field for various temperatures is presented in Figure 4.9. This shows that the singlet-triplet transition occurs at lower magnetic field strength in the presence of e-e interaction and the peak is sharper in the absence of it. The sharpness of the peak decreases with temperature.
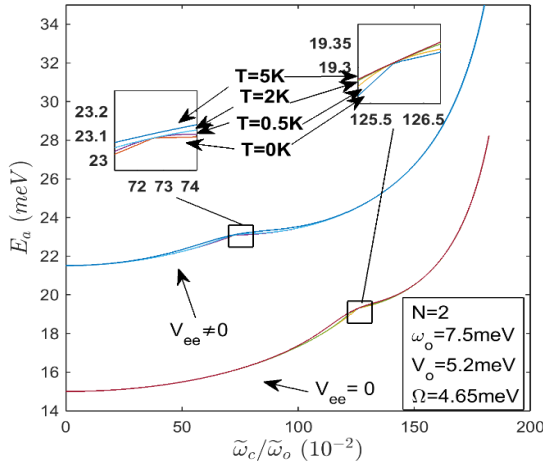
Fig. 4.9 Average thermodynamic energy Vs. magnetic field with and without e-e interaction.

The heat capacity of a two-electron quantum dot with and without e-e interaction is presented in Fig. 4.10 for various temperatures. The heat capacity as a function of magnetic field shows a peak structure wherever the two energy levels are close enough to show Schottky anomaly. A sudden rise in heat capacity is observed when the thermal energy is comparable to the energy

level separation. At the transition point, heat capacity falls as the energy level separation is zero which causes no state change.
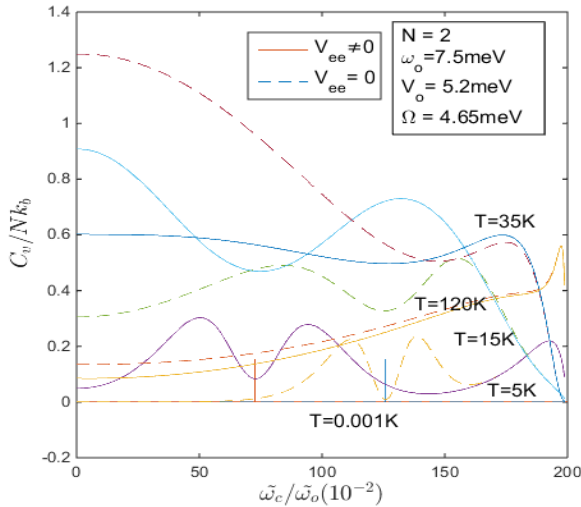
Fig. 4.10 Heat capacity Vs. magnetic field with and without e-e interaction.

Therefore, both before the singlet-triplet transition point and immediately after the transition point, a peak in the heat capacity is observed. At $T = 0.001K$ a double peak structure with negligibly small width is observed. At $T = 5K$, one more peak is observed in the heat capacity at larger magnetic fields, where the separation between the energy levels again becomes comparable to the thermal energy. The e-e interaction shifts the double

peak structure in the heat capacity towards lower magnetic fields and also makes the peak shorter and wider. At very large magnetic fields, there is no apparent difference in the heat capacity with and without e-e interactions. At low temperatures, the e-e interaction in general raises the heat capacity while at very high temperatures, it reduces the heat capacity. As temperature increases, the first peak becomes wider and shorter and at a sufficiently high temperature it disappears. i. e., the system becomes more triplet like as temperature increases. Beyond this temperature the heat capacity gradually falls to zero. At larger temperatures and large magnetic fields, a peak is always observed as at the large field regime, some energy level separation will be equal to the thermal energy resulting in the transition similar to Schottky anomaly.

A study of behavior of entropy with and without e-e interaction as a function of magnetic field for various temperatures is shown in Fig 4.11. At zero temperature and zero applied field, entropy is found to be zero. At the transition point of singlet-triplet transition, entropy increases and after the transition, entropy again falls back to zero. This is an obvious consequence of Schottky anomaly in the heat capacity behavior as a function of magnetic field. Finally, at very large magnetic fields,

entropy approaches $Nk_b \ln(3/2)$ which is same as the entropy of a diatomic molecule.
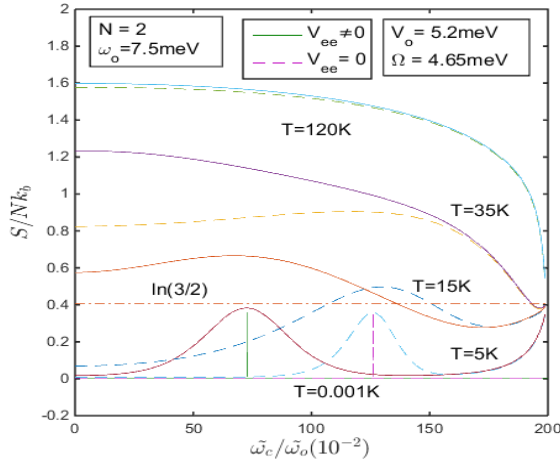
Fig. 4.11 Entropy Vs. magnetic field a) with and b) without e-e interaction.

As temperature increases, entropy increases. However, at a large magnetic field, the entropy saturates as the system becomes fully ordered. The e-e interaction raises the entropy peak in the low temperature regime while at the higher temperatures it reduces the value of the entropy in general. However, in the high field regime, the entropy curves with and without e-e interaction merge with each other.

A study of the variation of heat capacity with and without e-e interaction as a function of temperature for various magnetic field strengths is presented in Fig. 4.12.
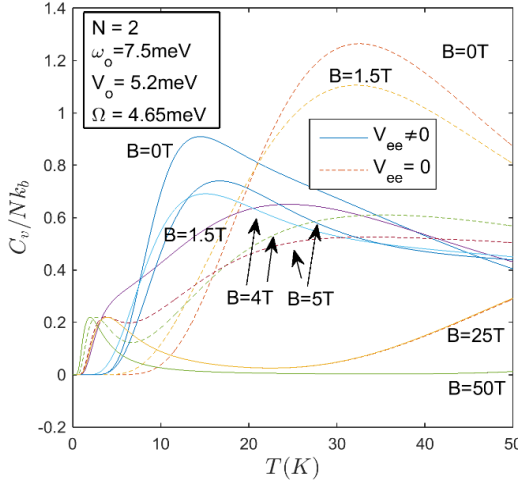
Fig. 4.12 Heat capacity Vs Temperature, with and without e-e interaction.

At zero applied field and low temperatures, heat capacity remains zero up to certain critical temperature, beyond which the system absorbs heat resulting in a Schottky peak. With e-e interaction on, the peak shifts to lower temperatures in the low field regime as the magnetic field brings the singlet, triplet energy levels closer which results in a Schottky peak at lower temperatures. Similar effect is observed with an increment in the applied magnetic field. In the high field regime, e-e interaction has no effect on the heat capacity at high temperature.

Also at high temperature and high applied field, heat capacity falls to zero as system will be mostly in triplet like state.

A plot of entropy with and without e-e interaction as a function of temperature for various magnetic field strengths is presented in Fig. 4.13. Entropy remains zero up to certain temperature and then starts increasing and at very large temperatures, saturates to a value $Nk_b \ln(3/2)$. The height of the peak decreases and the width of the peak increases with both applied magnetic field and e-e interaction. Also entropy increases from zero in the $T \to 0$ case with the applied magnetic field.
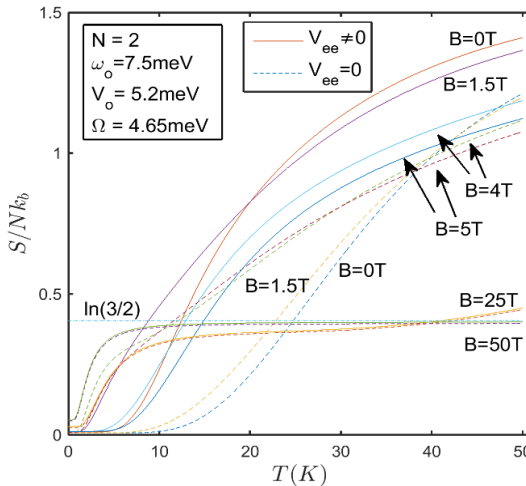
Fig. 4.13 Entropy Vs Temperature, with and without e-e interaction.

To understand the effect of SOI on the heat capacity and entropy of two electron quantum dot, it is quite convenient to consider the spin-polarized system because both RSOI and DSOI have similar effect on electrons with opposite spins and opposite effect on the electrons with same spin. In the rest of the paper, we consider a two-electron PQD with spin polarized states.

The energy spectrum of spin-polarized system with and without e-e interaction is presented in Fig. 4.14 a and Fig. 4.14 b respectively. This shows that the ground state is doubly degenerate at $B = 0$. This can be explained as follows. If the first electron is in the single-electron state $(0,0)$ where the state is labled as (N, L), N standing for principle quantum number and L for orbital angular momentum quantum number, then the second electron has to enter either $(0, +1)$ or $(0, -1)$ state as it cannot enter $(0,0)$ state due to Pauli's exclusion principle if the system is spin-polarized. This explains the degeneracy of the ground state at zero field.
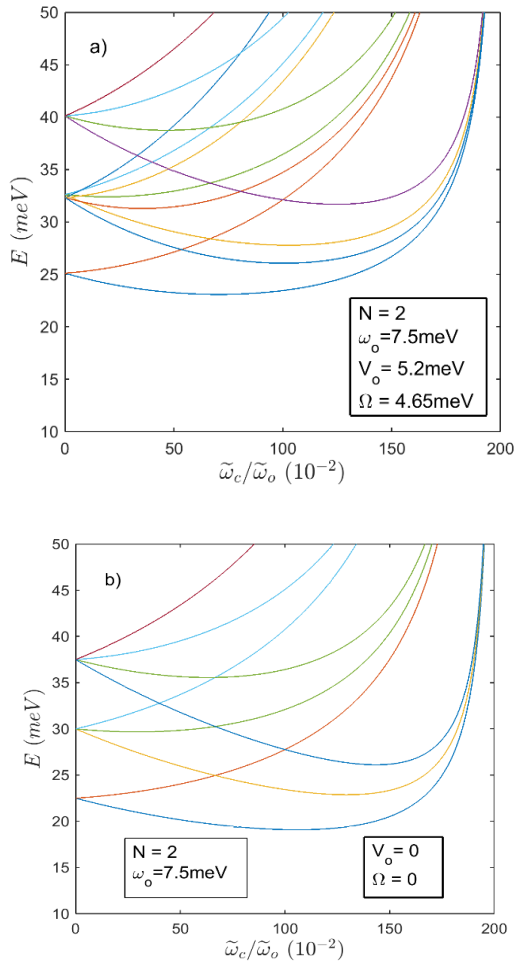
Fig. 4.14 Energy spectrum of spin polarized system a) with and b) without e-e interaction.

The heat capacity of such a system with and without e-e interaction as a function of magnetic field for various

temperatures is presented in Fig. 4.15. The plot shows a sharp peak at $B = 0$ for the $T = 0.001K$ case. As temperature lifts degeneracy of the ground state even at zero field. The height of the peak reduces and the width increases as the temperature increases.
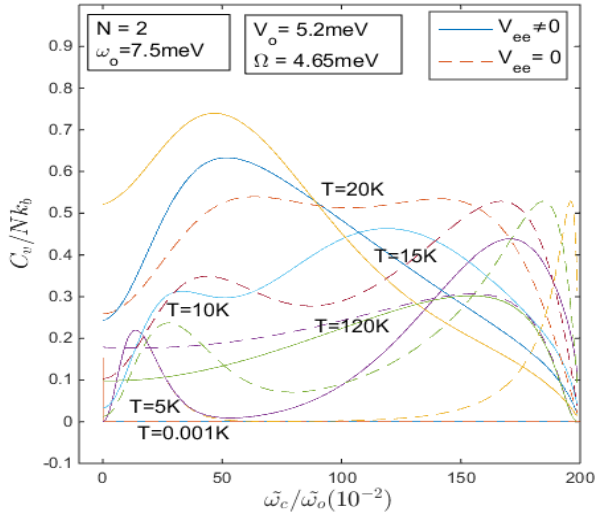
Fig. 4.15 Heat capacity vs. magnetic field with and without e-e interaction.

Also the peak shifts to larger applied fields with increase in temperature. At a very large magnetic field, one more peak is observed in the heat capacity plot which is due to the closely packed energy levels prevailing at large fields. With an increase in temperature, the height of the second peak increases and shifts to lower applied fields. At very low temperature and small applied field, the heat

capacity with e-e interaction and that without it have same value. Furthermore, at very low temperatures and low applied fields, the e-e interaction lowers the heat capacity while at very large temperatures, it enhances the heat capacity.
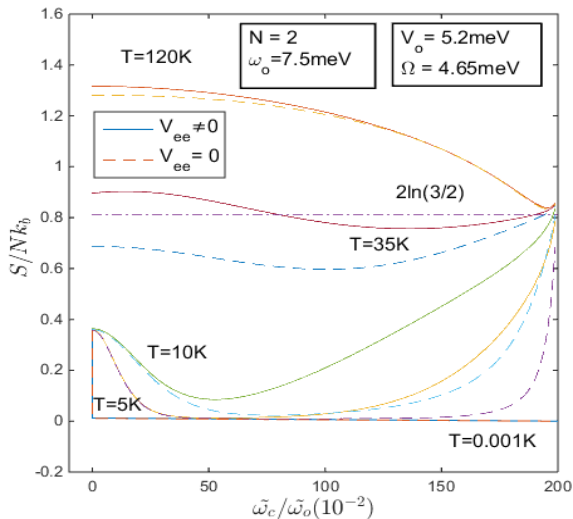
Fig. 4.16 Entropy Vs. magnetic field with and without e-e interaction.

The variation of entropy of a spin-polarized system with and without e-e interaction as a function of magnetic field for various temperatures is presented in Fig. 4.16. The plot shows that there is a sharp peak in entropy at zero applied field and $T = 0.001K$. With increasing temperature, the height of the peak reduces and the width increases and beyond a certain

temperature, the peak disappears. However, the entropy increases with temperature. As the applied magnetic field increases, the entropy asymptotically saturates to $2Nk_b \ln(3/2)$ approximately. The factor 2 arises as we have considered the spin-polarized system.

The variation of heat capacity without SOI, with RSOI and with DSOI as a function of magnetic field with e-e interaction is presented in Fig. 4.17. At very low magnetic fields and at very high magnetic fields, the heat capacity reduces with RSOI and increases with DSOI as compared to the case without both SOI. In the intermediate field strengths, the effect of RSOI and DSOI changes sign at every field strength where Schottky peak occurs. As $T \rightarrow 0$, both RSOI and DSOI have negligible effects on heat capacity. The variation of entropy with RSOI, with DSOI and without the SOI's has been compared as a function of applied magnetic field in Fig. 4.18. The plot shows that DSOI reduces the entropy and RSOI enhances the entropy of the system. As $T \rightarrow 0$, the effect of RSOI and DSOI on the entropy reduces to zero.
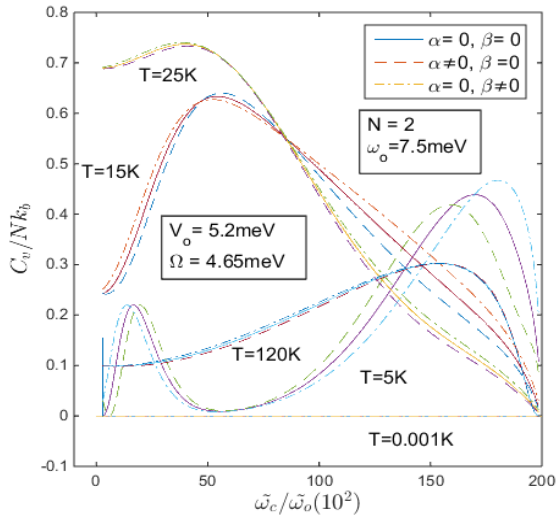
Fig. 4.17 Heat capacity Vs. magnetic field with RSOI,
DSOI and without SOI's.
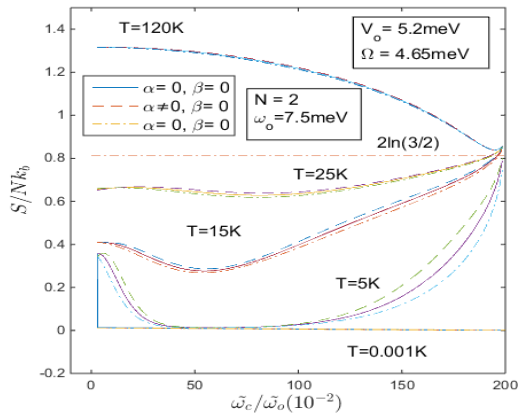
Fig. 4.18 Vs magnetic field with RSOI, DSOI and
without SOI's
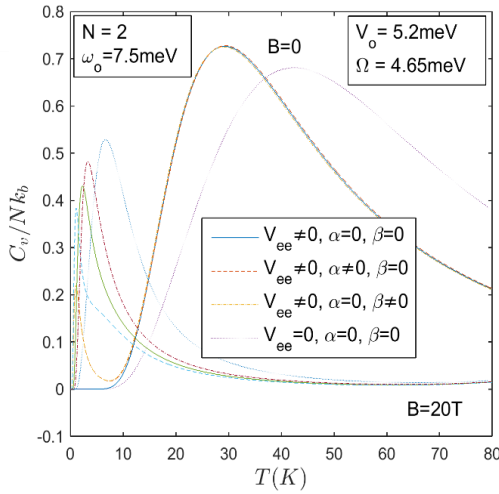
Fig. 4.19 Heat capacity Vs temperature with RSOI, DSOI, without both SOI and e-e interaction.
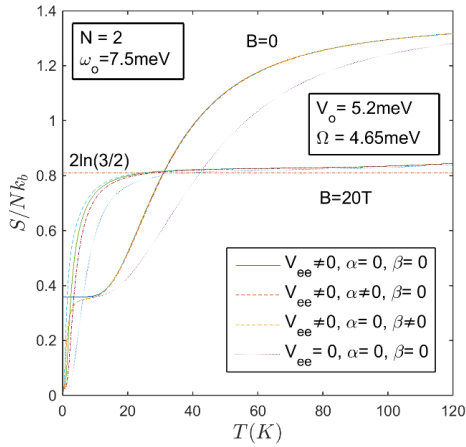
Fig. 4.20 Entropy Vs temperature with RSOI, DSOI, without both SOI and e-e interaction.

The results for the variation of heat capacity and entropy of a spin-polarized system with RSOI, with DSOI and without SOI's, in the presence and absence of an e-e interaction are presented as a function of temperature in Fig. 4.19 and 4.20. In the zero applied field case, and in the absence of SOI, the entropy remains zero up to certain range of temperature and then starts increasing. Finally at very large temperatures, heat capacity falls to zero. Similar behavior is observed both in the presence and absence of e-e interaction. In the presence of SOI, heat capacity shows a peak structure due to the zero field spin splitting. Both RSOI and DSOI have similar effect on heat capacity in the absence of applied field. In the presence of the applied field, RSOI reduces the height of the peak and shifts it to lower temperatures whereas DSOI enhances the heat capacity and shifts the peak to higher temperatures. At very large temperatures, e-e interaction has no effect on the heat capacity.

In the presence of RSOI and DSOI and the zero applied field case, entropy starts from zero and merges with that without SOI after certain temperature limit. In the presence of applied field, RSOI enhances the entropy and DSOI reduces the entropy in the low temperature regime. Finally at large temperatures, entropy with and

without e-e interaction match with each other and again that with and without SOI also match with each other.

4.4   Conclusions

The magnetization, susceptibility, heat capacity and entropy of a two-electron quantum dot with e-e interaction and with and without RSOI and DSOI have been studied as a function of B and T. It has been observed that the e-e interaction V_{ee} reduces the field required to cause the s-t transition in the magnetization plot. Furthermore, the height and width of the s-t transition peak in the magnetization plot are found to decrease with temperature. We have shown that V_{ee} has no effect in the paramagnetic region whereas it reduces both **M** and χ in the diamagnetic region. **M** and χ are unaffected by temperature in the diamagnetic region whereas the temperature reduces the height of the d-p transition peak. The RSOI shifts the d-p transition peak towards a higher value of B, whereas the DSOI shifts it towards a lower value of B. In the diamagnetic region, both RSOI and DSOI enhance the B-dependence of **M.** Similar behavior is also observed in the behavior of χ as a function of B. At $B = 0$, as $T \to 0$, **M** is $+ve$ in the presence of RSOI and is $-ve$ in the presence of DSOI. But

at larger T, SOI seems to have no effect on **M**. On the other hand, at $B = 0$ and small T, V_{ee} has no effect on **M** but at larger T, it enhances **M**. The height of the paramagnetic peak of χ as a function of T is finite In the presence of SOI, while it is infinite in the absence of SOI. χ seems to be independent of SOI at large values of T.

It has been observed that the e-e interaction shifts the peak in the magnetic behavior of heat capacity towards lower field strengths. Also it increases the width of the peak and reduces its height. But at very high magnetic fields, e-e interaction has no effect on the heat capacity. In the low field regime, e-e interaction increases with increasing temperature up to a certain temperature. Once the heat capacity reaches its maximum, thereafter, the heat capacity with e-e interaction is lower to that without e-e interaction. Heat capacity shows a peak due to Schottky anomaly as a function of temperature whose height reduces and width increases with both e-e interaction and the applied magnetic field. Entropy as a function of temperature starts from zero and saturates. RSOI and DSOI have no effect on the heat capacity at zero applied field and at any temperature. But in the nonzero field case, RSOI reduces the heat capacity and DSOI enhances the heat capacity and they have exactly the opposite effect on the entropy as a function of

magnetic field. Similar effect is observed in the case of heat capacity and entropy as a function of temperature also. In the low field regime, and as $T \to 0$, the heat capacity as a function of temperature shows Schottky anomaly due to zero-field spin splitting in the presence of RSOI and DSOI which is not observed in the absence of SOI. Thus the effect of zero-field spin splitting can be easily demonstrated by measuring heat capacity and entropy.

References

[1]   P. a. Maksym, T. Chakraborty, *Quantum dots in a magnetic field: Role of electron-electron interactions*, Phys. Rev. Lett. **65**, 108, (1990). doi:10.1103/PhysRevLett.65.108.

[2]   Q.P. Li, K. Karraï, S.K. Yip, S. Das Sarma, H.D. Drew, *Electrodynamic response of a harmonic atom in an external magnetic field*, Phys. Rev. B. **43**, 5151, (1991). doi:10.1103/PhysRevB.43.5151.

[3]   Y. Meir, O. Entin-Wohlman, Y. Gefen, *Magnetic-field and spin-orbit interaction in restricted geometries: Solvable models*, Phys. Rev. B. **42**, 8351, (1990). doi:10.1103/PhysRevB.42.8351.

[4]   P.A. Maksym, T. Chakraborty, *Effect of electron-electron interactions on the magnetization of quantum*

dots, Phys. Rev. B. **45**, 1947, (1992).
doi:10.1103/PhysRevB.45.1947.

[5]   M. Wagner, U. Merkt, A. V. Chaplik, *Spin-singlet–spin-triplet oscillations in quantum dots*, Phys. Rev. B. **45**, 1951, (1992). doi:10.1103/PhysRevB.45.1951.

[6]   J.-J.S. De Groote, J.E.M. Hornos, A. V. Chaplik, *Thermodynamic properties of quantum dots in a magnetic field*, Phys. Rev. B. **46**, 12773, (1992). doi:10.1103/PhysRevB.46.12773.

[7]   M. Governale, *Quantum dots with Rashba spin-orbit coupling.*, Phys. Rev. Lett. **89**, 206802, (2002). doi:10.1103/PhysRevLett.89.206802.

[8]   W. Sheng, H. Xu, *Quantum dots with interacting electrons: Energy spectra and magnetization*, Phys. B Condens. Matter. **256-258**, 152, (1998). doi:10.1016/S0921-4526(98)00556-0.

[9]   L.G.G. V. Dias da Silva, M.A.M. de Aguiar, *Short-range interactions in a two-electron system: Energy levels and magnetic properties*, Phys. Rev. B. **66**, 165309, (2002). doi:10.1103/PhysRevB.66.165309.

[10]   L.G.G. V. Dias da Silva, C.H. Lewenkopf, N. Studart, *Orbital magnetic properties of quantum dots: The role of electron-electron interactions*, Phys. Rev. B. **69**, 075311, (2004). doi:10.1103/PhysRevB.69.075311.

[11]   B. BOYACIOGLU, A. CHATTERJEE, *MAGNETIC*

PROPERTIES OF SEMICONDUCTOR QUANTUM DOTS WITH GAUSSIAN CONFINEMENT, Int. J. Mod. Phys. B. **26**, 1250018, (2012). doi:10.1142/S021797921250018X.

[12]   B. Boyacioglu, A. Chatterjee, *Dia- and paramagnetism and total susceptibility of GaAs quantum dots with Gaussian confinement*, Phys. E Low-Dimensional Syst. Nanostructures. **44**, 1826, (2012). doi:10.1016/j.physe.2012.05.001.

[13]   A. Boda, B. Boyacioglu, A. Chatterjee, *Ground state properties of a two-electron system in a three-dimensional GaAs quantum dot with Gaussian confinement in a magnetic field*, J. Appl. Phys. **114**, 044311, (2013). doi:10.1063/1.4816314.

[14]   B. Boyacioglu, A. Chatterjee, *Heat capacity and entropy of a GaAs quantum dot with Gaussian confinement.*, J. Appl. Phys. **112**, 83514, (2012). doi:10.1063/1.4759350.

[15]   J.H. Oh, K.J. Chang, G. Ihm, S.J. Lee, *Electronic structure of three-dimensional quantum dots in tilted magnetic fields*, Phys. Rev. B. **50**, 15397, (1994). doi:10.1103/PhysRevB.50.15397.

[16]   H. Müller, S. Koonin, *Phase transitions in quantum dots.*, Phys. Rev. B. Condens. Matter. **54**, 14532, (1996). doi:10.1103/PhysRevB.54.14532.

[17]   Z.-Y. Zhai, Y.-Q. Li, X.-Y. Pan, *Effects of anisotropy and magnetic fields on the specific heat of a quasi-two-dimensional Boltzmann gas in an elliptical parabolic quantum dot*, Chinese Phys. B. **21**, 070506, (2012). doi:10.1088/1674-1056/21/7/070506.

[18]   F. Gao, D.J.D. Beaven, J. Fulcher, C.H. Yang, Z. Zeng, W. Xu, C. Zhang, *Thermodynamic properties of two-dimensional semiconductors with spin–orbit coupling*, Phys. E Low-Dimensional Syst. Nanostructures. **40**, 1454, (2008). doi:10.1016/j.physe.2007.09.039.

[19]   S.C. Lee, S.W. Kim, *Heat capacity in a quantum-dot superlattice with the Zeeman effect*, J. Korean Phys. Soc. **61**, 162, (2012). doi:10.3938/jkps.61.162.

[20]   S.C. Lee, H.S. Ahn, S.W. Kim, *Angular dependence of the heat capacity in a quantum-dot superlattice with the Zeeman effect in tilted magnetic fields*, J. Korean Phys. Soc. **65**, 792, (2014). doi:10.3938/jkps.65.792.

[21]   P. Pietilainen, T. Chakraborty, *Energy levels and magneto-optical transitions in parabolic quantum dots with spin-orbit coupling*, Phys. Rev. B. **73**, 155315, (2005). doi:10.1103/PhysRevB.73.155315.

[22]   A. Kumar, S. Laux, F. Stern, *Electron states in a GaAs quantum dot in a magnetic field*, Phys. Rev. B. **42**, 5166, (1990). doi:10.1103/PhysRevB.42.5166.

[23]   P.L. McEuen, E.B. Foxman, J. Kinaret, U. Meirav, M.A.

Kastner, N.S. Wingreen, S.J. Wind, *Self-consistent addition spectrum of a Coulomb island in the quantum Hall regime*, Phys. Rev. B. **45**, 11419, (1992). doi:10.1103/PhysRevB.45.11419.

[24] M. Rontani, F. Rossi, F. Manghi, E. Molinari, *Coulomb correlation effects in semiconductor quantum dots: The role of dimensionality*, Phys. Rev. B. **59**, 10165, (1999). doi:10.1103/PhysRevB.59.10165.

[25] M. Dineykhan, R.G. Nazmitdinov, *Two-electron quantum dot in a magnetic field: Analytical results*, Phys. Rev. B. **55**, 13707, (1997). doi:10.1103/PhysRevB.55.13707.

[26] R.G. Nazmitdinov, N.S. Simonović, J.M. Rost, *Semiclassical analysis of a two-electron quantum dot in a magnetic field: Dimensional phenomena*, Phys. Rev. B. **65**, 155307, (2002). doi:10.1103/PhysRevB.65.155307.

[27] R.G. Nazmitdinov, N.S. Simonović, *Finite-thickness effects in ground-state transitions of two-electron quantum dots*, Phys. Rev. B. **76**, 193306, (2007). doi:10.1103/PhysRevB.76.193306.

[28] J.L. Birman, R.G. Nazmitdinov, V.I. Yukalov, *Effects of symmetry breaking in finite quantum systems*, Phys. Rep. **526**, 1, (2013). doi:10.1016/j.physrep.2012.11.005.

[29]   N.F. Johnson, M. Payne, *Exactly solvable model of interacting particles in a quantum dot*, Phys. Rev. Lett. **67**, 1157, (1991). http://journals.aps.org/prl/abstract/10.1103/PhysRevLett.67.1157.

5

As a part of application, we study the effect of Rashba spin-orbit interaction (RSOI) and Dresselhaus spin-orbit interaction (DSOI) in two different systems. First we study of effect of RSOI on the binding energy of D^0 center in a *GaAs* Gaussian quantum dot (GQD) (see Section 5.1) and next we study the transmission and reflection coefficients and tunneling conductance across a metal-semiconductor barrier, where semiconducting material possesses non-zero values of Rashba and Dresselhaus spin-orbit interaction constant (see Section 5.2).

5.1 RSOI on the binding energy of D^0 center in a Gaussian quantum dot

5.1.1 Introduction

The impurity states are known to have much importance in determining the electrical properties of semiconductors [1]. There are two kinds of these states, the so called donor and acceptor states. Neutral electronic energy states associated with donor impurity levels in semiconductors can sometimes be understood

by means of a hydrogen model of the impurity [2,3]. In such a case, the impurity wave function can be considered as hydrogenic wave function where the electron will have mass m^* and experience a nuclear charge of e/ε, where ε is the dielectric constant of the medium[4]. The study of donor impurity levels in quantum wells started [5] soon after the invention of semiconductor heterostructures. The first study of donor states in quantum dots (QDs) was started by Zhu [6] in 1989.

Last three decades have witnessed some extensive investigations on the subject of impurity states in semiconductor QDs [7–12]. Impurity being a rule rather than an exception, as such studies are extremely useful for their importance in the nanotechnology [13]. J. Bruning *et al.* [14] have studied the existence of infinitely many bound states below the continuous spectrum for short-range perturbations of a much larger class of the Rashba and Dresselhaus spin-orbit Hamiltonians. Li *et al.* [15] have studied the electronic states of a hydrogen donor impurity in a *GaAs/GaAlAs* Quantum Well (QW) including the Rashba spin-orbit coupling. However, to our knowledge, no investigation has been reported so far on the effect of RSOI on a donor complex in a QD with Gaussian confinement. Since we are interested in

studying the binding energy of a donor impurity in QD, we need to consider a finite well and here we choose to work with a Gaussian confinement potential [16–18].

5.1.2 Model and Formulation

According to the effective-mass theory, the Hamiltonian of a hydrogenic donor in a three–dimensional *GaAs* QD with Gaussian confinement in the presence of RSOI can be written as

$$H = H_1 + H_2 \tag{5.1}$$

with

$$H_1 = \left(\frac{\boldsymbol{p}^2}{2m^*} - \frac{e^2}{\varepsilon r} - V_0\, e^{-\frac{r^2}{2R^2}} \right) I, \tag{5.2}$$

$$H_2 = \frac{\alpha_R}{\hbar} (\boldsymbol{\sigma} \times \boldsymbol{p})_Z, \tag{5.3}$$

where the first term in Eq. (5.2) represents the electron kinetic energy, $\boldsymbol{p}$ being the electron momentum operator canonically conjugate to the electron position $\boldsymbol{r}$ (x, y, z) and m^* the effective electron mass, the second term denotes the Coulomb interaction between the electron with the donor nucleus, ε being the dielectric constant of the medium, the third term describes the Gaussian confining potential, V_0 being the depth of the potential and R the range and I is a 2×2 unit matrix. The range R may be considered to give a measure of the effective size of the QD. α_R is the RSO coupling constant and $\boldsymbol{\sigma}\ (\sigma_x, \sigma_y, \sigma_z)$ are the Pauli spin matrices. To proceed further we perform a unitary transformation on H [19] with the generator $S = (i\alpha_R m^*/\hbar^2)(y\sigma_x - x\sigma_y)$ and expand the transformed Hamiltonian in powers of

$$\tilde{H} = \left(\frac{\boldsymbol{p}^2}{2m^*} - \frac{e^2}{\varepsilon r} - V_0\, e^{-\frac{r^2}{2R^2}} - \frac{m^*}{\hbar^2}\alpha_R^2 \right) I - \frac{m^*}{\hbar^3}\alpha_R^2 \sigma_z L_z \qquad (5.4)$$

α_R and retain terms up to quadratic in α_R to obtain the Eq. (5.4); where $L_z = (xp_y - yp_x)$ is the z-component of the angular momentum. One can immediately see that the second term involving L_z commutes with the first term and since we are interested in the ground state (GS)

of the system, we can drop the second term. We seek a variational solution for the GS of D^0 in the presence of the RSOI and choose a simple trial function: $\psi(r) = Ne^{-\alpha r^2 - \beta r}$, which we expect to describe the GS of the Hamiltonian well (see Eq. 5.4). An explanation for such a choice may be in order. The potential in the Hamiltonian shown Eq. 5.4 has two pieces: one is a Gaussian potential and the other is an attractive Coulomb potential and therefore it makes sense to choose a trial wave function which is a product of a Gaussian function and an exponential function. The chosen wave function will describe the GS because it is nodeless. The variational parameters α and β will be finally obtained by minimizing the GS energy with respect to them. Throughout this chapter, we use the donor Rydberg $R_y^* = (m^* e^4 / \varepsilon^2 \hbar^2)$ as the unit of energy, and the donor Bohr radius $a_B^* = (\varepsilon \hbar^2 / m^* e^2)$ as the unit of length. Finally, however, the integrations and minimizations are done numerically. The binding energy of the D^0 centre $((E_B(D^0))$ is defined as: $E_B(D^0) = E(e^-) - E(D^0)$, where $E(D^0)$ is the GS energy of the D^0 complex in the QD, and $E(e^-)$ is the GS energy of the QD with an electron detached from the donor complex.

5.1.3 Numerical results and discussion

We apply our theory to a GaAs QD for which we take $\varepsilon = 12.4$ and $m^* = 0.06m_0$, where m_0 is the bare electron mass. Thus the energy is expressed in units of $R_y^* = 12 meV$ and the length in units of $a_B^* = 9.8\,nm$. In Fig. 5.1, we plot the GS energy of an electron in a Gaussian GaAs QD as a function of the QD size R for a few values of V_0 and α_R.

Fig. 5.1 Variation of GS energy of an electron in a Gaussian QD as a function of QD size R.
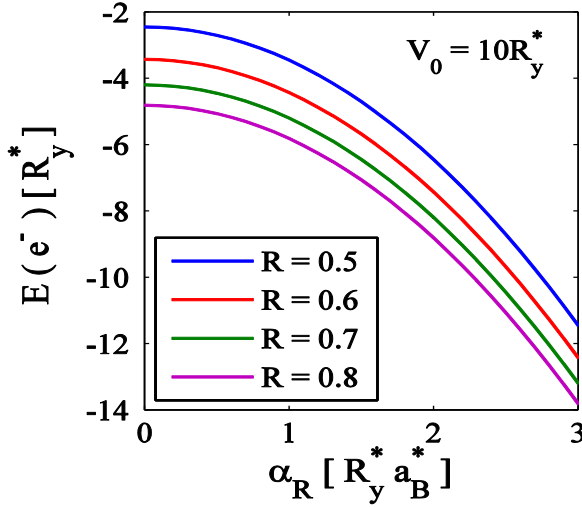
Fig. 5.2 Variation of GS energy of a D^0 complex in a GaAs QD as a function of QD size R.

In Fig. 5.2 we plot that of the D^0 complex for the same set of parameter values. To obtain the explicit $\alpha_R -$ dependence we present in Figs. 5.3 and 5.4, the GS energies of two systems as a function of α_R for different values of R. Figs. 5.3 and 5.4 show the GS energy decreases in a nonlinearly with α_R for both the systems. However, quantitatively the GS energy of a D^0 complex is lower than that of an electron for the same set of parameter values.
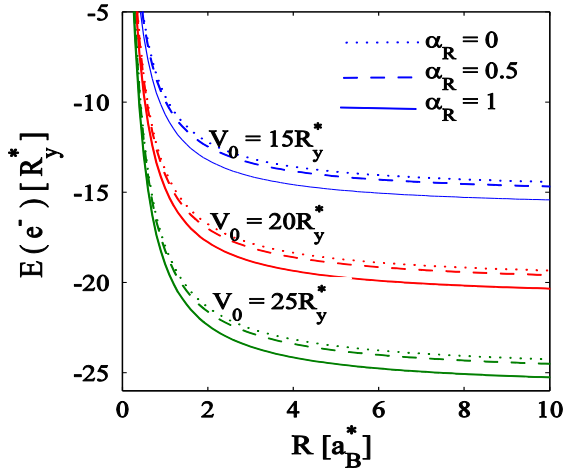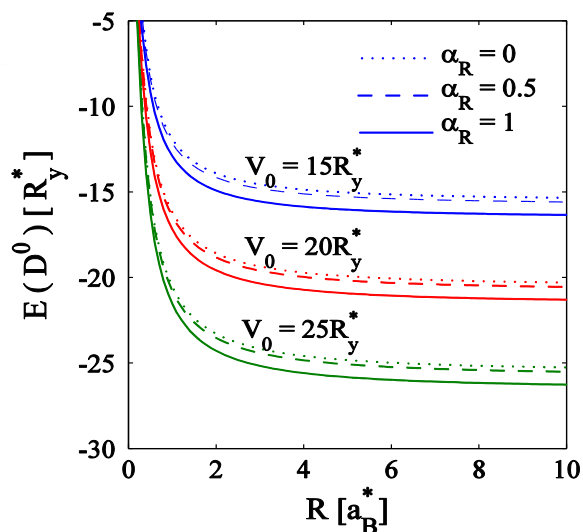
Fig. 5.3 Variation of GS energy of an electron in a
Gaussian QD as a function of α_R.
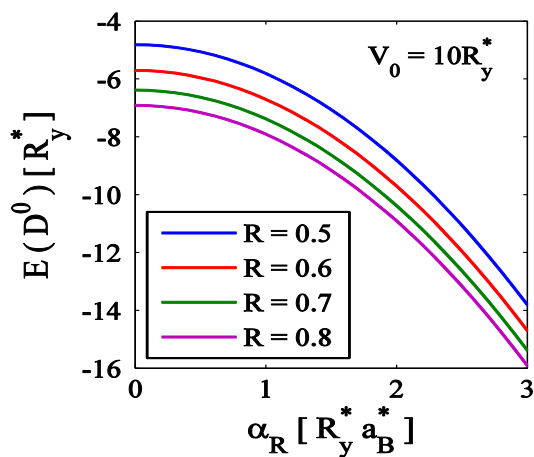
Fig. 5.4 Variation of GS energy of a D^0 centre in a
Gaussian QD as a function of α_R.

The GS binding energies of a D^0 complex system are shown in Fig. 5.5 as a function of the QD radius for two different values of the confinement potentials in the absence of RSOI. Fig. 5.5 shows that the binding energy of a D^0 complex is positive which implies that a D^0 system is a stable system. This is of course a well-known fact and arises due to the Coulomb interaction effect.

Fig. 5.5 BE of a D^0 complex in a GaAs QD
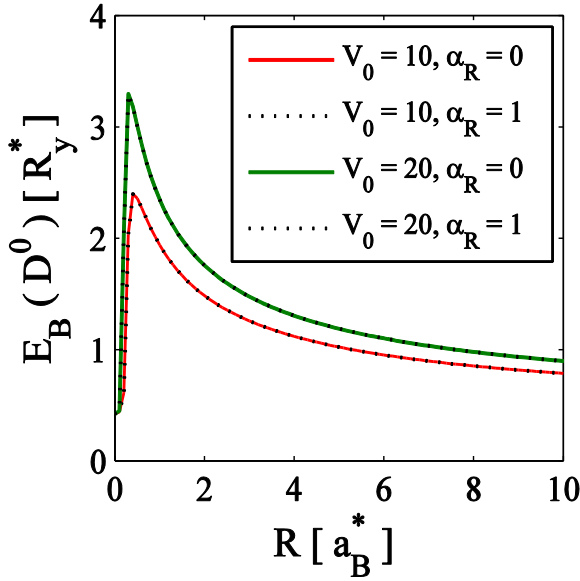
as a function of R for $\alpha_R = 0$ and $\alpha_R = 1$.

One can see that the binding energy decreases as the size of the quantum dot increases, and we find that

it finally saturates to a limiting value which is the bulk result. Since the binding energy increases as the dot size decreases from the bulk value, one can conclude that quantum confinement enhances the stability of the D^0 system. However, there seems to exist a critical confinement length (L_c) at which the stability becomes maximum and below this length the binding starts weakening very fast. The reduction in binding below L_c is purely a quantum mechanical effect. As the QD size becomes very small, the uncertainty in position also becomes very small and then the uncertainty in the momentum must become very large and concomitantly the momentum as well as the kinetic energy become very large. It then becomes difficult to keep the electron bound to the D^0 centre and as a result the binding energy falls sharply. This gives a peak in the binding energy graph. This happens when the size of the QD becomes comparable to the size of the D^0 complex. Though the peak structure is understandable from the argument of uncertainty principle, the sharpness of the peak may as well be an artefact of the approximation employed in the analysis. About the effect of the RSOI on the energies we make an interesting observation. It is evident from Figs. 5.1 and 5.3 that the spin-orbit interaction reduces the GS energies of both the electron and the D^0 centre.

Interestingly, however, the binding energy of a D^0 centre is not affected by the RSOI. This assertion remains valid even when higher-order terms of α_R are included. This can be understood in the following way: the approximate (transformed) Hamiltonian commutes with the operator L_z and therefore the energy shift due to RSOI happens to be the same for the quantum dot with and without the donor centre for the fact that the variational wave function assumes $L_z = 0$. Thus, though RSOI has an impact on the GS energies of the electron and the D^0 centre; however, it does not imply any dissociation process.

Finally we are interested in donor electron distribution which gives the probability of finding the electron at a distance r from the centre of the QD. In Fig. 5.6, we plot the donor electron distribution as a function of r for dots with different confinement lengths and a given confinement strength. It is clear that an electron becomes more and more localized with decreasing size of the QD. We furthermore find that the electron becomes more and more localized with increasing depth of the potential V_0.
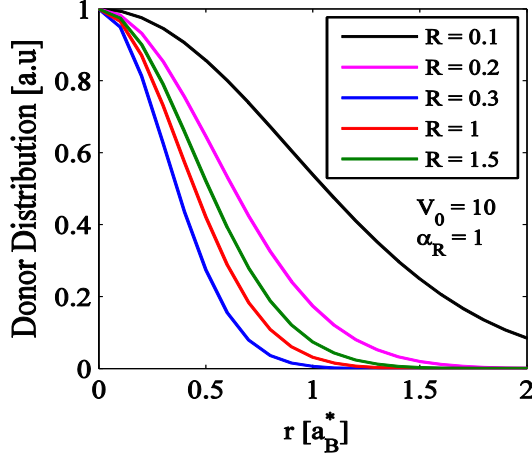
Fig. 5.6 Donor distribution in a GaAs QD with $V_0 = 10R_y^*$ and for various values of R.

One would have expected a peak structure in the donor electron distribution too, as observed in the binding energy. The donor electron distribution however shows only a maximum that saturates at $r = 0$, but no peak. It is not clear why our variational method could not capture this behaviour.

5.1.4 Conclusion

In this work, we have considered the problem of a D^0 centre in a GQD and calculated the GS energy of the electron and the D^0 centre as function of the QD radius and RSOI constant. We have shown that the GS energies

of the electron and the D^0 complex increase as the effective quantum dot size decreases and decrease as the confinement strength increases. It is also shown that with increasing RSOI constant GS energies of both the electron and the D^0 system decrease. However, the GS binding energy of the D^0 system turns out to be independent of the RSOI. Finally, we have shown the variation of the donor electron distributions as a function of the distance of the electron from the centre of the quantum dot for various QD sizes.

5.2   Tunnelling conductance across metal-semiconductor junction with SOI

5.2.1   Introduction

After the proposal of spin field effect transistor by Datta and Das [20], a new area of research evolved in the field of magneto-electronics and quantum computation [21]. The major requirement for all these experiments is a reliable source of spin-polarized electron generator. These spin-polarized electrons have majority of their applications in the field of elementary particle physics, astrophysics, nuclear physics, atomic, ionic, molecular physics, optics, condensed matter physics and surface

studies of magnetic materials [22–27]. There are different ways to achieve this spin polarization, the most general methods include ferromagnetic-metal interfaces [28] and dilute magnetic semiconductors [29]. There are also other methods that use ferromagnetic-superconducting interfaces [30,31] to achieve the same. Studies on grapheme-based [32–34] spin filters are still in their infancy; nevertheless, spin filters developed using hetero- structures have their own advantages. High quality hetero-structures can be easily prepared with the currently available fabrication techniques. Besides, in semiconductor hetero-structures there are no stray magnetic fields which may cause undesirable effects on the spin-polarized electrons. The theoretical study to exploit the SOI effects in spin-filtering applications started with the works of Koga *et al.* [35] and further extended by several authors to apply it to the transmission and reflection of electrons across ferromagnetic/semiconductor/ferromagnetic interfaces [36–40].

In our study we have extended the proposal of Khodas *et al.* [41], Zhang and Dargys [42–45] for the transmission and reflection of electrons across a metal-semiconductor junction [46–51] where the semiconductor material is a semi-infinite two

dimensional electron gas (2DEG) with a non-zero RSOI and DSOI.

5.2.2 The model

We consider an infinite 2D system in an XY-plane, where the metallic 2D lead and a semiconductor system with spin-orbit interactions occupy the $x < 0$ and $x > 0$ regions respectively. The two regions are separated by a flat interface at $x = 0$. The Hamiltonian of the system is given by

$$H = H_{\text{I}} + H_{\text{II}} \tag{5.4}$$

where

$$H_{\text{I}} = \frac{p_x^2}{2m} + \frac{p_y^2}{2m} \quad for \; -\infty \leq x < 0 \tag{5.5}$$

$$H_{\text{II}} = \frac{p_x^2}{2m} + \frac{p_y^2}{2m} + \frac{\alpha}{\hbar}\left(\sigma_y p_x - \sigma_x p_y\right) + \frac{\beta}{\hbar}\left(\sigma_y p_y - \sigma_x p_x\right)$$
$$+ V_o \quad for \quad 0 \leq x \leq \infty. \tag{5.6}$$

The corresponding Schrodinger equation is written as

$$H_I \psi_I = E\psi_I \quad ; \quad H_{II}\psi_{II} = E\psi_{II} \tag{5.7}$$

where the wave functions ψ_I and ψ_{II} are chosen such that

$$\psi_I(0, y) = \psi_{II}(0, y) \tag{5.8}$$

$$\left. \frac{\partial}{\partial x}\psi_I(x, y)\right|_{x=0} = \left.\frac{\partial}{\partial x}\psi_{II}(x, y)\right|_{x=0} \tag{5.9}$$

Let the wave function in region II be

$$\psi_{II} = A_{II}e^{i(k_x x + k_y y)} + B_{II}e^{-i(k_x x - k_y y)} \tag{5.10}$$

This leads to

$$\left[\frac{\hbar^2}{2m}k^2 + \alpha\left(\sigma_y k_x - \sigma_x k_y\right) + \beta\left(\sigma_y k_y - \sigma_x k_x\right)\right]A_{II}$$
$$+ V_0 A_{II} = E A_{II} \tag{5.11}$$

$$\left[\frac{\hbar^2}{2m}k^2 - \alpha(\sigma_y k_x + \sigma_x k_y) + \beta(\sigma_y k_y + \sigma_x k_x)\right]B_{\text{II}}$$
$$+ V_0 B_{\text{II}} = E B_{\text{II}} \qquad (5.12)$$

Eq. (5.11) can be written in a matrix form as

$$\begin{bmatrix} \epsilon_k & (-\alpha k_y - \beta k_x) - i(\alpha k_x + \beta k_y) \\ -(\alpha k_y + \beta k_x) + i(\alpha k_x + \beta k_y) & \epsilon_k \end{bmatrix} \begin{bmatrix} A_{\text{II}}^{(1)} \\ A_{\text{II}}^{(2)} \end{bmatrix}$$
$$= E' \begin{bmatrix} A_{\text{II}}^{(1)} \\ A_{\text{II}}^{(2)} \end{bmatrix} \qquad (5.13)$$

where $E' = E - V_o$. With the definitions $\gamma_k = \alpha k_y + \beta k_x = (\alpha \sin \theta_k' + \beta \cos \theta_k')k$, $\delta_k = \alpha k_x + \beta k_y = (\alpha \cos \theta_k' + \beta \sin \theta_k')k$,

we obtain

$$\gamma_k^2 + \delta_k^2 = k^2[(\alpha \sin \theta_k' + \beta \cos \theta_k')^2 + (\alpha \cos \theta_k' + \beta \sin \theta_k')^2]$$
$$= k^2[\alpha^2 + \beta^2 + 4\alpha\beta \sin \theta_k' \cos \theta_k'],$$

so that Eq. (5.11) becomes

$$\begin{bmatrix} E' - \epsilon_k & \gamma_k + i\,\delta_k \\ \gamma_k - i\,\delta_k & E' - \epsilon_k \end{bmatrix} \begin{bmatrix} A_{\text{II}}^{(1)} \\ A_{\text{II}}^{(2)} \end{bmatrix} = 0 \qquad (5.14)$$

The eigenvalues E' are given by

$$E'_{k^+} = \epsilon_{k^+} + k^+ \sqrt{\alpha^2 + \beta^2 + 4\alpha\beta \sin\theta'_{k^+} \cos\theta'_{k^+}} \qquad (5.15)$$

$$E'_{k^-} = \epsilon_{k^-} - k^- \sqrt{\alpha^2 + \beta^2 + 4\alpha\beta \sin\theta'_{k^-} \cos\theta'_{k^-}} \qquad (5.16)$$

Using the definitions

$$\phi_k = \tan^{-1}\frac{\delta_k}{\gamma_k} = \tan^{-1}\left(\frac{\alpha\cos\theta'_k + \beta\sin\theta'_k}{\alpha\sin\theta'_k + \beta\cos\theta'_k}\right)$$

$$\lambda(\theta'_k) = \sqrt{\alpha^2 + \beta^2 + 4\alpha\beta \sin\theta'_k \cos\theta'_k}$$

one can write

$$\gamma_k + i\,\delta_k = \sqrt{\gamma_k^2 + \delta_k^2}\, e^{i\phi_{k^+}} \quad ; \quad \gamma_k - i\,\delta_k = \sqrt{\gamma_k^2 + \delta_k^2}\, e^{-i\phi_{k^-}}$$

and thus we may rewrite Eq.(5.15) and Eq.(5.16) as

$$k^+$$

$$= -\frac{m}{\hbar^2}\lambda\big(\theta'_{k^+}\big) + \sqrt{\left(\frac{m\lambda(\theta'_{k^+})}{\hbar^2}\right)^2 + \frac{2m}{\hbar^2}(E_{k^+} - V_0)} \qquad (5.17)$$

$$\text{for } k^+ > 0$$

$$k^- = \frac{m}{\hbar^2}\lambda(\theta'_{k^-}) + \sqrt{\left(\frac{m\lambda(\theta'_{k^-})}{\hbar^2}\right)^2 + \frac{2m}{\hbar^2}(E_{k^-} - V_0)} \qquad (5.18)$$

Since there is no reflection in semiconductor region, one can write

$$B_{\mathrm{II}}^{(1)} = B_{\mathrm{II}}^{(2)} = 0$$

and

$$\psi_{\mathrm{II}}(x,y) = \Bigg[A_{\mathrm{II}}^{(1)} \begin{bmatrix} 1 \\ -e^{-i\phi_{k^+}} \end{bmatrix} e^{ik_x^+ x}$$
$$+ A_{\mathrm{II}}^{(2)} \begin{bmatrix} e^{i\phi_{k^-}} \\ 1 \end{bmatrix} e^{ik_x^- x} \Bigg] e^{ik_y y} \qquad (5.19)$$

The energy eigenvalue in region I is given by

$$E = \frac{\hbar^2}{2m}\left(k_x^2 + k_y^2\right) = \frac{\hbar^2 k^2}{2m} \tag{5.20}$$

and the wave function in region I is given by

$$
\begin{aligned}
\psi_I &= [A_1 e^{ik_x x} + B_1 e^{-ik_x x}] e^{ik_y y} \\
&= \frac{1}{\sqrt{2}}\begin{bmatrix}1\\1\end{bmatrix} e^{i(k_x x + k_y y)} \\
&\quad + \begin{bmatrix}b_\uparrow\\b_\downarrow\end{bmatrix} e^{-i(k_x x - k_y y)}
\end{aligned}
\tag{5.21}
$$

Here the first term corresponds to the incoming wave with equally probable up-spin and down-spin electrons and the second term corresponds to the reflected wave with $b_\uparrow$ and $b_\downarrow$ representing the spin-up and spin-down probability amplitudes, respectively. Since the system is translationally symmetric along y direction, $k_y^+ = k_y$ and $k_y^- = k_y$. Let us define $\tan\theta = \frac{k_y}{k_x}$. At the boundary between the two media (i.e., at $x = 0$), the projection of the wave vector on to the boundary should be conserved i.e.,

$$k \sin\theta = k^+ \sin\theta'_{k+} \;\Rightarrow\; n_{k+} = \frac{k^+}{k} = \frac{\sin\theta}{\sin\theta'_{k+}} \;\Rightarrow\; \sin\theta'_{k+}$$

$$= \frac{1}{n_{k+}}\sin\theta$$

and

$$k \sin \theta = k^- \sin \theta'_{k^-} \;\Rightarrow\; n_{k^-} = \frac{k^-}{k} = \frac{\sin \theta}{\sin \theta'_{k^-}} \;\Rightarrow\; \sin \theta'_{k^-}$$

$$= \frac{1}{n_{k^-}} \sin \theta$$

where n_{k^+} and n_{k^-} are the refractive indices of the two transmitted waves. In the region II, since the incoming beam splits into two, there will be two critical angles corresponding to each of the transmitted wave. Thus we have

$$n_{k^+} = \sin \theta_c^+ = \frac{k^+ \left(\lambda \left(\frac{\pi}{2} \right) \right)}{k}$$

$$= \left(-\frac{m}{\hbar^2} \lambda \left(\frac{\pi}{2} \right) + \sqrt{\left(\frac{m\lambda \left(\frac{\pi}{2} \right)}{\hbar^2} \right)^2 + \frac{2m}{\hbar^2} \left(E_{k^+} \left(\frac{\pi}{2} \right) - V_0 \right)} \right) \Big/ \sqrt{\frac{2m}{\hbar^2} E} \;,$$

$$n_{k^-} = \sin \theta_c^- = \frac{k^- \left(\lambda \left(\frac{\pi}{2} \right) \right)}{k}$$

$$= \left(\frac{m}{\hbar^2} \lambda \left(\frac{\pi}{2} \right) + \sqrt{ \left(\frac{m \lambda \left(\frac{\pi}{2} \right)}{\hbar^2} \right)^2 + \frac{2m}{\hbar^2} \left(E_{k^-} \left(\frac{\pi}{2} \right) - V_0 \right) } \right) \Big/ \sqrt{ \frac{2m}{\hbar^2} E } \ .$$

Using boundary conditions given in Eq.(5.7) and Eq.(5.8) one can obtain

$$A_{\text{II}}^{(1)} = \frac{\sqrt{2}}{\left(1 + \frac{k_x^+}{k_x} \right)} \frac{\left(e^{-i\phi_{k^-}} - 1 \right)}{\left(e^{-i\phi_{k^+}} + e^{-i\phi_{k^-}} \right)} \tag{5.22}$$

$$A_{\text{II}}^{(2)} = \frac{\sqrt{2}}{\left(1 + \frac{k_x^-}{k_x} \right)} \frac{\left(e^{i\phi_{k^+}} + 1 \right)}{\left(e^{i\phi_{k^+}} + e^{i\phi_{k^-}} \right)} \tag{5.23}$$

$$\begin{aligned} b_\uparrow = &\frac{\sqrt{2}}{\left(1 + \frac{k_x^+}{k_x} \right)} \frac{\left(1 - e^{i\phi_{k^-}} \right)}{\left(1 + e^{-i(\phi_{k^+} - \phi_{k^-})} \right)} \\ &+ \frac{\sqrt{2}}{\left(1 + \frac{k_x^-}{k_x} \right)} \frac{\left(1 + e^{i\phi_{k^+}} \right)}{\left(1 + e^{i(\phi_{k^+} - \phi_{k^-})} \right)} \\ &- \frac{1}{\sqrt{2}} \end{aligned} \tag{5.24}$$

$$b_\downarrow = \frac{\sqrt{2}}{\left(1 + \frac{k_x^+}{k_x}\right)} \frac{\left(1 - e^{-i\phi_{k^-}}\right)}{\left(1 + e^{i(\phi_{k^+} - \phi_{k^-})}\right)}$$

$$+ \frac{\sqrt{2}}{\left(1 + \frac{k_x^-}{k_x}\right)} \frac{\left(1 + e^{-i\phi_{k^+}}\right)}{\left(1 + e^{-i(\phi_{k^+} - \phi_{k^-})}\right)} \qquad (5.25)$$

$$- \frac{1}{\sqrt{2}}$$

Using Eq.(5.22) - Eq.(5.25), one can write the reflection and transmission coefficients as

$$R_\uparrow = 2|b_\uparrow|^2 \quad ,$$

$$R_\downarrow = 2|b_\downarrow|^2 \quad ,$$

$$T_+ = 2 \frac{k_x^+}{k_x} \left|A_{\mathrm{II}}^{(1)}\right|^2 \quad ,$$

$$T_- = 2 \frac{k_x^-}{k_x} \left|A_{\mathrm{II}}^{(2)}\right|^2 \quad .$$

Here pre-factor 2 corresponds to the spin degrees of freedom of the incident unpolarized electron.

The differential conductance at zero temperature can be obtained as [50,52]

$$G(V) = G_o \int\limits_{-\theta_m}^{+\theta_m} d\theta \, \cos\theta \, \sqrt{1 + \frac{eV}{E_F} (T_+ + T_-)} \qquad (5.26)$$

where $G_o = e^2 A k_F / 2\pi h$ and A is the area of the metal, θ_m is the maximum possible angle of incidence.

One can define polarizability for transmitted and reflected electrons as

$$P_{trans} = \frac{T_+ - T_-}{T_+ + T_-} \quad ,$$

$$P_{refl} = \frac{R_\uparrow - R_\downarrow}{R_\uparrow + R_\downarrow} \quad .$$

5.2.3 Numerical results and discussion

In our numerical calculations we consider the energy of the incident electron as $20 meV$ and the height of the potential barrier as $V_o = 12 meV$. The variation of the refracted angle as a function of the incident angle is shown in Fig. 5.7. Here we have considered the strengths

of RSOI and DSOI as $\alpha = 5meV - nm$ and $\beta = 5meV - nm$. For normal incidence ($\theta = 0$), angle of refraction is also zero.
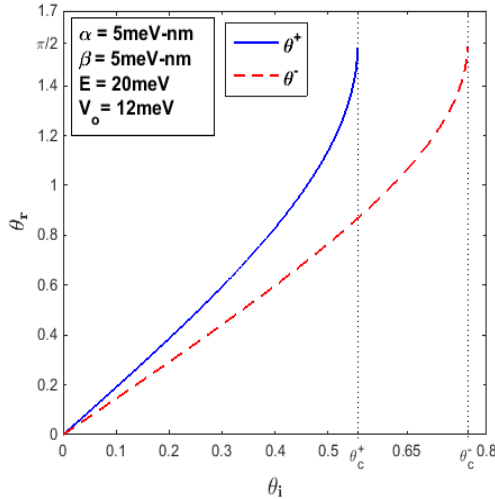

Fig. 5.7 Angle of refraction as a function of angle of incidence.

In the absence of both the SOI's in the region II, the angle of refraction remains the same as the angle of incidence. But in the presence of it, the electron with energy E'_{k+}, has a larger refraction angle and the electron with energy E'_{k-}, has a smaller angle of refraction compared to angle of incidence. With the increment in the strength of RSOI and DSOI, the splitting between the curves increases more and more. Also the critical angle at which the angle of refraction becomes $\pi/2$, shifts towards the lower

values for an electron with energy E'_{k+} (+ mode), and towards higher values for an electron with energy E'_{k-} (− mode).

Fig. 5.8 represents the variation of transmission and reflection coefficients as a function of angle of incidence. The figure shows that $R_\uparrow$ is almost zero and it further reduces with the incident angle. Similar stable behavior is observed in the case of T_+ as well; but, it increases with incident angle with an additional shift up in the numerical value. $R_\downarrow$ falls off as a function of incident angle and T_- increases as a function
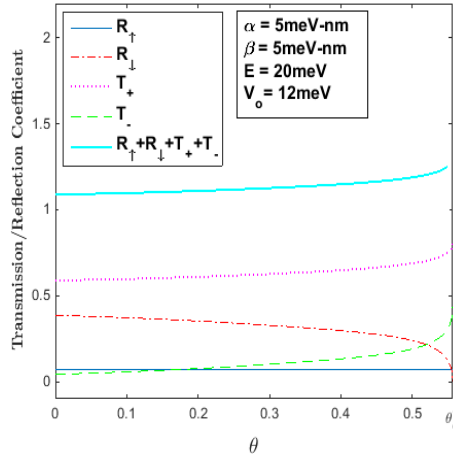

Fig. 5.8: The variation of transmission and reflection coefficients vs. angle of incidence.

of the incident angle. Both the $R_\downarrow$ and T_- have opposite behavior as is shown in the Fig. 5.8. This also shows that the sum $R_\uparrow + R_\downarrow + T_+ + T_- \neq 1$. This is due to the fact that the environment on either side of the barrier is different and we did not take into account the effective mass of the electron in the region II. We would like to emphasize that similar qualitative behavior can be obtained by considering the effective mass of electron or by fixing the height of the step potential V_o [47].

The variation of polarizability of incident and reflected electrons is shown if Fig. 5.9 as a function of incident angle.
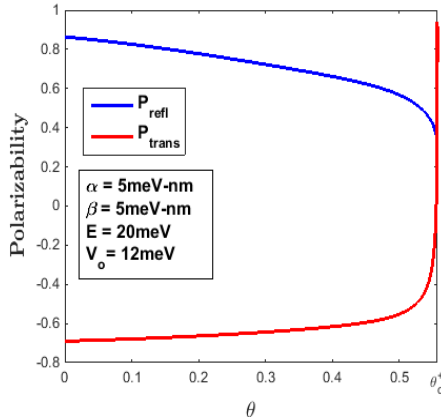

Fig. 5.9: Reflected and transmitted polarizability vs. incident angle.

The figure shows that the polarization in the reflected electrons falls gradually as a function of the incident angle while that of transmitted electrons increases. At the critical angle, there is a steep rise in polarizability of transmitted electron and a steep fall in that of the reflected electron. Also the sum of the transmitted electron polarizability and the reflected electron polarizability is finite positive throughout the range of the angle of incidence; however, at the critical angle, the respective polarizabilities change their sign.

Fig. 5.10 shows the variation of differential conductivity as a function of the Fermi energy and applied voltage for various incident energies. To calculate differential conductivity, we consider $E_F = 15meV$ and the applied voltage $V = 25meV$. In both the cases, we observe an obvious functional dependence as given in Eq. 5.22. i. e., the differential conductivity varies as the inverse square root of Fermi energy and as the square root of applied voltage. This shows that the differential conductivity decreases with an increase in the incident angle. It falls very rapidly to some negative values as the angle of incident approaches the critical angle. The variation of differential conductivity as a function of strength of SOI is shown in Fig. 5.11 for various incident energies. The figure shows that the differential conductivity decreases

quadratically with the SOI strength. One can also observe that the differential conductivity increases with
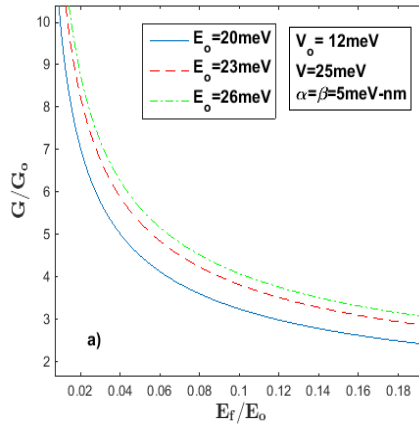
an increment in incident energy.
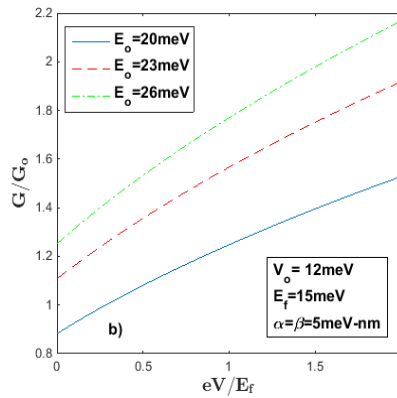
Fig. 5.10 The variation of differential conductivity vs. a) Fermi energy b) Applied voltage.
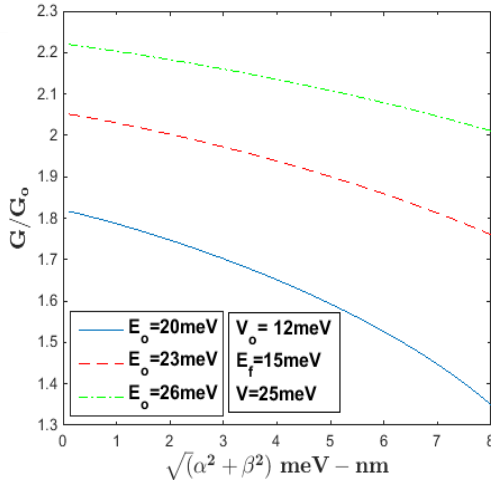
Fig. 5.11   Differential conductivity vs. SOI strength.

The variation of reflection and transmission coefficients as a function of SOI strength is shown in Fig. 5.12 for various incident energies. The figures show that both the $R_\uparrow$ and $R_\downarrow$ increase quadratically with an increase in the SOI strength. Likewise, both of them decrease with increasing incident energy. T_+ increases as the square root of SOI strength whereas T_- decreases quadratically with an increase in the SOI strength. Both the transmission coefficients increase with an increment in the incident energy.

a)

$R_\uparrow$

$V_o = 12\text{meV}$
$E_f = 15\text{meV}$
$V = 25\text{meV}$

$E_o = 20\text{meV}$
$E_o = 23\text{meV}$
$E_o = 26\text{meV}$

$\sqrt{(\alpha^2 + \beta^2)}\ \text{meV} - \text{nm}$

b)

$R_\downarrow$

$V_o = 12\text{meV}$
$E_f = 15\text{meV}$
$V = 25\text{meV}$

$E_o = 20\text{meV}$
$E_o = 23\text{meV}$
$E_o = 26\text{meV}$

$\sqrt{(\alpha^2 + \beta^2)}\ \text{meV} - \text{nm}$
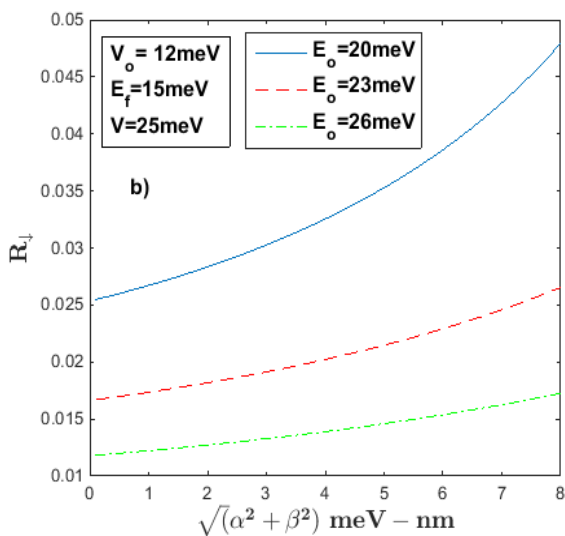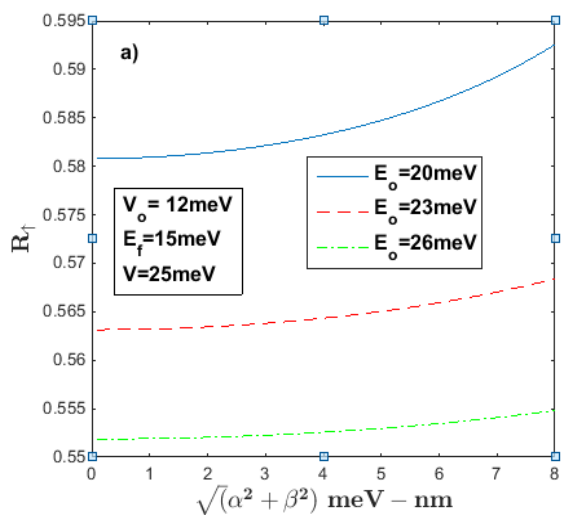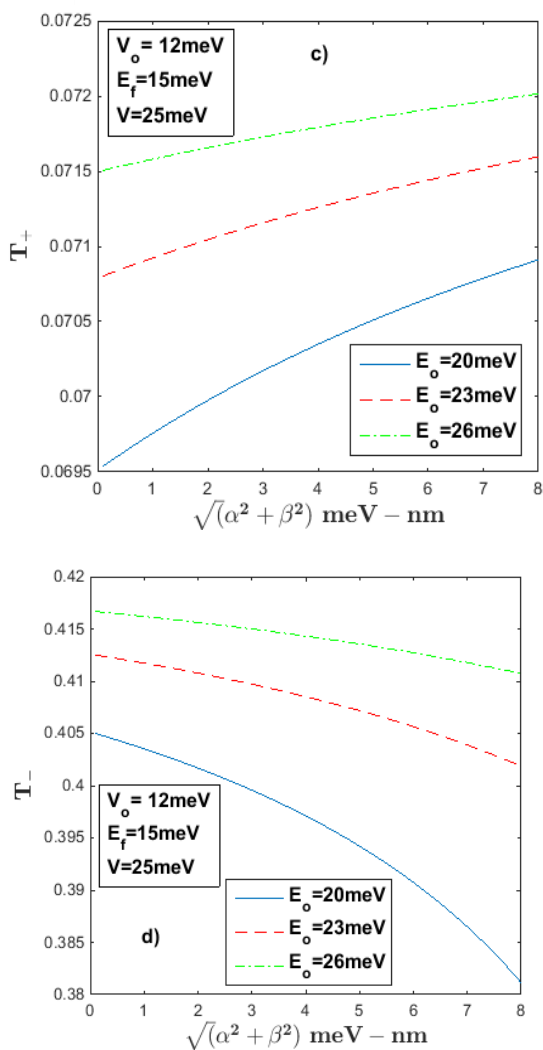
Fig. 5.12: Reflection and transmission coefficients
vs. SOI strength. a) $R_\uparrow$, b) $R_\downarrow$, c) T_+, d) T_-.

The variation of polarizability as a function of SOI strength is shown in Fig. 5.13 for various incident energies.
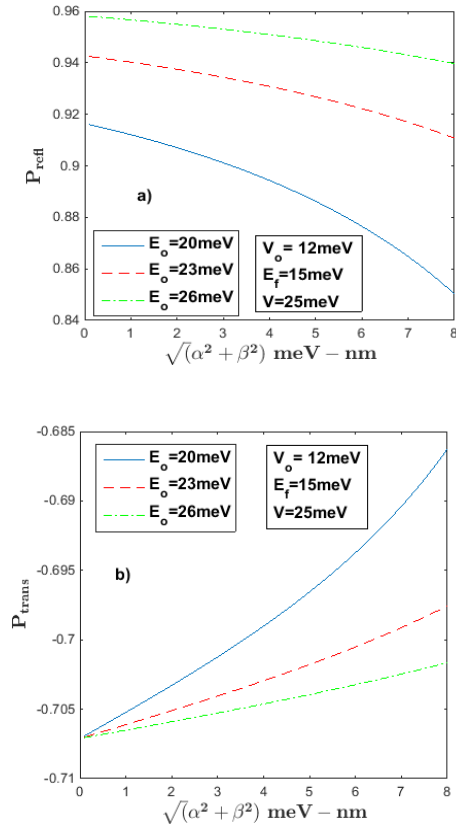

Fig. 5.13: Polarizability vs. SOI strength a) for reflected electrons b) for transmitted electrons.

The figures show that the polarizability of reflected electrons decreases quadratically with SOI strength and that of transmitted electrons increases quadratically. Also, polarizability of the reflected electrons increases with incident energy and decreases in the case of transmitted electrons.

5.2.4 Conclusions

The spin polarization effects due to the transmission and reflection of electrons across a barrier separating a metal and a semiconductor with RSOI and DSOI have been studied in this work. The transmission and reflection coefficients have been calculated and experimentally measurable quantities like differential conductance, polarizability have been obtained. The effects of the incident angle, incident energy, applied voltage, and the SOI strength on the differential conductance and spin polarizability have been studied. It has been observed that the incident electron energy enhances the transmission coefficient and reflection polarizability, while opposite effects are observed in case of their counter parts. The SOI is found to reduce the transmission coefficient and reflection polarizability

while it is found to enhance their counterparts. The transmission coefficient corresponding to the +ve mode has an interesting behavior, it increases as a square root of the SOI strength. The polarizability of the reflected electron is found to be positive and that of the transmitted electron turns out be negative. Both change sign at the critical angle of + mode. The present work has potential applications in spin filtering and spin polarizing devices.

References

1. S.N.F. Mott, R.W. Gurney, *Electronic processes in ionic crystals*, Clarendon Press, , (1948).

2. G.L. Pearson, J. Bardeen, *Electrical Properties of Pure Silicon and Silicon Alloys Containing Boron and Phosphorus*, Phys. Rev. **75**, 865, (1949). doi:10.1103/PhysRev.75.865.

3. W. Kohn, J.M. Luttinger, *Theory of Donor States in Silicon*, Phys. Rev. **98**, 915, (1955). doi:10.1103/PhysRev.98.915.

4. Y. Yafet, R.W. Keyes, E.N. Adams, *Hydrogen atom in a strong magnetic field*, J. Phys. Chem. Solids. **1**, 137, (1956). doi:10.1016/0022-3697(56)90020-8.

5. G. Bastard, *Hydrogenic impurity states in a quantum well: A simple model*, Phys. Rev. B. **24**, 4714, (1981).

doi:10.1103/PhysRevB.24.4714.

6. J.-L. Zhu, *Exact solutions for hydrogenic donor states in a spherically rectangular quantum well*, Phys. Rev. B. **39**, 8780, (1989). doi:10.1103/PhysRevB.39.8780.

7. C. Bose, C.K. Sarkar, *Binding Energy of Impurity States in Spherical GaAs-Ga1-xAlxAs Quantum Dots*, Phys. Status Solidi. **218**, 461, (2000). doi:10.1002/1521-3951(200004)218:2<461::AID-PSSB461>3.0.CO;2-U.

8. C.-C. Yang, L.-C. Liu, S.-H. Chang, *Eigenstates and fine structure of a hydrogenic impurity in a spherical quantum dot*, Phys. Rev. B. **58**, 1954, (1998). doi:10.1103/PhysRevB.58.1954.

9. J.J. Vivas-Moreno, N. Porras-Montenegro, *The Effects of Quantum Confinement and Magnetic Fields on the Binding Energy of Hydrogenic Impurities in Low-Dimensional Systems*, Phys. Status Solidi. **210**, 723, (1998). doi:10.1002/(SICI)1521-3951(199812)210:2<723::AID-PSSB723>3.0.CO;2-T.

10. P.G. Bolcatto, C.R. Proetto, *Shape and dielectric mismatch effects in semiconductor quantum dots*, Phys. Rev. B. **59**, 12487, (1999). doi:10.1103/PhysRevB.59.12487.

11. A. Corella-Madueño, R. Rosas, J.L. Marín, R. Riera, *Hydrogenic impurities in spherical quantum dots in a magnetic field*, J. Appl. Phys. **90**, 2333, (2001).

doi:10.1063/1.1329143.

12.   B. Szafran, J. Adamowski, B. Stébé, *Energy spectrum of centres in spherical quantum dots*, J. Phys. Condens. Matter. **10**, 7575, (1998). doi:10.1088/0953-8984/10/34/011.

13.   E. Bernardes, J. Schliemann, M. Lee, J.C. Egues, D. Loss, *Spin-orbit interaction in symmetric wells with two subbands.*, Phys. Rev. Lett. **99**, 076603, (2007). doi:10.1103/PhysRevLett.99.076603.

14.   J. Brüning, V. Geyler, K. Pankrashkin, *On the discrete spectrum of spin-orbit Hamiltonians with singular interactions*, Russ. J. Math. Phys. **14**, 423, (2007). doi:10.1134/S1061920807040073.

15.   S.-S. Li, J.-B. Xia, *Spin-orbit splitting of a hydrogenic donor impurity in GaAsGaAlAs quantum wells*, Appl. Phys. Lett. **92**, 022102, (2008). doi:10.1063/1.2833692.

16.   W. Xie, *Binding energy of an off-center hydrogenic donor in a spherical Gaussian quantum dot*, Phys. B Condens. Matter. **403**, 2828, (2008). doi:10.1016/j.physb.2008.02.017.

17.   A. Boda, A. Chatterjee, *Ground state and binding energies of (D0), (D−) centres and resultant dipole moment of a (D−) centre in a GaAs quantum dot with Gaussian confinement*, Phys. E Low-Dimensional Syst.

Nanostructures. **45**, 36, (2012). doi:10.1016/j.physe.2012.06.021.

18.   S.S. Gomez, R.H. Romero, *Binding energy of an off-center shallow donor in a spherical quantum dot*, Phys. E Low-Dimensional Syst. Nanostructures. **42**, 1563, (2010). doi:10.1016/j.physe.2009.12.045.

19.   I.L. Aleiner, V.I. Fal'ko, *Spin-orbit coupling effects on quantum transport in lateral semiconductor dots.*, Phys. Rev. Lett. **87**, 256801, (2001). doi:10.1103/PhysRevLett.87.256801.

20.   S. Datta, B. Das, *Electronic analog of the electro-optic modulator*, Appl. Phys. Lett. **56**, 665, (1990). doi:10.1063/1.102730.

21.   G.A. Prinz, *Magnetoelectronics*, Science (80-.). **282**, 1660, (1998). doi:10.1126/science.282.5394.1660.

22.   C.Y. Prescott, W.B. Atwood, R.L.A. Cottrell, H. DeStaebler, E.L. Garwin, A. Gonidec, R.H. Miller, L.S. Rochester, T. Sato, D.J. Sherden, C.K. Sinclair, S. Stein, R.E. Taylor, J.E. Clendenin, V.W. Hughes, N. Sasao, K.P. Schüler, M.G. Borghini, K. Lübelsmeyer, W. Jentschke, *Parity non-conservation in inelastic electron scattering*, Phys. Lett. B. **77**, 347, (1978). doi:10.1016/0370-2693(78)90722-0.

23.   C.Y. Prescott, $e^+ e^-$ Collisions at the SLC: The Left-right asymmetry, in: Proceedings, Int. Conf.

Neutral Curr. Twenty Years Later, : pp. 379–390. http://inspirehep.net/record/359111 (accessed December 19, 2015).

24. B.R. Heckel, C.E. Cramer, T.S. Cook, E.G. Adelberger, S. Schlamminger, U. Schmidt, *New CP-violation and preferred-frame tests with polarized electrons.*, Phys. Rev. Lett. **97**, 021603, (2006). doi:10.1103/PhysRevLett.97.021603.

25. R. Feder, *Polarized Electrons in Surface Physics*, World Scientific, , (1985). https://books.google.com/books?id=d-z-sb7eUOAC&pgis=1 (accessed December 19, 2015).

26. P.D. Johnson, *Spin-polarized photoemission*, Reports Prog. Phys. **60**, 1217, (1997). doi:10.1088/0034-4885/60/11/002.

27. G. Baum, W. Blask, P. Freienstein, L. Frost, S. Hesse, W. Raith, P. Rappolt, M. Streun, *Spin asymmetries for triple-differential electron-impact ionization of lithium at 54.4 eV.*, Phys. Rev. Lett. **69**, 3037, (1992). doi:10.1103/PhysRevLett.69.3037.

28. T. Schäpers, J. Nitta, H.B. Heersche, H. Takayanagi, *Interference ferromagnet/semiconductor/ferromagnet spin field-effect transistor*, Phys. Rev. B. **64**, 125314, (2001). doi:10.1103/PhysRevB.64.125314.

29. J.C. Egues, *Spin-Dependent Perpendicular*

Magnetotransport through a Tunable ZnSe / Zn 1 − x Mn x Se Heterostructure: A Possible Spin Filter?, Phys. Rev. Lett. **80**, 4578, (1998). doi:10.1103/PhysRevLett.80.4578.

30. H. Li, X. Yang, W. Chen, *Spin-polarization transport in ferromagnetic semiconductor/ferromagnetic -wave superconductor junctions*, Solid State Commun. **150**, 772, (2010). doi:10.1016/j.ssc.2010.01.011.

31. P. Högl, A. Matos-Abiague, I. Žutić, J. Fabian, *Magnetoanisotropic Andreev reflection in ferromagnet-superconductor junctions.*, Phys. Rev. Lett. **115**, 116601, (2015). doi:10.1103/PhysRevLett.115.116601.

32. F. Aghel, R. Safaiee, M.M. Golshan, *Dynamical spin polarization in single-layer graphene*, Phys. E Low-Dimensional Syst. Nanostructures. **54**, 133, (2013). doi:10.1016/j.physe.2013.06.010.

33. M. Shiraishi, M. Ohishi, R. Nouchi, N. Mitoma, T. Nozaki, T. Shinjo, Y. Suzuki, *Robustness of Spin Polarization in Graphene-Based Spin Valves*, Adv. Funct. Mater. **19**, 3711, (2009). doi:10.1002/adfm.200900989.

34. A. Dyrdał, J. Barnaś, *Current-induced spin polarization and spin-orbit torque in graphene*, Phys. Rev. B. **92**, 165404, (2015). doi:10.1103/PhysRevB.92.165404.

35. T. Koga, J. Nitta, H. Takayanagi, S. Datta, *Spin-filter*

device based on the Rashba effect using a nonmagnetic resonant tunneling diode., Phys. Rev. Lett. **88**, 126601, (2002). doi:10.1103/PhysRevLett.88.126601.

36.   K. Chang, F.M. Peeters, *Spin polarized tunneling through diluted magnetic semiconductor barriers*, Solid State Commun. **120**, 181, (2001). doi:10.1016/S0038-1098(01)00370-2.

37.   Y.-C. Xiao, R. Zhu, W.-J. Deng, *Ballistic transport in extended Datta–Das spin field effect transistors*, Solid State Commun. **151**, 1214, (2011). doi:10.1016/j.ssc.2011.06.005.

38.   R. Vali, S.M. Mirzanian, *Effect of Rashba spin–orbit coupling on the spin polarized transport in diluted magnetic semiconductor barrier structures*, Solid State Commun. **149**, 2032, (2009). doi:10.1016/j.ssc.2009.08.027.

39.   V.M. Ramaglia, D. Bercioux, V. Cataudella, G. De Filippis, C.A. Perroni, *Spin polarization of electrons with Rashba double-refraction*, J. Phys. Condens. Matter. **16**, 9143, (2004). doi:10.1088/0953-8984/16/50/005.

40.   D. Dragoman, *Optical analogues of nanostructures with Rashba–Dresselhaus interactions*, J. Opt. **16**, 015710, (2014). doi:10.1088/2040-8978/16/1/015710.

41.   M. Khodas, A. Shekhter, A.M. Finkel'stein, *Spin*

polarization of electrons by nonmagnetic heterostructures: the basics of spin optics., Phys. Rev. Lett. **92**, 086602, (2004). doi:10.1103/PhysRevLett.92.086602.

42. A. Dargys, *Double reflection of electron spin in 2D semiconductors*, Superlattices Microstruct. **48**, 221, (2010). doi:10.1016/j.spmi.2010.05.015.

43. A. Dargys, *Boundary conditions and transmission reflection of electron spin in a quantum well*, Semicond. Sci. Technol. **27**, 045009, (2012). doi:10.1088/0268-1242/27/4/045009.

44. A. Dargys, *Control of two-dimensional electron spin by an abrupt change of physical parameters of a quantum well*, Lith. J. Phys. **51**, 53, (2011). doi:10.3952/lithjphys.51108.

45. A. Dargys, Double reflection of electron spin in semiconductors, in: Acta Phys. Pol. A, : pp. 161–163. http://www.scopus.com/inward/record.url?eid=2-s2.0-79751484364&partnerID=tZOtx3y1.

46. P. Shao, W. Deng, *Electronic double refraction due to the Rashba effect: Analytical and numerical results*, Front. Phys. China. **2**, 44, (2007). doi:10.1007/s11467-007-0015-6.

47. T. Yokoyama, Y. Tanaka, J. Inoue, *Charge transport in two-dimensional electron gas/insulator/superconductor*

junctions with Rashba spin-orbit coupling, Phys. Rev. B. **74**, 035318, (2006). doi:10.1103/PhysRevB.74.035318.

48.   A. Reynoso, G. Usaj, C.A. Balseiro, *Spin Hall effect in clean two-dimensional electron gases with Rashba spin-orbit coupling*, Phys. Rev. B. **73**, 115342, (2006). doi:10.1103/PhysRevB.73.115342.

49.   B. Lv, Z. Ma, *Electronic equivalence of optical negative refraction and retroreflection in the two-dimensional systems with inhomogeneous spin-orbit couplings*, Phys. Rev. B. **87**, 045305, (2013). doi:10.1103/PhysRevB.87.045305.

50.   B. Srisongmuang, P. Pairor, M. Berciu, *Tunneling conductance of a two-dimensional electron gas with Rashba spin-orbit coupling*, Phys. Rev. B. **78**, 155317, (2008). doi:10.1103/PhysRevB.78.155317.

51.   V.M. Ramaglia, D. Bercioux, V. Cataudella, G. De Filippis, C.A. Perroni, F. Ventriglia, *Conductance of a large point contact with Rashba effect*, Eur. Phys. J. B - Condens. Matter. **36**, 365, (2003). doi:10.1140/epjb/e2003-00355-4.

52.   G. Papp, F.M. Peeters, *Spin filtering in a magnetic–electric barrier structure*, Appl. Phys. Lett. **78**, 2184, (2001). doi:10.1063/1.1360224.

6 Chapter 6 Conclusions

In this thesis entitled *"Spin − orbit interactions in parabolic quantum dots"* we have studied the effect of Rashba spin-orbit interaction (RSOI) and Dresselhaus spin-orbit (DSOI) interaction in a parabolic quantum dot (PQD) with interacting electrons. We have investigated various experimentally measurable quantities related to quantum dots (QDs) and investigated the effect of both RSOI and DSOI on them. We have also applied some of our results to a couple of realistic quantum dots.

We began the thesis with an introductory chapter on quantum dots where we have first presented a brief description of the chronological development in semiconductor technology that led to the discovery and developments in QDs research. Then we have introduced a few theoretical models that have been very useful for the understanding of the physics of QDs. In this context we have discussed the role of confining potential in a quantum dot and gave reasons for choosing the parabolic potential as the model confinement potential for our work. We have also introduced here the exactly soluble

Johnson-Payne model potential as a reasonable model for the electron-electron interaction potential in an interacting $N-$ electron QD. Finally we have given a short description about the Rashba and Dresselhaus spin-orbit interactions and introduced the unitary transformations required to solve the QD Hamiltonian with RSOI and DSOI.

In the next chapter we have studied the effect of RSOI and e-e interaction on the ground state energy of a parabolic QD with N interacting electrons in a perpendicular magnetic field. We have also studied the effect of these interactions on the resonance tunneling energy. We have observed that RSOI reduces the GS energy and the reduction effect increases as we go to the higher magnetic field regime. Also the dependence of GS energy on the RSOI term is slightly more complex than just quadratic. We have observed that RSOI and the e-e interaction are independent of each other. The e-e interaction energy increases with number of electrons and also increases linearly with applied magnetic field. Resonant tunneling energy also increases almost linearly with applied magnetic field. Sometimes with a change in number of electrons on the dot, a valley structure is also observed. RSOI has a constant reduction effect on resonant tunneling energy also. Our results are found to

be in good agreement with the numerical results reported in the literature.

Next we have taken up for study in In Chapter 3, the effect of RSOI, DSOI and the e-e interaction on the entire energy spectrum of an $N-$ electron PQD in a perpendicular magnetic field. We have also studied the effect of these interactions on the chemical potential, addition energy and spin splitting energy. It is shown that both the SOI's reduce the energy of the system. As we go to higher excited states, the reduction effect of DSOI decreases and after a certain excited state, DSOI increases the energy of the system, whereas RSOI reduces the energy of the system and the reduction effect increases as we go to higher excited states. It is also shown that RSOI enhances the effect of Zeeman term, whereas DSOI reduces it. The e-e interaction energy as a function of applied field increases linearly for low-lying excited states and almost quadratically for higher excited states and at larger applied fields it saturates. It is furthermore shown that RSOI marginally enhances the e-e interaction effect and DSOI reduces it slightly. The effect of SOI on the chemical potential is found to be same as that on the total energy. It is observed that in the absence of any external field, RSOI enhances the addition energy and DSOI reduces it. But with the

application of an external field, the effect reduces and beyond a certain critical field, the effect of the SOI's on the addition energy reverses. It is shown that in the presence of RSOI, the spin-splitting energy initially increases quadratically with the magnetic field and once complete polarization occurs, it becomes flat and eventually decreasing linearly. A similar behavior is also observed in the case of DSOI except for a sign change. For a zero angular momentum state, neither RSOI nor DSOI has any effect on the spin-splitting energy whereas RSOI enhances the spin splitting for a negative orbital angular momentum state and DSOI enhances it for a positive orbital angular momentum state.

In Chapter 4, we have the studied the effect of RSOI, DSOI and e-e interaction on some thermodynamic and magnetic properties namely, the magnetization, susceptibility, heat capacity and entropy of an $N-$ electron parabolic quantum dot in a perpendicular magnetic field and explicit numerical results have been obtain and graphs plotted a two-electron QD system. Both magnetization and susceptibility show a paramagnetic peak wherever a singlet-triplet transition occurs in the energy spectrum. RSOI shifts the paramagnetic peak to the higher magnetic field side while DSOI shifts it to the lower magnetic field regime.

The e-e interaction reduces the magnetization in the diamagnetic region and has no effect in the paramagnetic region. The height of the paramagnetic peak of susceptibility as a function of T is finite In the presence of SOI, while it is infinite in the absence of SOI. The susceptibility seems to be independent of SOI at large values of T. The heat capacity curve shows a Schottky anomaly kind of peak just before and after the singlet-triplet transition and also at very large magnetic fields where the energy levels are close enough to resemble a two level system. It is shown that temperature increases the width and reduces the height of the peak and at a very high temperature only one peak is observed at a very high magnetic field. At very low and high magnetic fields, the heat capacity reduces with RSOI and increases with DSOI as compared to the case without any SOI. In the intermediate field regime, the effect of RSOI and DSOI changes sign for every peak transition in the heat capacity curve. As $T \rightarrow 0$, both RSOI and DSOI have negligible effects on heat capacity. The e-e interaction has no effect on heat capacity at very large magnetic fields. But at low magnetic field strengths, the e-e interaction enhances the heat capacity at lower temperatures and reduces it at high temperatures. In the absence of the applied field, the heat capacity as a

function of temperature shows a sharp peak at a low temperature in the presence of both RSOI and DSOI whereas no peak is observed in the absence of SOI which is a direct consequence of zero-field spin splitting. As temperature increases, the entropy increases and saturates to a constant value for a larger magnetic field. It is shown that RSOI enhances the entropy and DSOI reduces it. The e-e interaction is found to enhance the entropy.

Finally we have extended our study of the effect of SOI on the binding energy of a D^0 complex in a Gaussian quantum dot D^0 complex in a Gaussian quantum dot and on the tunneling conductance of an electron across a barrier separating a metal and a semiconductor where the semiconducting medium imposes RSOI and DSOI. It is shown that RSOI reduces the energy of the electron in D^0 complex quadratically, but It has no effect on the binding energy of the electron. The barrier transmission problem has been studied at for zero temperature in the absence of an applied magnetic field. Therefore, both RSOI and DSOI show a similar effect without even a sign change. The effects of incident electron energy and the strength of SOI on reflection and transmission coefficients, reflected and transmitted electron polarizabilities and differential conductivity are studied.

It is observed that the increase in the incident electron energy enhances the transmission coefficient, and the reflection polarizability. Opposite effect is observed on their counter parts i.e, reflection coefficient and transmission polarizability. We also show that SOI reduces the transmission coefficient and reflection polarizability and enhances their counterparts. It is further more shown that SOI reduces the differential conductivity quadratically. This work has potential applications in spin filtering and spin polarizing devices.

List of Publications

List of publications based on which the present Thesis has been written:

D. Sanjeev Kumar, S. Mukhopadhyay, A. Chatterjee, Effect of Rashba interaction and Coulomb correlation on the ground state energy of a GaAs quantum dot with parabolic confinement. Physica E, Volume **47**, 270 (2013).

D. Sanjeev Kumar, A. Boda, S. Mukhopadhyay, A. Chatterjee; Effect of Rashba spin-orbit interaction on the ground state energy of a D^0 centre in a GaAs quantum dot with Gaussian confinement. Superlattices Microstruct. **88**, 174 (2015).

D. Sanjeev Kumar, S. Mukhopadhyay, A. Chatterjee, Magnetization and susceptibility of a parabolic InAs quantum dot with electron-electron and spin-orbit interactions in the presence of a magnetic field at finite temperature, JMMM, (2016) (in press, doi: 10.1016/j.jmmm.2016.02.071).

D. Sanjeev Kumar, S. Mukhopadhyay, A. Chatterjee Effect of Rashba and Dresselhaus interactions on the energy spectrum, chemical potential, addition energy and spin-splitting in a many-electron parabolic GaAs quantum dot in a magnetic field, (To be communicated)

D. Sanjeev Kumar, S. Mukhopadhyay, A. Chatterjee; Heat capacity and Entropy of a parabolic InAs quantum

dot with electron-electron and spin-orbit interactions in the presence of a magnetic field at finite temperature. (To be communicated)

D. Sanjeev Kumar, S. Sil, A. Chatterjee; Double refraction of electron spin across metal-semiconductor junction with Rashba and Dresselhaus spin-orbit interactions; (To be communicated)
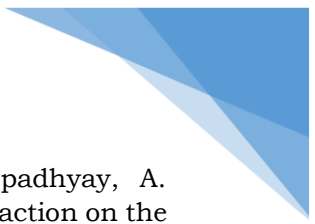
Other publication:

Effect of electron–electron interaction on the magnetic moment and susceptibility of a parabolic GaAs quantum dot. Aalu Boda, D. Sanjeev Kumar, I.V. Sankar, Ashok Chatterjee; JMMM, (2016) (in press, doi: 10.1016/j.jmmm.2016.04.015)

Publications in Conference proceedings:

D. Sanjeev Kumar, S. Mukhopadhyay, A. Chatterjee; Effect of Rashba interaction on the energy levels of a GaAs quantum dot with parabolic confinement. AIP Conf. Proc. **1536**, 211 (2013).

D. Sanjeev Kumar, S. Mukhopadhyay, A. Chatterjee; Magnetization Of A Parabolic Quantum Dot In The Presence Of Rashba And Dresselhaus Spin-Orbit Interactions. AIP Conf. Proc. **1661**, 080019 (2015).

A. Boda, D. Sanjeev Kumar, S. Mukhopadhyay, A. Chatterjee, Effect of Rashba spin-orbit interaction on the ground state of a Hydrogenic D^0 complex in a Gaussian quantum dot. AIP Conf. Proc. **1665**, 120035 (2015).

D. Sanjeev Kumar, S. Mukhopadhyay, A. Chatterjee; Specific heat of parabolic quantum dot with Dresselhaus spin-orbit interaction, AIP Conf. Proc. **1724**, 020093 (2016)

Spin-Orbit interactions in parabolic quantum dots